

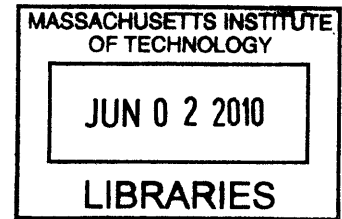
Engineering Artificial Cell Membranes

by

Ting F. Zhu

B.E., Engineering Mechanics (2003)
Tsinghua University

M.S., Mechanical Engineering (2005)
Massachusetts Institute of Technology



Submitted to the Division of Health Sciences and Technology in Partial Fulfillment of the
Requirements for the Degree of Doctor of Philosophy in Biomedical Engineering

at the

Massachusetts Institute of Technology

ARCHIVES

May 2010
[June 2010]

© 2010 Massachusetts Institute of Technology
All rights reserved

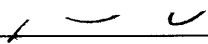
Signature of Author: _____
Harvard-MIT Division of Health Sciences and Technology
May 7, 2010

Certified By: _____
Jack W. Szostak, Ph.D.
Investigator, HHMI; Professor of Genetics, Harvard Medical School
Alex Rich Distinguished Investigator, Massachusetts General Hospital
Thesis Supervisor

Accepted By: _____
Ram Sasisekharan, Ph.D.
Director, Harvard-MIT Division of Health Sciences and Technology
Edward Hood Taplin Professor of Health Sciences and Technology and Biological Engineering


This doctoral thesis has been examined by a Thesis Committee of the following:

Professor Brian Seed, Ph.D.




Committee Chairman

Professor Jack W. Szostak, Ph.D.



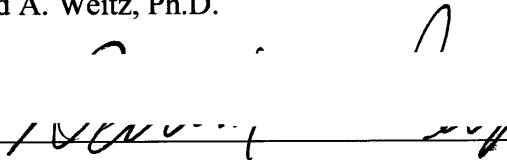
Thesis Supervisor

Professor David P. Bartel, Ph.D.



Committee Member

Professor David A. Weitz, Ph.D.



Committee Member

Abstract

Growth and division are essential biological processes of cellular life. A crucial question concerning the origin of cellular life is how primitive cells (protocells) lacking complex biological machinery could grow and divide. To address this question, we first developed an effective method for preparing large monodisperse (uniform-sized) vesicles through a combination of extrusion and large-pore dialysis. The development of this preparation method has led us to the discovery of a simple but efficient pathway for the growth and division of the membrane envelope of a model protocell: growth of a large multilamellar fatty acid vesicle after being fed with fatty acid micelles leads to a series of remarkable shape transformations, from an initially spherical state to a long thread-like vesicle; under modest shear forces, the thread-like vesicle divides into multiple daughter vesicles. We have also discovered a different pathway that allows the long thread-like vesicles to divide without relying on external forces. Furthermore, in the course of studying fatty acid vesicles, we have discovered a striking phenomenon: intense illumination causes dye-packed vesicles of a few microns in diameter to explode, rapidly and locally releasing the encapsulated contents. The photoactivated release of substances from exploding vesicles in a highly spatio-temporally controlled manner suggests potential applications of this phenomenon in many areas across disciplines.

Thesis Supervisor: Jack W. Szostak, Ph.D.

Investigator, HHMI; Professor of Genetics, Harvard Medical School;

Alex Rich Distinguished Investigator, Massachusetts General Hospital

To Mom and Dad

Acknowledgements

On an afternoon of late April 2005, a young graduate student from MIT's Mechanical Engineering Department walked into the office of Prof. Jack Szostak, a prominent biologist and a leader in the origins of life field. That student was me. Five years, 1000 microscope hours, 5000 emails, 10000 pipettes later, here I am, specializing in membrane vesicle studies. Such a transformation could be seen as more dramatic than the shape transformation of growing vesicles that surprised us both. How I have benefited the most from working with Jack is from his amazing ability to come up with brilliant ideas (such as putting *Tetrahymena* telomeres into yeasts, or adding DTT to vesicles) and to identify the ones that are going to work with greater than 90% accuracy—and he can do this in many different fields. He has led me through the door of science, showing me how to ask key questions, how to take risks, how to have fun, and how to explore and unite different areas across disciplines. I am soon to become the 28th Ph.D. from the Szostak Lab. I am both excited and nervous about this moment, not only because “28” is supposed to be a mathematically “perfect number” (the last one was 6, Jennifer Doudna, and the next one is 496), but also because I am about to leave his group and to establish myself like Jack and his prior 27 all-star graduates.

I also would especially like to thank my fantastic thesis committee. Prof. Brian Seed is one of the rare people in the world who seems to have more in-depth knowledge of different areas across disciplines than everyone else in his surroundings combined. His insightful advice on my research and his tremendous support for my career development have helped me greatly during the years I studied here. Prof. Dave Bartel is one of the all-star graduates from the Szostak Lab. Taking his classes at MIT was a wonderful introduction to the origins of life research, and was

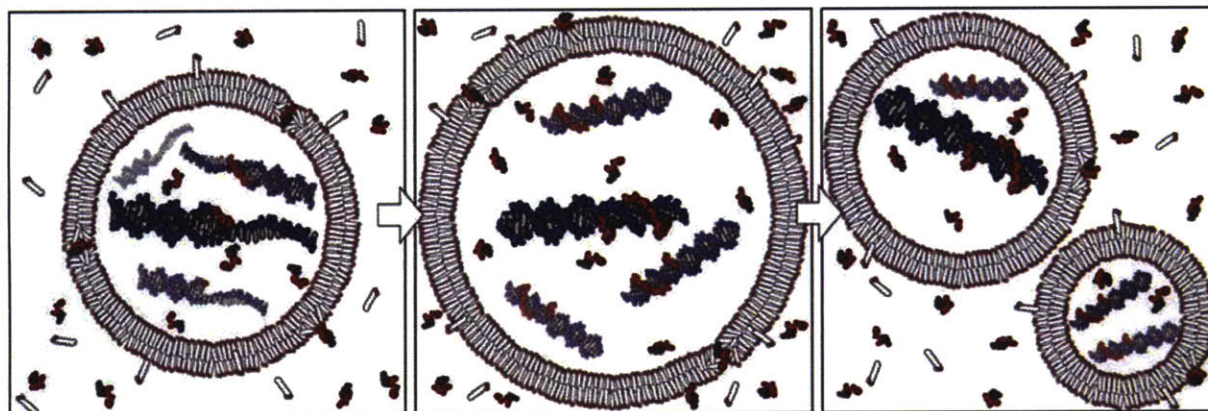
part of how I got interested in the field. I am also very lucky to have Prof. Dave Weitz on my thesis committee, who has provided me with valuable insights on membrane biophysics and great support of my job applications. I would also like to thank Prof. Fred Schoen, with whom I had my first TA experience in his HST.521 class, which I truly enjoyed and valued. Dr. Schoen has become a great mentor and friend since then, and has supported me in my teaching, research, and career development over the years.

I would also like to thank my wonderful labmates, Kate Adamala, Craig Blain, Raphael Bruckner, Itay Budin, Quentin Dufton, Mark Elenko, Ben Heuberger, Jeannie Jackson, Chi-Wang Lin, Matt Powner, Alonso Ricardo, Yollete Guillen Schlippe, Jason Schrum, Pam Svec, Sylvia Tobé, Simon Trevino, Na Zhang, and Shenglong Zhang, as well as former lab members Irene Chen, Andrej Luptak, Sheref Mansy, and Doug Treco, for their friendly and tireless support of my work over the past five years.

My friends and colleagues at MIT and Harvard have given me tremendous help in writing this thesis, and there is no way I could have finished this without them. Finally, I would like to thank my parents, who have always been behind me and supporting me from thousands of miles away. You are the best parents I could ever ask for.

Table of Contents	Page
Thesis Committee	ii
Abstract	iii
Acknowledgements	v
Table of Contents	vii
Chapter I: Introduction: The Origins of Cellular Life	1
Background	2
Recent Results	6
Challenges and Future Directions	23
Chapter II: Preparation of Large Monodisperse Vesicles	36
Summary	37
Introduction	38
Methods	40
Results	43
Discussion	45
Chapter III: Coupled Growth and Division of Model Protocell Membranes	53
Summary	54
Introduction	55
Methods	59
Results	68
Discussion	78
Chapter IV: Vesicle Pearling and Division	99
Summary	100
Introduction	101
Methods	102
Results	104
Discussion	107
Chapter V: Exploding Vesicles	116
Summary	117
Introduction	118
Methods	119
Results	124
Discussion	130
Appendix A: Preparation of Fatty Acid or Phospholipid Vesicles	144
Appendix B: Vesicle Extrusion through Track-etched Membranes	157
Appendix C: Preparation of Fatty Acid Micelles	169

Introduction: The Origins of Cellular Life



A portion of this chapter has been published in the *Cold Spring Harbor Book on Origins of Cellular Life*.

Background

The emergence of the first cells on the early Earth was the culmination of a long history of prior chemical and geophysical processes. While recognizing the many gaps in our knowledge of prebiotic chemistry and the early planetary setting in which life emerged, we will assume for the purpose of this review that the requisite chemical building blocks were available, in appropriate environmental settings. This assumption allows us to focus on the various spontaneous and catalyzed assembly processes that could have led to the formation of primitive membranes and early genetic polymers, their co-assembly into membrane-encapsulated nucleic acids, and the chemical and physical processes that allowed for their replication. We will discuss recent progress towards the construction of laboratory models of a protocell (Figure I.1), evaluate the remaining steps that must be achieved before a complete protocell model can be constructed, and consider the prospects for the observation of spontaneous Darwinian evolution in laboratory protocells. While such laboratory studies may not reflect the specific pathways that led to the origin of life on Earth, they are proving to be invaluable in uncovering surprising and unanticipated physical processes that help us to reconstruct plausible pathways and scenarios for the origin of life.

The term protocell has been used loosely to refer to primitive cells or to the first cells. Here we will use the term protocell to refer specifically to cell-like structures that are spatially delimited by a growing membrane boundary, and that contain replicating genetic information. A protocell differs from a true cell in that the evolution of genomically encoded advantageous functions has not yet occurred. With a genetic material such as RNA (or perhaps one of many other heteropolymers that could provide both heredity and function) and an appropriate

environment, the continued replication of a population of protocells will lead inevitably to the spontaneous emergence of new coded functions by the classical mechanism of evolution through variation and natural selection. Once such genomically encoded and therefore heritable functions have evolved, we would consider the system to be a complete, living biological cell, albeit one much simpler than any modern cell (Szostak et al., 2001).

Membranes as compartment boundaries. All biological cells are membrane-bound compartments. The cell membrane fulfills the essential function of creating an internal environment within which genetic materials can reside and metabolic activities can take place without being lost to the environment. Modern cell membranes are composed of complex mixtures of amphiphilic molecules such as phospholipids, sterols, and many other lipids as well as diverse proteins that perform transport and enzymatic functions. Phospholipid membranes are stable under a wide range of temperature, pH, and salt concentration conditions. Such membranes are extremely good permeability barriers, so that modern cells have complete control over the uptake of nutrients and the export of wastes through the specialized channel, pump and pore proteins embedded in their membranes. A great deal of complex biochemical machinery is also required to mediate the growth and division of the cell membrane during the cell cycle. The question of how a structurally simple protocell could accomplish these essential membrane functions is a critical aspect of understanding the origin of cellular life.

Vesicles formed by fatty acids have long been studied as models of protocell membranes (Gebicki and Hicks, 1973; Hargreaves and Deamer, 1978; Walde et al., 1994a). Fatty acids are attractive as the fundamental building block of prebiotic membranes in that they are chemically

simpler than phospholipids. Fatty acids with a saturated acyl chain are extremely stable compounds and therefore might have accumulated to significant levels, even given a relatively slow or episodic synthesis. Moreover, the condensation of fatty acids with glycerol to yield the corresponding glycerol esters provides a highly stabilizing membrane component (Monnard et al., 2002). Finally, phosphorylation and the addition of a second acyl chain yields phosphatidic acid, the simplest phospholipid, thus providing a conceptually simple pathway for the transition from primitive to more modern membranes.

The best reason for considering fatty acids as fundamental to the nature of primitive cell membranes is not, however, their chemical simplicity. Rather, fatty acid molecules in membranes have dynamic properties that are essential for both membrane growth and permeability. Because fatty acids are single chain amphiphiles with less hydrophobic surface area than phospholipids, they assemble into membranes only at much higher concentrations. This equilibrium property is mirrored in their kinetics: fatty acids are not as firmly anchored within the membrane as phospholipids; they enter and leave the membrane on a time scale of seconds to minutes (Chen and Szostak 2004). Fatty acids can also exchange between the two leaflets of a bilayer membrane on a sub-second time scale. Rapid flip-flop is essential for membrane growth when new amphiphilic molecules are supplied from the environment. New molecules enter the membrane primarily from the outside leaflet, and flip-flop allows the inner and outer leaflet areas to equilibrate, leading to uniform growth.

Considering that protocells on the early Earth did not, by definition, contain any complex biological machinery, they must have relied on the intrinsic permeability properties of their

membranes. Membranes composed of fatty acids are in fact reasonably permeable to small polar molecules and even to charged species such as ions and nucleotides (Mansy et al., 2008). This appears to be largely a result of the ability of fatty acids to form transient defect structures and/or transient complexes with charged solutes, which facilitate transport across the membrane.

Prebiotic vesicles were almost certainly composed of complex mixtures of amphiphiles. Amphiphilic molecules isolated from meteorites (Deamer, 1985; Deamer and Pashley, 1989) as well as those synthesized under simulated prebiotic conditions (McCollum et al., 1999; Dworkin et al., 2001; Rushdi and Simoneit, 2001) are highly heterogeneous, both in terms of acyl chain length and head group chemistry. Membranes composed of mixtures of amphiphiles often have superior properties to those composed of single pure species. For example, mixtures of fatty acids together with the corresponding alcohols and/or glycerol esters generate vesicles that are stable over a wider range of pH and ionic conditions (Monnard et al., 2002), and are more permeable to nutrient molecules including ions, sugars and nucleotides (Chen et al., 2004; Sacerdote and Szostak, 2005; Mansy et al., 2008). This is in striking contrast to the apparent requirement for homogeneity in the nucleic acids, where even low levels of modified nucleotides can be de-stabilizing or can block replication.

Recent Results

Pathways for vesicle growth. Fatty acid vesicle growth has been shown to occur through at least two distinct pathways: growth through the incorporation of fatty acids from added micelles, and growth through fatty acid exchange between vesicles. The growth of membrane vesicles from micelles has been observed following the addition of micelles or fatty acid precursors to pre-formed vesicles (Walde et al., 1994a; Walde et al., 1994b; Berclaz et al., 2001). When initially alkaline fatty acid micelles are mixed with a buffered solution at a lower pH, the micelles become thermodynamically unstable. As a consequence, the fatty acid molecules can either be incorporated into pre-existing membranes, leading to growth (Berclaz et al., 2001), or can self-assemble into new vesicles (Blochliger et al., 1998; Luisi et al., 2004). These pioneering studies were done by cryo-TEM, which does not allow growth to be followed in real time, and by light scattering, which is difficult to interpret in the case of samples with heterogeneous size distributions. We therefore adapted a fluorescence assay based on FRET (Förster resonance energy transfer) to measure changes in membrane area in real time. This assay is based on the distance dependence of energy transfer between donor and acceptor fluorescent dyes; thus when a membrane grows in area by incorporating additional fatty acid molecules, the dyes are diluted and the efficiency of FRET decreases. Studies on small (typically 100 nm in diameter) unilamellar fatty acid vesicles using this assay showed that the slow addition of fatty acid micelles led to vesicle growth with an efficiency of ~90% (Hanczyc et al., 2003).

The real-time FRET assay allowed for a kinetic dissection of the growth process, revealing a surprisingly complex series of events after the rapid addition of micelles (Chen and Szostak, 2004). Two major processes were observed. The first fast phase resulted in membrane area

growth that was limited to ~40% increase in area, independent of the amount of added micelles. A second much slower phase led to a further increase in membrane area that varied with the amount of added micelles. We interpreted the fast phase as reflecting the rapid assembly of a layer of adhering micelles around the pre-formed vesicles, with rapid monomer exchange resulting in the efficient incorporation of this material into the pre-formed membrane. We interpreted the slow phase as the consequence of micelle-micelle interactions leading to the assembly of intermediate structures that could partition between two pathways - with some monomers dissociating and contributing to membrane growth and the remainder ultimately assembling into new membrane vesicles. Although these interpretations are consistent with our data, the experiments are rather indirect, and further exploration of the mechanism of membrane growth is certainly desirable.

A second, distinct pathway for vesicle growth involves fatty acid exchange between vesicles. Under certain conditions this exchange can lead to growth of a sub-population of vesicles at the expense of their surrounding neighbors. Within populations of osmotically relaxed vesicles, such exchange processes do not result in significant changes in size distribution with time. Similarly, a population of uniformly osmotically swollen vesicles does not change in size distribution, but such vesicles are in equilibrium with a lower solution concentration of fatty acids because the tension in the membrane of the swollen vesicles makes it more energetically favorable for fatty acid molecules to reside in membrane. When osmotically swollen vesicles are mixed with osmotically relaxed (isotonic) vesicles, rapid fatty acid exchange processes result in growth of the swollen vesicles and corresponding shrinkage of the relaxed vesicles (Chen et al., 2004). Since vesicles can be osmotically swollen as a result of the encapsulation of high concentrations

of nucleic acids such as RNA, this process allows for the growth of vesicles containing genetic polymers at the expense of empty vesicles (or vesicles that contain less internal nucleic acid). Because faster replication would increase the internal nucleic acid concentration, this pathway of competitive vesicle growth provides the potential for a direct physical link between the rate of replication of an encapsulated genetic polymer and the rate of growth of the protocell as a whole.

Assuming that the division of osmotically swollen vesicles could occur either stochastically or at some threshold size, protocells that developed some heritable means of faster replication and growth would have a shorter cell cycle, on average, and would therefore gradually take over the population. This simple physical mechanism might therefore lead to the emergence of Darwinian evolution by competition at the cellular level. However, if replication is limited by the rapid reannealing of complementary strands (see below), it may be difficult to reach osmotically significant concentrations. Furthermore, osmotically swollen vesicles are intrinsically difficult to divide owing to the energetic cost of reducing the volume of a spherical vesicle to that of two daughter vesicles of the same total surface area. One possibility is that osmotically driven competitive growth might alternate with the faster membrane growth that follows micelle addition. If new fatty acid material was only available sporadically, rapid membrane growth might follow an influx of fresh fatty acids, facilitating division (see below).

All of the experiments discussed above were done with small unilamellar vesicles prepared by extrusion through 100 nm pores in filters. In contrast, fatty acid vesicles that form spontaneously by rehydrating dry fatty acid films tend to be several microns in diameter and multilamellar (Hargreaves and Deamer, 1978; Hanczyc et al., 2003). Such large multilamellar

fatty acid vesicles are so heterogeneous that quantitative studies of growth and division are difficult. We have recently developed a simple procedure for the preparation of micron-sized, monodisperse (homogeneous in size) multilamellar vesicles by large-pore dialysis (Zhu and Szostak, 2009b). The preparation of large monodisperse multilamellar vesicles has allowed us to directly observe an unusual mode of vesicle growth (Zhu and Szostak, 2009a). We showed that feeding a micron-sized multilamellar fatty acid vesicle with fatty acid micelles results in the formation of a thin membranous protrusion which extends from the side of the initially spherical parental vesicle. Over time, this thin membrane tubule elongates and thickens, gradually incorporating more and more of the parental vesicle, until eventually the entire vesicle is transformed into a long, hollow thread-like vesicle (Figure I.2). This pathway occurs with vesicles ranging in size from 1 to at least 10 μm in diameter, composed of a variety of different fatty acids and related amphiphiles. Only multilamellar vesicles grow in this manner and only when vesicle volume increases slowly (relative to surface area growth) due to a relatively impermeable buffer solute. Confocal microscopy has provided insight into the mechanism of this mode of growth: the outermost membrane layer grows first, and because there is little volume between it and the next membrane layer, and that volume cannot increase on the same time scale, the extra membrane area is forced into the form of a thin tubule. Over time, this tubule grows, and as a result of poorly understood exchange processes, the entire original vesicle is ultimately transformed into a long thread-like hollow vesicle (Figure I.3).

Pathways for vesicle division. Vesicle division by the extrusion of large vesicles through small pores is a way in which mechanical energy can be used to drive division (Hanczyc et al., 2003). Vesicle growth by micelle feeding followed by division by extrusion can be carried out

repetitively, resulting in cycles of growth and division in which both membrane material and vesicle contents are distributed to daughter vesicles in each cycle. However, division by extrusion results in the loss of 30-40% of the encapsulated vesicle contents to the environment during each cycle (Hanczyc et al., 2003; Hanczyc and Szostak, 2004). Most of this loss is a result of the unavoidable geometric constraint of dividing a spherical vesicle into two spherical (or sub-spherical) daughter vesicles with conservation of surface area; some additional loss may occur as a result of pressure-induced membrane rupture. Although extrusion is a useful laboratory model for vesicle division, an analogous extrusion process appears unlikely to occur in a prebiotic scenario on the early Earth because vesicle extrusion from the flow of suspended vesicles through a porous rock would require both the absence of any large pores or channels and a very high pressure gradient (Zhu and Szostak, 2009a).

The above problems stimulated a search for a more realistic pathway for vesicle division. The possible spontaneous division of small unilamellar vesicles after micelle addition has been reported (Luisi et al., 2004; Luisi, 2006), and electron microscopy has revealed structures that are possible intermediates in growth and division, notably pairs of vesicles joined by a shared wall (Stano et al., 2006). However, the mechanism of the proposed division as well as the nature of the energetic driving force remain unclear. Additional studies are required to clearly distinguish between the vesicle-stimulated assembly of new vesicles, and the more biologically relevant processes of growth and division.

We have recently found that the growth of large multilamellar vesicles into long thread-like vesicles, described above, provides a pathway for coupled vesicle growth and division (Zhu and

Szostak, 2009a). The long thread-like vesicles are extremely fragile, and divide spontaneously into multiple daughter vesicles in response to modest shear forces. In an environment of gentle shear, growth and division become coupled processes since only the filamentous vesicles can divide (Figure I.3). If the initial parental vesicle contains encapsulated genetic polymers such as RNA, these molecules are distributed randomly to the daughter vesicles and are thus inherited. The robustness and simplicity of this pathway suggests that similar processes might have occurred under prebiotic conditions. The mechanistic details of this mode of division remain unclear. One possibility, supported by some microscopic observations, is that the long thin membrane tubules are subject to the “pearling instability” (Bar-Ziv and Moses, 1994), and minimize their surface energy by spontaneously transforming from a cylindrical shape to a string of beads morphology. The very thin tether joining adjacent spherical beads may be a weak point that can be easily disrupted by shear forces.

RNA-catalyzed RNA replication on the early Earth and the modern laboratory. A core assumption of the RNA world hypothesis is that the RNA genomes of primitive cells were replicated by a ribozyme RNA polymerase (Gilbert, 1986). The idea of RNA-catalyzed RNA replication provides a solution to the apparent paradox of DNA replication catalyzed by proteins that are encoded by DNA. This simplification of early biochemistry gained instant plausibility from the discovery of catalytic RNAs almost 30 years ago (Kruger et al., 1982; Guerrier-Takada et al., 1983). In the time after the discovery of the first ribozymes, the RNA World hypothesis has continued to gain support, most dramatically from the discovery that the ribosome is a ribozyme (Nissen et al., 2000), and that all proteins are assembled through the catalytic activity of the ribosomal RNA. Support has also come from the *in vitro* evolution of a wide range of new

ribozymes, including *bona fide* RNA polymerases made of RNA (Johnston et al., 2001). On the other hand, no ribozyme polymerase yet comes close to being a self-replicating RNA, like the replicase envisaged as the core of the RNA World biochemistry.

Why has the *in vitro* evolution of an RNA replicase been so much more difficult than originally expected? It is clear that the problem is not with catalysis of the chemical step, even with catalytically demanding triphosphate substrates. Evolutionarily optimized versions of the Class I ligase carry out multiple-turnover ligation reactions at $> 1 \text{ s}^{-1}$, with over 50,000 turnovers overnight (Ekland et al., 1995), and optimized versions of the smaller, simpler DSL ligase carry out sustained multiple turnover ligation reactions at rates $> 1 \text{ min}^{-1}$ (Voytek and Joyce, 2007). These catalytic rates are more than sufficient to carry out the replication of a 100-200 nt ribozyme in minutes to hours, if these rates could be maintained in the context of a polymerase reaction using monomer substrates. However, even the best available polymerase ribozyme requires 1-2 days to copy 10-20 nucleotides of a template strand, apparently as a consequence of poor binding to both the ribonucleoside triphosphate (NTP) monomers and the primer-template substrate. The need to overcome the electrostatic repulsion between negatively charged NTP and RNA substrates and ribozyme is thought to contribute to the very high Mg^{2+} requirement for the polymerase ribozyme (Glasner et al., 2000). Such high levels of Mg^{2+} lead to hydrolytic degradation of the ribozyme, and are also not compatible with known fatty acid based membranes due to crystallization of the fatty acid - magnesium salt. In addition, fatty acid membranes are almost impermeable to NTPs (Mansy et al., 2008).

The incompatibility between currently available ribozyme polymerases and fatty acid based vesicles suggests either that early replicases were quite different, or that RNA replication in early cells proceeded in a very different manner. For example, less charged and more activated nucleotides might be easier for a ribozyme polymerase to bind, with little or no Mg^{2+} . Many potential leaving groups, such as imidazole, adenine or 1-Me-adenine have been examined in template-directed and non-templated polymerization reactions, but have not yet been tested as substrates for ribozyme polymerases (Prabakar and Ferris, 1997; Huang and Ferris, 2006). The tethering of ribozyme and primer-template to hydrophobic aggregates has been examined as a way of increasing local substrate concentration (Müller and Bartel, 2008). However, this approach did not lead to a dramatic improvement in the extent of template copying, apparently as a result of ribozyme inhibition at high effective RNA concentrations. It may be possible to evolve polymerases that operate well at high RNA concentrations, but membrane localization by chemical derivatization adds further complexity to a replication pathway due to the need for a specific catalyst for the derivatization step. Alternative means of facilitating the interaction of a ribozyme with a primer-template substrate, such as the presence of basic peptides or other cofactors, might overcome this problem. Finally it is noteworthy that very small self-aminoacylating ribozymes have been obtained using RNA libraries that have an unconstrained sequence at their 3'-end (Chumachenko et al., 2009). This strategy may also be fruitful in selections for ribozyme polymerases.

Given the above constraints and uncertainties, what can we say about the emergence of RNA-catalyzed RNA replication in the origin of life? It is still possible that under the proper conditions, and using the right substrates, a small simple ribozyme could effectively catalyze

RNA replication. However, a replicase must do more than catalyze a simple phospho-transfer reaction. Binding in a non-sequence-specific manner to a primer-template complex, facilitating binding of the proper incoming monomer, catalyzing primer extension, and repeating this process until the end of the template (or set of templates for a mutli-component replicase) is reached might require a complex replicase structure. Such a replicase would presumably be rare in collections of random RNA sequences. If life required a very special sequence to get started, then the origin of life on earth could have been a low probability event and life on other earth-like planets might be very rare. If, on the other hand, RNA-catalyzed RNA replication could have emerged gradually in a series of simpler steps, it might have been easier and thus more likely for life to begin, and life elsewhere might be common. For this reason, we now turn to a consideration of non-enzymatic template-directed replication chemistry.

Chemical template replication revisited. The non-enzymatic template-directed polymerization of activated ribonucleotides was studied in depth by Leslie Orgel, together with his students and colleagues, over a period of several decades (Orgel, 2004). Here, the template itself acts as a catalyst by helping to align and orient the monomers so that they are pre-organized for polymerization. The main lesson from this work is that spontaneous chemical copying of RNA sequences is indeed possible, but is subject to several important constraints and limitations. The constraints make template-directed RNA copying incompatible with currently available membrane vesicle systems, and the limitations have, so far at least, made it impossible to obtain repeated cycles of RNA replication through chemical copying.

In order to obtain reasonable reaction rates, Orgel made use of nucleoside monophosphates activated with a good leaving group such as imidazole. The ribonucleotide 5'-phosphorimidazolides spontaneously assemble on a template oligonucleotide and polymerize over several days, generating a complementary strand. However, monomer binding to RNA templates is weak and concentrations on the order of 0.1 M were required for optimal copying. In addition, a Mg^{2+} concentration of ~ 0.1 M, which as noted above is incompatible with the presence of fatty acid based membranes, is required for optimal polymerization. Even under these rather extreme conditions, polymerization proceeds at only 1-2 nucleotides per day, and is therefore limited by monomer hydrolysis. Beyond these constraints, three aspects of the copying reaction present major hurdles to multiple rounds of replication. First, the chemical structure of RNA results in a problem of regiospecificity, since new linkages can be either 3'-5' or 2'-5' phosphodiester bonds. Surprisingly, under most conditions, it is the 2'-5' phosphodiester bonds that are most common in polymerization products. This problem can be ameliorated by the choice of ions and leaving groups; for unknown reasons, Zn^{2+} ions and the 2-methylimidazole leaving group favor the synthesis of 3'-5' linkages (Lohrmann et al., 1980; Inoue and Orgel, 1982). Studies of oligonucleotide ligation showed that the helical context of an extended RNA duplex also favors the formation of 3'-5' linkages (Rohatgi et al., 1996). However, it remains difficult to obtain a homogeneous RNA backbone without enzymatic catalysis. Second, adenine (A) residues in the template are difficult to copy, and two or more As in succession block chain growth (Inoue and Orgel, 1983), presumably as a result of the poor base-stacking propensity of the incoming U monomers. It has recently been found that template copying at subzero temperatures can proceed past multiple A residues in the template (Vogel and Richert, 2007), but this required sequential additions of oxyazabenzotriazole-activated monomer together with a

series of helper oligos. Third, there is the issue of fidelity. The copying of G and C residues is remarkably accurate, with error rates estimated at 0.5% or less. However, the addition of A and U residues causes problems, most significantly the formation of G:U wobble base-pairs (Wu and Orgel, 1992), which would lead to significant error rates in a four base system. Might an alternative genetic polymer, perhaps even a close relative of RNA, overcome these problems and enable chemical replication? The identification of such a system might ultimately lead to the discovery of plausible progenitors of RNA, or, alternatively, to the discovery of new replication strategies that allow for the chemical replication of RNA itself.

Phosphoramidate nucleic acids. Early studies of template copying using more reactive nucleotide derivatives were carried out by Orgel et al., who examined both 2'- and 3'-amino ribonucleotide 5'-phosphorimidazolides (Lohrmann and Orgel, 1976; Zielinski and Orgel, 1985; Tohidi et al., 1987). Polymerization of these nucleotides yields phosphoramidate nucleic acids, which are generally similar to standard phosphodiester linked nucleic acids except that the phosphoramidate linkage is more acid labile. As expected, replacing a sugar hydroxyl in the monomer with a more nucleophilic amino group resulted in a large increase in monomer reactivity. The activated 3'-amino ribonucleotides participated in rapid copying of short oligonucleotide templates 5-13 nucleotides in length, yielding N3'→P5' linked complementary oligonucleotides (Tohidi et al., 1987). The increased reactivity also led to faster intramolecular monomer cyclization, which depleted the template copying reactions of activated substrate molecules (Hill et al., 1988).

More recently, the Richert group has begun to explore the potential of 3'-amino-nucleotide analogues in template-directed condensation reactions. Deoxyribonucleotide monomers, activated with an oxyazabenzotriazole leaving group, completed a template-directed reaction with a 3'-amino-terminated primer in seconds (Rothlingshofer et al., 2008). The fidelity of this reaction is sufficient to allow for sequencing by non-enzymatic primer extension. However, the monomer is rapidly consumed by internal cyclization.

The high intrinsic reactivity of the amino-sugar modified nucleotides suggested to us that an alternative phosphoramidate nucleic acid might act as a good platform for chemical self-replication. Our group has therefore started to study a series of phosphoramidate nucleic acids with sugar phosphate backbones that vary in their degree of conformational flexibility or constraint. We are currently focusing on the 2'-5' linked phosphoramidate analog of DNA, and the corresponding monomers, the 2'-amino dideoxyribonucleotide 5'-phosphorimidazolides (Figure I.4). The 2'-amino ImpddNs are advantageous as monomers because they cannot undergo intramolecular cyclization due to the steric constraint of the ribose ring; they are only depleted during polymerization reactions by competing hydrolysis.

Our first experiments with 2'-amino ImpddG led to rapid and efficient primer-extension across a dC₁₅ template, generating full-length product in ~6 hours (Mansy et al., 2008). Encouraged by the rapid copying of oligo-dC templates by 2'-amino ImpddG, we carried out a more extensive study of the copying of templates with differing sugar-phosphate backbones, lengths and sequences (Schrum et al., 2009). The most important property contributing to good template activity appears to be pre-organization in the form of an A-type helix. Thus, RNA

templates were uniformly superior to DNA templates of the same sequence, and LNA (locked nucleic acid) templates, which are chemically locked in a C3'-endo sugar conformation, were superior to RNA templates. This result is consistent with previous observations that under most conditions RNA-template directed polymerization of ribonucleotides leads to a majority of 2'-5' linkages; it appears that an A-type helical geometry generally favors polymerization through attack by a 2' nucleophile. A second key factor is that enhanced monomer affinity for the template increases the reaction efficiency. Thus G:C base-pairs lead to efficient copying, whereas A:U base-pairs were very poorly copied. Replacing A with D (diaminopurine) results in a D:U base-pair with three hydrogen bonds, and slightly improved primer-extension. However, the poor base stacking of U residues must also be improved in order to obtain efficient template copying. When we replaced U with C5-propynyl-U, the resulting A:U^p base-pairs led to improved copying, but the D:U^p combination had a clearly synergistic effect (Figure I.5). In the context of a DNA duplex, the D:U^p base-pair has previously been shown to be energetically almost equivalent to a C:G base-pair (Chaput et al., 2002). When we used G, C, D and U^p as the four monomer and template bases, we were able to copy mixed-sequence RNA templates over 15 nts in length in about a day. This represents a significant step towards developing a robust, generalized chemical replication system.

This system is, however, far from ideal, and there are strong indications that the fidelity of template copying becomes an issue when all four nucleotides are present, largely due to the formation of G:U wobble base-pairs. Given that primer-extension on 2'-5' linked DNA templates is approximately similar to that on the corresponding RNA templates, we are currently synthesizing 2'-5' linked phosphoramidate DNA templates to assess self-replication in this

system. In light of the efficient templating of LNA oligonucleotides, we are also interested in exploring prebiotically plausible nucleic acids that are more conformationally constrained than RNA. A particularly interesting candidate is TNA (threose nucleic acid) (Schöning et al., 2000) and its 2'-amino substituted phosphoramidate version, NP-TNA (Wu et al., 2002). These are both base-pairing systems that form standard Watson-Crick duplexes, despite having only 5 atoms per backbone repeat unit (vs. 6 for RNA and DNA). It will be of great interest to see if the resulting decrease in flexibility leads to increased fidelity in template copying reactions.

Protocell assembly. In principle, protocell-like objects could form spontaneously as new membranes self-assemble and encapsulate genetic molecules in solution. Recently, simple physical processes that would enhance the efficiency of the co-assembly of nucleic acids and membrane vesicles have been proposed. One such alternative scenario is based on the fact that the clay mineral montmorillonite is not only a catalyst of RNA polymerization (Ferris et al., 1996; Huang and Ferris, 2006) but also catalyzes membrane assembly (Hanczyc et al., 2003). Experiments with clay particles containing surface-adsorbed RNA showed that such particles stimulated vesicle assembly, and frequently became trapped inside the vesicles whose assembly they had catalyzed. Thus, a common mineral can catalyze both the assembly of a genetic polymer and the assembly of a membrane vesicle, and bring these two components together to generate a protocell-like structure consisting of a genetic polymer trapped within a membrane compartment. While the effectiveness of this process is attractive, some means of releasing at least some of the bound nucleic acid from the mineral surface, and/or replicating it on the surface, would be necessary for subsequent replication to occur.

More recent experiments suggest a very different geochemical scenario leading to the assembly of similar protocell-like structures. The hollow channels within the rocks of the alkaline off-axis hydrothermal vents provide a protected compartmentalized environment where it has been suggested that primitive metabolic activities might have originated (Martin and Russell, 2003). Recent theoretical studies suggested that the strong thermal gradients present in hydrothermal vents, together with the thin channels produced by mineral precipitation, could greatly concentrate small organic molecules such as nucleotides as well as larger nucleic acids from a very dilute external reservoir (Baaske et al., 2007). Work from our laboratory (Budin et al., 2009) has confirmed the predicted concentration effect, and has also shown that sub-critical concentrations of fatty acids can be concentrated to the extent that they self-assemble into vesicles at the bottom of the capillary channels. Moreover, DNA oligonucleotides can also be greatly concentrated and can become encapsulated within the vesicles, resulting in the spontaneous assembly of protocell-like structures.

Encapsulated template replication: emergence of a protocell. The experiments discussed above suggest that the assembly of protocell-like structures is not that difficult, since it appears to be possible through multiple distinct mechanisms. The more challenging question is, how could such a structure replicate? We have already considered the replication of the protocell membrane and the genetic material as separate entities. To address the question of their replication as a combined structure we must consider in more detail the molecular constituents of the protocell membrane and the molecular nature of the encapsulated genetic material.

Genome replication within a protocell can only occur if the building blocks used to copy template strands are able to enter the fatty acid vesicle compartment. Early work using phospholipid-based vesicles and protein enzymes demonstrated the feasibility of constructing primitive cell-like compartments (Chakrabarti et al., 1994; Luisi et al., 1994). More recent permeability studies showed that nucleotides could spontaneously diffuse across simple fatty acid membranes, but that net negative charge is a critical determinant of permeability. Thus, nucleotides that are chemically activated, e.g. by conversion of the 5'-phosphate to a 5'-phosphorimidazolidine, equilibrate across vesicle membranes much more rapidly on account of the reduction of the net negative charge. In addition, mixtures of fatty acids with their glycerol esters generate membranes that are more permeable to polar and charged molecules. By combining these observations, we were able to show that activated 2'-amino-2',3'-dideoxyguanosine-5'-phosphorimidazolidine, the same nucleotide previously shown to rapidly copy oligo-dC templates, could be added to the outside of fatty acid vesicles containing an encapsulated primer-template complex, and copy the internal dC₁₅ template. Copying of the encapsulated dC₁₅ template by primer-extension reached >95% completion in 12-24 hours (Mansy et al., 2008), compared to 6-12 hours in free solution. The longer time required for copying encapsulated templates reflects the time required for entry of external nucleotides to the interior of the vesicles. Importantly, the presence of high concentrations (5-10 mM) of highly reactive activated nucleotides did not have any disruptive effects on the integrity of the vesicle membrane, as no leakage of encapsulated primer-template complexes was observed. It is also important to note that control experiments with phospholipid membranes showed no copying of internal template, because the activated nucleotides could not enter the vesicle; similarly, "modern" activated nucleotides such as nucleoside triphosphates cannot cross fatty acid based membranes. Successful copying of

encapsulated templates therefore requires both “primitive” nucleotides with reduced charge, and “primitive” membranes composed of single chain amphiphiles.

The copying of a genetic polymer inside a membrane compartment is an important step toward the realization of a self-replicating system capable of Darwinian evolution. What, then, are the remaining barriers to the assembly of such a system? The copying of a single-stranded template produces a double-stranded product; these strands would have to separate before a second cycle of genome replication could begin. Separate follow up experiments by our group demonstrated that some fatty acid based vesicles are able to retain encapsulated DNA and RNA oligonucleotides over a temperature range of 0 °C to 100 °C (Mansy and Szostak, 2008). As with permeability, mixtures of amphiphiles lead to improved thermostability, with glycerol esters being particularly stabilizing, possibly due to the additional hydrogen bond donors and acceptors provided by the glycerol head group. Furthermore, we found that encapsulated double-stranded DNA could be denatured at elevated temperatures, with the strands reannealing once the temperature was lowered (Mansy and Szostak, 2008). This implies that thermal fluctuations could provide a mechanism for strand separation that is compatible with the integrity of fatty acid vesicles, potentially allowing for complete cycles of replication of encapsulated genetic polymers. The mutual compatibility of nucleic acid replication and fatty acid compartment growth is very encouraging because it alleviates concerns related to the permeability and stability of membrane vesicles. Vesicles therefore do seem to be a physically plausible way to segregate and spatially localize genomes, keep emergent catalytic polynucleotides physically close to their encoding genome, and protect the nascent evolving system from parasitic polymers.

Challenges and Future Directions

Prospects for a complete protocell model. Although considerable progress has been made toward the assembly of model protocells, several remaining issues must be solved before multiple cycles of protocell replication can be achieved in the laboratory. These factors are also relevant to protocell replication on the early Earth. The most important factor at this time appears to be the competition between strand reannealing and strand copying, after thermal strand separation. PCR reactions generally plateau at about 1 μM DNA strand concentration, which is the concentration at which strand reannealing and strand copying occur on a similar time scale of about 1 minute. However, non-enzymatic template copying requires on the order of a day for completion, which implies that either template copying must be much faster, or reannealing must be much slower. One way to make reannealing sufficiently slow is to keep strand concentrations sub-nanomolar. Low strand concentrations are possible in large vesicles, but it is hard to see how a few molecules of a genetic polymer could have any significant phenotypic effect on a large vesicle composed of millions of amphiphilic molecules. The emergence of metabolic ribozymes would be more plausible if nucleic acid strand concentrations were much higher, so that a catalyst of modest efficiency could generate enough product to influence cell properties.

What other factors might affect the rate of strand reannealing? Perhaps the most obvious possibility is that secondary structure, which can form extremely rapidly since the interactions are intramolecular, could greatly slow down strand annealing. This phenomenon is essential to the viability of single-stranded RNA phage such as Q β (Axelrod et al., 1991). Significant intra-strand secondary structure would also be an expected consequence of selection for sequences that fold into functional shapes with catalytic activity. On the other hand, chemical replication

through dense secondary structure would probably be much slower than replication of an unfolded, open template. The outcome of simultaneous selection for an open, accessible template sequence, and a folded functional structure remains unclear. An alternative but even more speculative solution might result from the rapid binding by base-pairing of short oligonucleotides or even monomers to freshly separated strands. If a template strand was largely occupied by monomers or short oligomers, even if these were in rapid exchange, the strand might be prevented from annealing to a complementary strand. This possibility has the advantage that it need not block or slow the copying reaction, however its effectiveness remains to be tested experimentally.

Another challenge faced by replicating protocells, whether on the early earth or in the modern laboratory, is the continuous dilution of protocells through the competing formation of new empty vesicles. When new fatty acids are supplied as micelles, the efficiency of incorporation into pre-formed vesicles (or protocells) can be quite high, but some new vesicles are always formed. Thus over time, the descendants of a given protocell will gradually be diluted out by the continuous formation of these new vesicles. In order to avoid extinction by dilution, the protocells must out-compete other vesicles either by having a more rapid cell cycle, thereby generating more progeny during division, or by surviving destructive processes more efficiently. We have previously proposed (Chen et al., 2004) that faster growth, driven by the osmotic pressure of encapsulated nucleic acid, could lead to an effectively shorter cell cycle for protocells that contain high copy numbers of their replicating genome. However, in light of the problems associated with this approach, it is of considerable interest to explore new ways in which a protocell genome could lead to faster growth or growth that occurs at the expense of empty

vesicles. An alternative strategy for surviving dilution would be for a protocell genome to colonize empty vesicles. This could occur through a low level of stochastic vesicle-vesicle fusion events, possibly catalyzed by low levels of divalent cations such as Ca^{2+} . Systematic efforts to measure vesicle fusion frequencies under different environmental conditions could therefore be quite useful. Finally, it is possible that this problem could be circumvented entirely if early life was discontinuous (Budin et al., 2009). For example, protocells could be occasionally disrupted by drying, or simply dissolve as a result of dilution with water to a level below the critical aggregate concentration; subsequent re-hydration or concentration would result in reformation of vesicles encapsulating genomic nucleic acids, thus generating a new “randomized” set of protocells. As long as such events were fairly uncommon, and assuming that genomic replication had kept ahead of vesicle replication so that each vesicle contained multiple genome copies prior to disruption, this process of disruption and reformation would lead to the spread of evolving genomic sequences through the “new” vesicles.

Laboratory models of protocell systems should be helpful in modeling many of the above scenarios. Assuming that protocell reproduction can be achieved, and made efficient enough to continue through many generations, it should then be possible to observe the spontaneous evolution of adaptive innovations in this relatively simple chemical system. The nature of such adaptations may provide clues as to how modern cells evolved from their earliest ancestors. Ultimately this line of research may also tell us whether the conserved biochemistry of life is driven by chemical necessity, or whether biochemically very different forms of life are also possible.

Figures

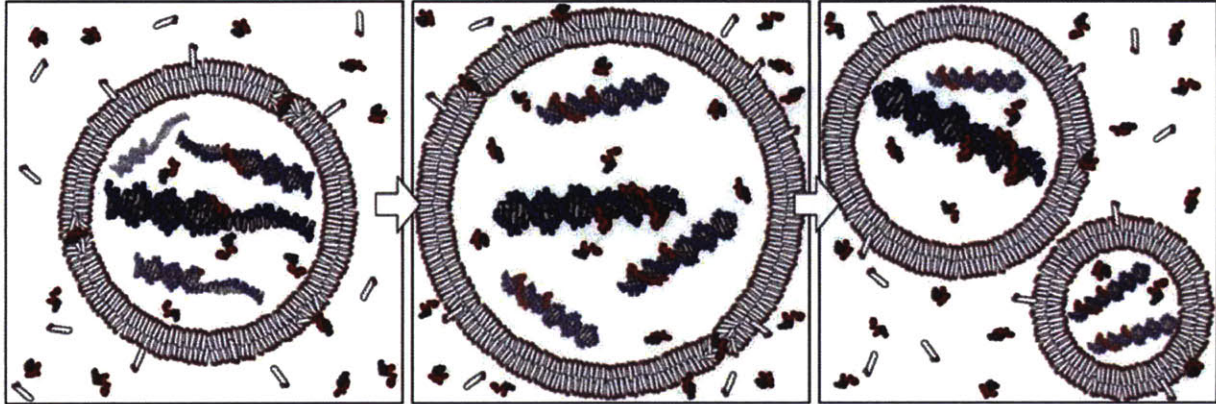


Figure I.1 A simple protocell model. A replicating vesicle for compartmentalization, and a replicating genome to encode heritable information. A complex environment provides lipids, nucleotides capable of equilibrating across the membrane bilayer, and sources of energy (left), which leads to subsequent replication of the genetic material and growth of the protocell (middle), and finally protocellular division through physical and chemical processes (right).

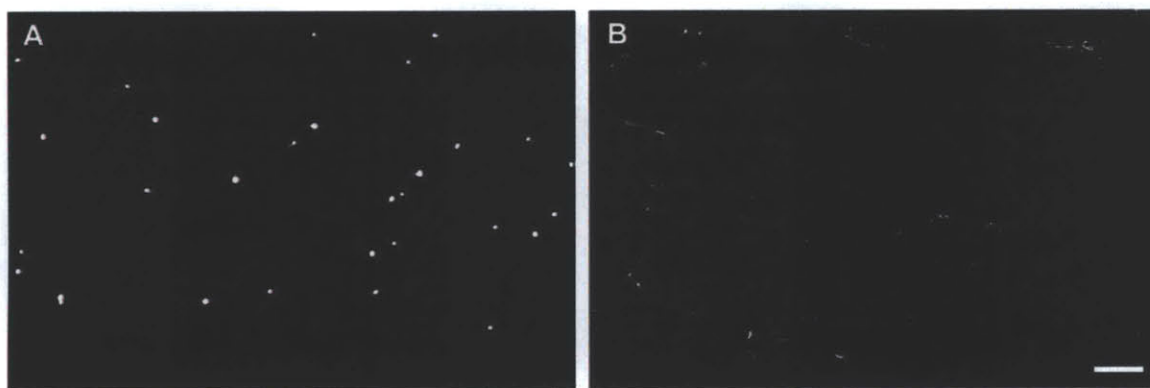


Figure I.2 Vesicle shape transformations during growth. All vesicles are labeled with 2 mM encapsulated HPTS, a water-soluble fluorescent dye, in their internal aqueous space. (A) 10 min and (B) 30 min after the addition of 5 equivalents of oleate micelles to oleate vesicles (in 0.2 M Na-bicine, pH 8.5). Scale bar, 50 μm .

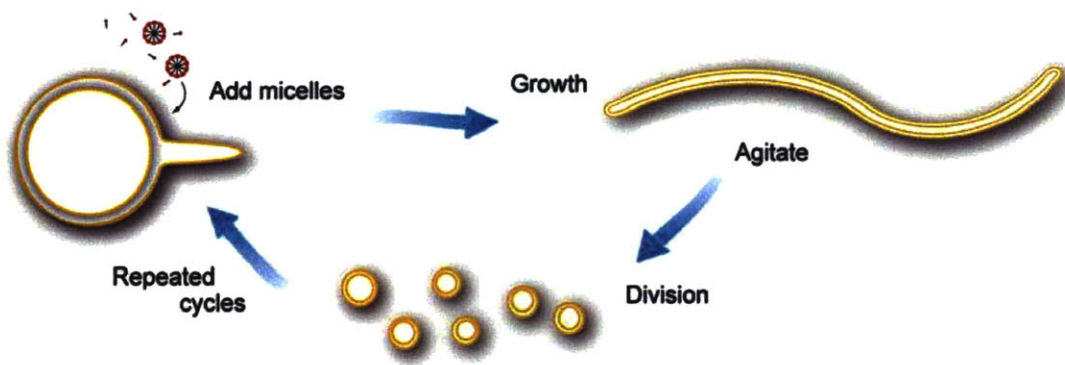


Figure I.3 Schematic diagram of coupled vesicle growth and division.

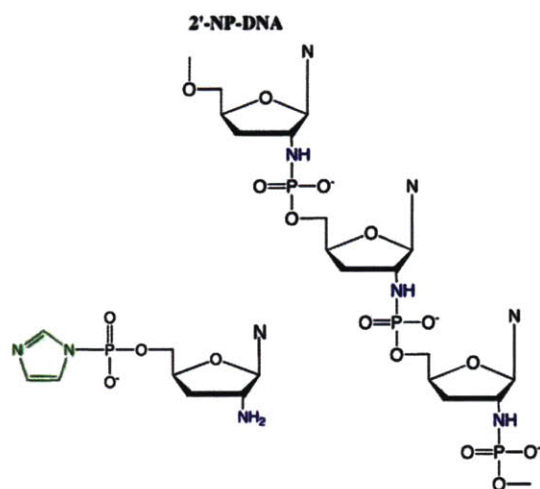


Figure I.4 2'-5' phosphoramidate DNA. Structures of 2'-5' phosphoramidate DNA, and the corresponding activated monomers.

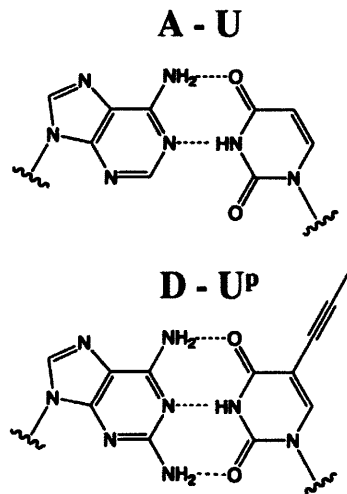


Figure I.5 Watson Crick base-pairs. Top: standard A:U base-pair. Bottom: alternative diaminopurine. (D):C5-propynyl-uracil (U^P) base-pair.

References

- Axelrod, V. D., Brown, E., Priano C., Mills, D. R. (1991). Coliphage Q beta RNA replication, RNA catalytic for single-strand release. *Virology* *184*, 595-608.
- Baaske, P., Weinert, F. M., Duhr, S., Lemke, K. H., Russell, M. J., and Braun, D. (2007). Extreme accumulation of nucleotides in simulated hydrothermal pore systems. *Proc Natl Acad Sci U S A* *104*, 9346-9351.
- Bar-Ziv, R. and Moses, E. (1994). Instability and "pearling" states produced in tubular membranes by competition of curvature and tension. *Phys Rev Lett* *73*, 1392-1395.
- Berclaz, N., Muller, M., Walde, P., and Luisi, P. L. (2001). Growth and transformation of vesicles studied by ferritin labeling and cryotransmission electron microscopy. *J Phys Chem B* *105*, 1056-1064.
- Blochliker, E., Blocher, M., Walde, P., and Luisi, P. L. (1998). Matrix effect in the size distribution of fatty acid vesicles. *J Phys Chem B* *102*, 10383-10390.
- Budin, I., Bruckner, R., and Szostak, J. W. (2009). Formation of protocell-like vesicles in a thermal diffusion column. *J Am Chem Soc* *131*, 9628–9629.
- Chakrabarti, A. C., Breaker, R. R., Joyce, G. F., and Deamer, D. W. (1994). Production of RNA by a polymerase protein encapsulated within phospholipid vesicles. *J Mol Evol* *39*, 555-9.
- Chaput, J. C., Sinha, S., Switzer, C. (2002). 5-propynyluracil.diaminopurine, an efficient base-pair for non-enzymatic transcription of DNA. *Chem Commun* *15*, 1568-9.
- Chen, I. A., Roberts, R. W., and Szostak, J. W. (2004). The emergence of competition between model protocells. *Science* *305*, 1474-1476.
- Chen, I. A. and Szostak, J. W. (2004). A kinetic study of the growth of fatty acid vesicles. *Biophys J* *87*, 988-998.
- Chumachenko, N. V., Novikov, Y., Yarus, M. (2009). Rapid and simple ribozymic aminoacylation using three conserved nucleotides. *J Am Chem Soc* *131*, 5257-63.
- Deamer, D. W. (1985). Boundary structures are formed by organic-components of the Murchison carbonaceous chondrite. *Nature* *317*, 792-794.

Deamer, D. W. and Pashley, R. M. (1989). Amphiphilic components of the Murchison carbonaceous chondrite, surface properties and membrane formation. *Orig Life Evol Biosph* 19, 21-38.

Dworkin, J., Deamer, D., Sandford, S., and Allamandola, L. (2001). Self-assembling amphiphilic molecules, Synthesis in simulated interstellar/precometary ices. *Proc Natl Acad Sci U S A* 98, 815-819.

Ekland, E. H., Szostak, J. W., Bartel, D. P. (2001). Structurally complex and highly active RNA ligases derived from random RNA sequences. *Science* 292, 1319-25.

Ferris, J. P., Hill, A. R. Jr., Liu, R., Orgel, L. E. (1996). Synthesis of long prebiotic oligomers on mineral surfaces. *Nature* 381, 59-61.

Gebicki, J. M. and Hicks, M. (1973). Ufasomes are stable particles surrounded by unsaturated fatty acid membranes. *Nature* 243, 232-234.

Gilbert, W. (1986). The RNA World. *Nature* 319, 618.

Glasner, M. E., Yen, C. C., Ekland, E. H., Bartel, D. P. (2000). Recognition of nucleoside triphosphates during RNA-catalyzed primer extension. *Biochemistry* 39, 15556-62.

Guerrier-Takada, C., Gardiner, K., Marsh, T., Pace, N., Altman, S. (1983). The RNA moiety of ribonuclease P is the catalytic subunit of the enzyme. *Cell* 35, 849-57.

Hanczyc MM, Fujikawa SM, and Szostak JW. (2003). Experimental models of primitive cellular compartments, encapsulation, growth, and division. *Science* 302, 618-622.

Hanczyc, M. M. and Szostak, J. W. (2004). Replicating vesicles as models of primitive cell growth and division. *Curr Opin Chem Biol* 8, 660-664.

Hargreaves, W. R. and Deamer, D. W. (1978). Liposomes from ionic, single-chain amphiphiles. *Biochemistry* 17, 3759-3768.

Hill, A. R. Jr., Nord, L. D., Orgel, L. E., Robins, R. K. (1988). Cyclization of nucleotide analogues as an obstacle to polymerization. *J Mol Evol* 28, 170-1.

Huang, W. and Ferris, J. P. (2006). One-step, regioselective synthesis of up to 50-mers of RNA oligomers by montmorillonite catalysis. *J Am Chem Soc* 128, 8914-9.

Inoue, T. and Orgel, L. E. (1982). Oligomerization of (guanosine 5'-phosphor)-2-methylimidazolid on poly(C). An RNA polymerase model. *J Mol Biol* 162, 201-17.

Inoue, T. and Orgel, L. E. (1983). A nonenzymatic RNA polymerase model. *Science* 219, 859-62.

Johnston, W. K., Unrau, P. J., Lawrence, M. S., Glasner, M. E., Bartel, D. P. (2001). RNA-catalyzed RNA polymerization: accurate and general RNA-templated primer extension. *Science* 292, 1319-25.

Kruger, K., Grabowski, P. J., Zaug, A. J., Sands, J., Gottschling, D. E., Cech, T. R. (1982). Self-splicing RNA, autoexcision and autocyclization of the ribosomal RNA intervening sequence of *Tetrahymena*. *Cell* 31, 147-57.

Lohrmann, R. and Orgel, L. E. (1976). Template-directed synthesis of high molecular weight polynucleotide analogues. *Nature* 261, 342-344.

Lohrmann, R., Bridson, P. K., Orgel, L. E. (1980). Efficient metal-ion catalyzed template-directed oligonucleotide synthesis. *Science* 208, 1464-5.

Luisi, P. L., Walde, P., Oberholzer, T. (1994). Enzymatic RNA synthesis in self-reproducing vesicles, an approach to the construction of a minimal synthetic cell. *Ber Bunsenges Phys Chem* 98, 1160-5.

Luisi, P.L., Stano, P., Rasi, S., and Mavelli, F. (2004). A possible route to prebiotic vesicle reproduction. *Artif Life* 10, 297-308.

Luisi, P. L. (2006). *The emergence of life, from chemical origins to synthetic biology*. Cambridge University Press, Cambridge.

Mansy, S. S., Schrum, J. P., Krishnamurthy, M., Tobé, S., Treco, D. A., and Szostak, J. W. (2008). Template-directed synthesis of a genetic polymer in a model protocell. *Nature* 454, 122-125.

Mansy, S. S., and Szostak, J. W. (2008). Thermostability of model protocell membranes. *Proc Natl Acad Sci U S A* 105, 13351-13355.

Martin, W., and Russell, M. J. (2003). On the origins of cells, a hypothesis for the evolutionary transitions from abiotic geochemistry to chemoautotrophic prokaryotes, and from prokaryotes to nucleated cells. *Philos Trans R Soc Lond B Biol Sci* 358, 59-83.

McCollom, T. M., Ritter, G., and Simoneit, B. R. (1999). Lipid synthesis under hydrothermal conditions by Fischer-Tropsch-type reactions. *Orig Life Evol Biosph* 29, 153-166.

Monnard, P. A., Apel, C. L., Kanavarioti, A., Deamer, D. W. (2002). Influence of ionic inorganic solutes on self-assembly and polymerization processes related to early forms of life, implications for a prebiotic aqueous medium. *Astrobiology* 2, 139-52.

Müller, U. F., Bartel, D. P. (2008). Improved polymerase ribozyme efficiency on hydrophobic assemblies. *RNA* 14, 552-62.

Nissen, P., Hansen, J., Ban, N., Moore, P. B., Steitz, T. A. (2000). The structural basis of ribosome activity in peptide bond synthesis. *Science* 289, 920-30.

Orgel, L. E. (2004). Prebiotic chemistry and the origin of the RNA world. *Crit Rev Biochem Mol Biol* 39, 99-123.

Prabahar, K. J., Ferris, J. P. (1997). Adenine derivatives as phosphate-activating groups for the regioselective formation of 3',5'-linked oligoadenylates on montmorillonite, possible phosphate-activating groups for the prebiotic synthesis of RNA. *J Am Chem Soc* 119, 4330-7.

Rohatgi, R., Bartel, D. P., Szostak JW. (1996). Nonenzymatic, template-directed ligation of oligoribonucleotides is highly regioselective for the formation of 3'-5' phosphodiester bonds. *J Am Chem Soc* 118, 3340-4.

Röthlingshöfer, M., Kervio, E., Lommel, T., Plutowski, U., Hochgesand, A., Richert, C. (2008). Chemical primer extension in seconds. *Angew Chem Int Ed Engl* 47, 6065-8.

Rushdi, A. I., and Simoneit, B. R. (2001). Lipid formation by aqueous Fischer-Tropsch-type synthesis over a temperature range of 100 to 400 degrees C. *Orig Life Evol Biosph* 31, 103-118.

Sacerdote, M. G. and Szostak, J. W. (2005). Semi-permeable lipid bilayers exhibit diastereoselectivity favoring ribose; implications for the origins of life. *Proc Natl Acad Sci U S A* 102, 6004-6008.

Schöning, K., Scholz, P., Guntha, S., Wu, X., Krishnamurthy, R., Eschenmoser, A. (2000). Chemical etiology of nucleic acid structure, the alpha-threofuranosyl-(3'-->2') oligonucleotide system. *Science* 290, 1347-51.

Schrump, J. P., Ricardo, A., Krishnamurthy, K., Blain, J. C. and Szostak, J. W. (2009). Efficient and Rapid Template-Directed Nucleic Acid Copying using 2'-amino-2', 3'-dideoxyribonucleoside-5'-phosphorimidazolide Monomers. *J Am Chem Soc* 131:14560-70.

Stano, P., Wehrli, E., and Luisi, P. L. (2006). Insights into the self-reproduction of oleate vesicles. *J Phys, Condens Matter* 18, S2231-S2238.

Szostak, J. W, Bartel, D. P, and Luisi, P. L. (2001). Synthesizing life. *Nature* 409, 387-390.

Tohidi, M., Zielinski, W. S., Chen, C. H., and Orgel, L. E. (1987). Oligomerization of 3'-amino-3'-deoxyguanosine-5'-phosphorimidazolidate on a d(CpCpCpCpC) template. *J Mol Evol* 25, 97-99.

Vogel, S. R., Richert, C. (2007). Adenosine residues in the template do not block spontaneous replication steps of RNA. *Chem Commun* 19, 1896-8.

Voytek, S. B., Joyce, G. F. (2007). Emergence of a fast-reacting ribozyme that is capable of undergoing continuous evolution. *Proc Natl Acad Sci U S A* 104, 15288-93.

Walde, P., Wick, R., Fresta, M., Mangone, A., and Luisi, P. L. (1994a). Autopoietic self-reproduction of fatty acid vesicles. *J Am Chem Soc* 116, 11649-11654.

Walde, P., Goto, A., Monnard, P-A., Wessicken, M., and Luisi, P. L. (1994b). Oparin's Reactions Revisited, Enzymatic Synthesis of Poly(adenylic acid) in Micelles and Self-Reproducing Vesicles. *J Am Chem Soc* 116, 7541-7547.

Wu, T., Orgel, L. E. (1992). Nonenzymatic template-directed synthesis on hairpin oligonucleotides. 3. Incorporation of adenosine and uridine residues. *J Am Chem Soc* 114, 7963-9.

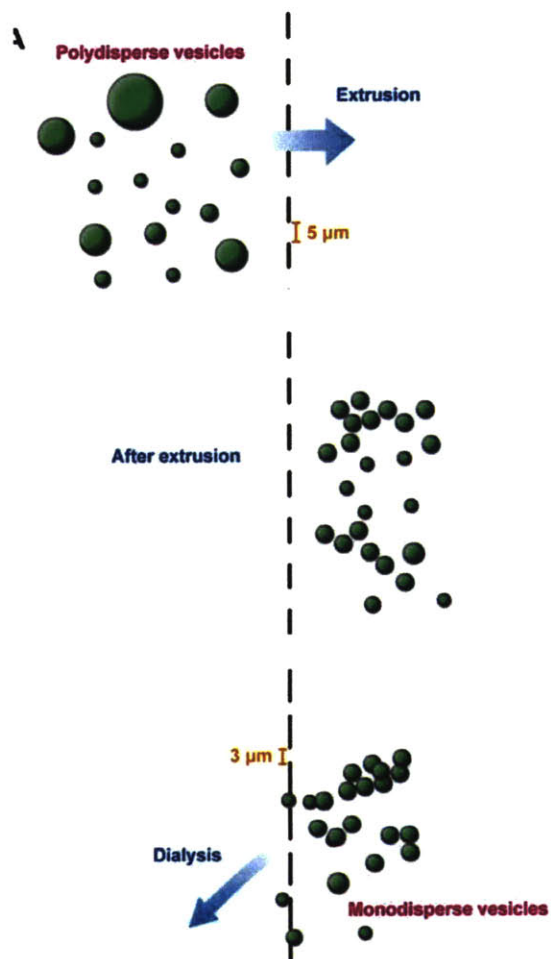
Wu, X., Guntha, S., Ferencic, M., Krishnamurthy, R., Eschenmoser, A. (2002). Base-pairing systems related to TNA: alpha-threofuranosyl oligonucleotides containing phosphoramidate linkages. *Org Lett* 4, 1279-82.

Zhu, T. F., and Szostak, J. W. (2009a). Coupled Growth and Division of Model protocell Membranes. *J Am Chem Soc* 131, 5705-5713.

Zhu, T. F., and Szostak, J. W. (2009b). Preparation of large monodisperse vesicles. *PLoS ONE* 4, e5009.

Zielinski, W. S., and Orgel, L. E. (1985). Oligomerization of activated derivatives of 3'-amino-3'-deoxyguanosine on poly(C) and poly(dC) templates. *Nucleic Acids Res* 13, 2469-2484.

Preparation of Large Monodisperse Vesicles



A portion of this chapter has been published in *PLoS ONE*.

Summary

Preparation of monodisperse vesicles is important for both research purposes and practical applications. While the extrusion of vesicles through small pores (~100 nm in diameter) results in relatively uniform populations of vesicles, extrusion to larger sizes results in very heterogeneous populations of vesicles. Here we report a simple method for preparing large monodisperse multilamellar vesicles through a combination of extrusion and large-pore dialysis. For example, extrusion of polydisperse vesicles through 5- μm -diameter pores eliminates vesicles larger than 5 μm in diameter. Dialysis of extruded vesicles against 3- μm -pore-size polycarbonate membranes eliminates vesicles smaller than 3 μm in diameter, leaving behind a population of monodisperse vesicles with a mean diameter of ~4 μm . The simplicity of this method makes it an effective tool for laboratory vesicle preparation with potential applications in preparing large monodisperse liposomes for drug delivery.

Introduction

Vesicles are closed bilayer membranes that encapsulate an aqueous compartment. Fatty acid vesicles have been studied as a model system for primitive cellular membranes at the origin of life (Hanczyc et al., 2003; Szostak et al., 2001). Phospholipid vesicles (liposomes), which are more stable under physiological conditions, have been widely used for drug delivery (Allen and Cullis, 2004). There are many advantages to being able to work with monodisperse vesicle preparations. In studies of vesicle growth, monodisperse vesicle preparations allow for the detection of changes in vesicle size by light scattering or by fluorescence microscopy (Chen and Szostak, 2004a; Hanczyc et al., 2003). The size distribution of vesicles is a crucial factor in determining the efficacy of drug delivery (Nagayasu et al., 1999). The accumulation of liposomes in tumors is size-dependent, as tumor capillaries have larger pores (100 to 700 nm in diameter) than normal blood vessels (typically < 50 nm). Thus liposomes between 90 and 200 nm in diameter can selectively penetrate tumor capillaries (Liu et al., 1992). The drug release profile from liposomes *in vivo* has also been shown to be size-dependent (Nagayasu et al., 1995). For inhaled liposomal drug delivery, the ideal liposome size is between 1 and 3 μm (Dhand, 2004; Edwards et al., 1998; Verschraegen et al., 2004), because particles in this size range can be delivered into the deep lung more effectively and avoid phagocytic clearance from the lung periphery (Edwards et al., 1998).

Vesicles formed by resuspending a dried film of lipids are highly heterogeneous in size (Knight et al., 1999; Korgel et al., 1998). Various methods have been used to directly prepare monodisperse vesicles, including vesicle extrusion and vesicle formation from double emulsions (Lorenceanu et al., 2005; Sugiura et al., 2008; Utada et al., 2005), or to purify monodisperse

vesicles from heterogeneous populations, such as gel filtration (Enoch and Strittmatter, 1979) and high performance size exclusion chromatography (HPSEC) (Grabielle-Madelmont et al., 2003). Extrusion is often used for making relatively homogeneous vesicles in the size range between 50 and 100 nm (Hope et al., 1985; Olson et al., 1979). This approach takes advantage of the fact that when vesicles are forced through membrane pores smaller than their diameter, they break down into smaller vesicles closer to the pore size (Patty and Frisken, 2003). While effective in making small (50 to 100 nm) monodisperse vesicles, this technique does not eliminate vesicles smaller than the membrane pore size. Because of the initial population heterogeneity, vesicles extruded through pores larger than ~200 nm remain quite heterogeneous. HPSEC has been used to purify vesicles prepared by extrusion (Grabielle-Madelmont et al., 2003; Korgel et al., 1998), but is only capable of producing monodisperse vesicles smaller than 300 nm because of limitations on the available pore sizes of the column gel. Double emulsions (e.g., water/oil/water emulsions) prepared using a microfluidic device (Lorenceanu et al., 2005; Sugiura et al., 2008; Utada et al., 2005) can be used to make giant monodisperse vesicles, but the process is complicated, and contamination by the oil phase remains an issue for drug delivery applications.

We have developed a simple method for preparing monodisperse vesicles through a combination of extrusion and large-pore dialysis. We use polycarbonate track-etched membranes with large pore sizes (submicron to several microns in diameter) first for extrusion, and then for dialysis to remove vesicles smaller than the membrane pores. For example, extruding through a polycarbonate membrane with 5- μm -diameter pores and dialyzing using membranes with 3- μm -diameter pores results in a vesicle population between 3-5 μm in diameter (Figure II.1).

Methods

Materials. Fatty acids and fatty acid derivatives were obtained from Nu-chek Prep (Elysian, MN). Fluorescent dyes were obtained from Molecular Probes, Inc. (Eugene, OR). Oleate (C18:1) vesicles were prepared by resuspending a dried film of oleic acid in 0.2 M Na-bicine (*N,N*-Bis(2-hydroxyethyl)glycine, Sigma-Aldrich, St. Louis, MO) containing 2 mM HPTS (8-hydroxypyrene-1,3,6-trisulfonic acid trisodium salt, a water-soluble, membrane-impermeable fluorescent dye) at pH 8.5, to a final concentration of 10 mM oleic acid in buffer. The vesicle suspension was vortexed briefly, and tumbled overnight. POPC (1-palmitoyl-2-oleoyl-*sn*-glycero-3-phosphocholine) vesicles were prepared by resuspending a dried film of POPC in 0.2 M Na-bicine containing 2 mM HPTS at pH 8.5, to a final concentration of 10 mM POPC in buffer. For oleate vesicles, the washing buffer for dialysis was prepared by resuspending 10 mM oleic acid in 0.2 M Na-bicine buffer at pH 8.5 but without fluorescent dye, to maintain the concentration of oleate acid above its cac (critical aggregation concentration) and avoid vesicle dissolution. Dialysis of POPC vesicles was performed using 0.2 M Na-bicine at pH 8.5 without POPC vesicles, since the cac of POPC vesicles is so low that vesicle dissolution was not a concern.

Vesicle extrusion and large-pore dialysis. Large-pore dialysis cassettes were made by modification of commercially available 500 μ l dialysis cassettes (Pierce, Rockford, IL). The original membranes on the cassette were replaced with polycarbonate track-etched membranes (Whatman, United Kingdom). Such membranes have sharply defined pore sizes, and have been used for vesicle extrusion in previous studies (Chen et al., 2004; Chen and Szostak, 2004a; Chen and Szostak, 2004b; Hanczyc et al., 2003). About 400 μ l of extruded vesicles encapsulating

HPTS were loaded onto the center of a modified dialysis cassette, after which the cassette was closed with metal clamps. A volume of ~30 ml washing buffer was used in each round of dialysis, which just submerged the horizontally placed dialysis cassette in a 150 ml beaker. The beaker was gently agitated on a table-top shaker at 60 rpm. The first 5-6 rounds of dialysis were for 5-10 min each, after which the free dye in the vesicle suspension was adequately eliminated. At least 6 more rounds of dialysis (each for 2 hrs minimum, one of which was overnight) were performed to eliminate vesicles smaller than the membrane pores. The vesicle sample was retrieved with a pipette tip by breaking the polycarbonate membrane after dialysis. For oleate vesicles, the resultant vesicle population contained large monodisperse vesicles encapsulating fluorescent dye and smaller vesicles from the washing buffer that were dye-free (since they are not fluorescent, their presence does not affect the imaging and the counting of large dye-labeled vesicles by fluorescence microscopy). Extrusion and large-pore dialysis of POPC vesicles were performed using the same method. The monodisperse POPC vesicle population did not contain any dye-free vesicles as the washing buffer did not contain any POPC vesicles.

Vesicle size distribution and lamellarity. To determine the size distribution of resuspended oleate vesicles before and after the removal of small vesicles, oleate vesicles (containing 2 mM HPTS) were extruded through a polycarbonate membrane with 5- μ m-diameter pores and dialyzed using conventional dialysis membranes (10 kDa cutoff) to eliminate the free dye (for the purpose of imaging) from the vesicle suspension. Vesicles were imaged using a Nikon TE2000S inverted epifluorescence microscope with extra long working distance (ELWD) objective lenses. Vesicle sizes were analyzed by Phylum Live software (Improvision, Lexington, MA). The size distribution of POPC vesicles was determined using the same method. To study

the lamellarity of the monodisperse oleate and POPC vesicles, confocal images were taken using a Leica SP5 AOBS scanning laser confocal microscope with Leica acquisition software (Leica, Germany). The vesicles were labeled with a membrane-anchored fluorescent dye, Rh-DHPE (LissamineTMrhodamine B 1,2-dihexadecanoyl-*sn*-glycero-3-phosphoethanolamine; excitation at 560 nm, emission at 586 nm).

Results

Oleic acid vesicles, after being extruded through a 5- μm -pore-size membrane, as shown in Figure II.2 (A), were almost all less than 5 μm in diameter. As expected, the vesicles were highly heterogeneous in size, with the bulk of the vesicles being smaller than 3 μm in diameter. The size distribution is shown in Figure II.2 (B). A large number of vesicles in the size range between 0 and 0.4 μm were too small to be accurately measured, and therefore were not counted. The fraction of 3-5 μm vesicles within this population was estimated as $\sim 4\%$. After 12 rounds of dialysis with 3- μm -pore-size membranes, vesicles smaller than 3 μm in the population were almost entirely eliminated, resulting in a relatively narrow population size distribution between 3 and 5 μm in diameter (Figure II.2, C, D). The average diameter was 4.2 μm , with a standard deviation of $\pm 15\%$. These vesicles contain $\sim 40\%$ of the total encapsulated volume of the original population, with the remaining $\sim 60\%$ of the encapsulated contents lost due to removal of the smaller vesicles. The recovered 3-5 μm vesicles retained the encapsulated fluorescent dye and remained monodisperse for at least several weeks.

We have used essentially the same procedures to prepare POPC vesicles of a different size range. Dye-labeled POPC vesicles extruded through a 1- μm -pore-size membrane, as shown in Figure II.3 (A, B), were heterogeneous in size. After dialyzing with 0.8- μm -pore-size membranes for 12 rounds, as shown in Figure II.3 (C, D), vesicles smaller than 0.8 μm were significantly reduced. The average final diameter was 1.0 μm with a standard deviation of $\pm 30\%$. Thus the preparation of POPC vesicles between 0.8 and 1 μm in diameter by the extrusion-dialysis method created a less monodisperse population of vesicles than we obtained for larger (3 to 5 μm in diameter) oleate vesicles. As shown in Figure II.4, both the oleate and POPC vesicles prepared

by extrusion-dialysis were multilamellar. This is as expected, since the vesicles were initially formed by the resuspension of dried lipid films, which is known to produce predominately multilamellar vesicles with variable numbers of internal membranes.

Discussion

The extrusion-dialysis method for preparing monodisperse vesicles that we have described is a hybrid preparation/purification method in which extrusion is used to prepare vesicles that are smaller than a given size, and then dialysis is used to eliminate vesicles smaller than a desired size threshold. This approach can be used to produce vesicles of different size ranges and with different lipid compositions. Since the extrusion-dialysis procedures are independent from how the vesicles are initially prepared (in the current study, via the resuspension of dried lipid films), this method should in principle be applicable to vesicles made in different ways, and to initial populations of vesicles with different lipid compositions, size ranges, and lamellarity. It may even be possible to develop a similar method to purify monodisperse solid particles from a population of polydisperse particles by removing particles above a size threshold by membrane filtration, followed by dialysis to eliminate particles below a smaller size threshold.

This method is most suitable for preparing large (several microns) monodisperse vesicles. This is convenient for applications involving fluorescence microscopy, because vesicles of several microns are ideal for imaging, as the optical resolution limit is ~ 0.25 to $0.5 \mu\text{m}$ for conventional microscopes. Standard methods for preparing monodisperse vesicles, such as extrusion, are typically used to produce vesicles of $< 200 \text{ nm}$ in diameter, thus the extrusion-dialysis method is an aptly complementary method. Though intravenous drug delivery typically uses liposomes smaller than $1 \mu\text{m}$, certain clinical applications such as inhaled liposomal drug delivery require larger liposomes of several microns in diameter (Dhand, 2004; Edwards et al., 1998; Verschraegen et al., 2004).

In addition to size control, control over the lamellarity of vesicles is also important for many applications. Since the method we used for initial vesicle formation (resuspension of dried lipid films) is known to produce predominately multilamellar vesicles, the monodisperse vesicles resulting from extrusion-dialysis were also multilamellar, as expected. Whether the extrusion-dialysis method can be applied to purify unilamellar vesicles prepared by other vesicle formation methods, such as electroformation, should be examined in future studies. Monodisperse multilamellar fatty acid vesicles are useful in origin-of-life studies as models of primitive cellular membranes, since vesicles that formed spontaneously in early earth environments (e.g., by the resuspension of dry fatty acid films or by the acidification of concentrated solutions of micelles) would be likely to be large and multilamellar (Hanczyc et al., 2003; Hargreaves and Deamer, 1978). Monodisperse multilamellar phospholipid vesicles may find applications in drug delivery, as the high membrane-to-volume ratio would allow them to carry more lipophilic drugs in their bilayer membranes.

Our experience indicates that this preparation/purification method is not very sensitive to changes in the operating parameters (duration of dialysis, etc.) and thus should be easy to reproduce using similar or modified methods. Practical applications of this method may currently be constrained by the overall duration of the procedures (~24 hr total), and by the low yield of monodisperse vesicles. On the other hand, the simplicity and versatility of the method should make large-scale preparation possible in practical applications.

Figures

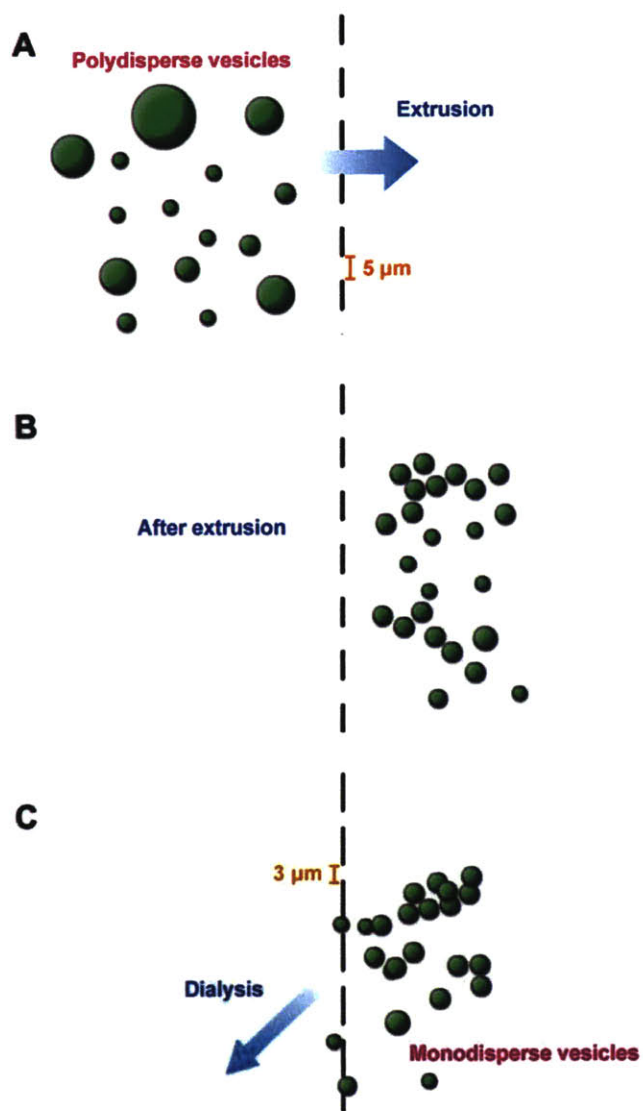


Figure II.1 Schematic diagram of vesicle extrusion-dialysis. (A, B) Extrusion of polydisperse vesicles through 5- μm -diameter pores eliminates vesicles larger than 5 μm in diameter. (C) Dialysis of extruded vesicles against 3- μm -pore-size polycarbonate membranes eliminates vesicles smaller than 3 μm in diameter, leaving behind a population of monodisperse vesicles.

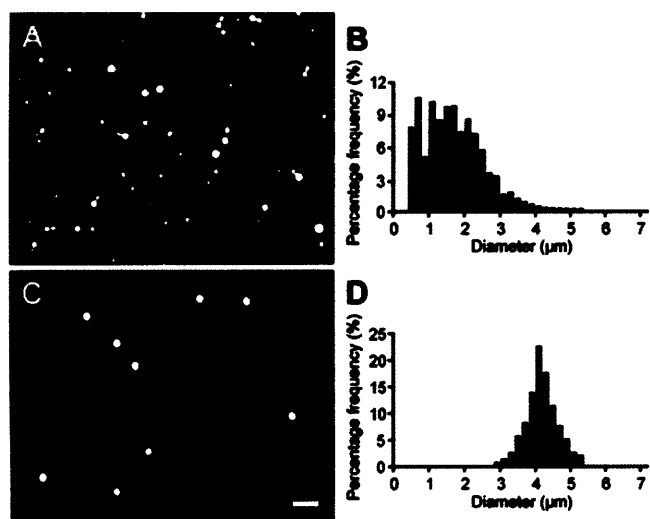


Figure II.2 Preparation of large monodisperse oleate vesicles. (A) Oleate vesicles (containing 2 mM HPTS, in 0.2 M Na-bicine, pH 8.5) after being extruded through 5- μm -diameter pores, and (B) the corresponding size distribution, shown as percent per 0.2 μm bin (vesicles between 0-0.4 μm in diameter were not counted). (C) After 12 rounds of dialysis using membranes with 3- μm -diameter pores, and (D) the corresponding size distribution. Scale bar, 10 μm .

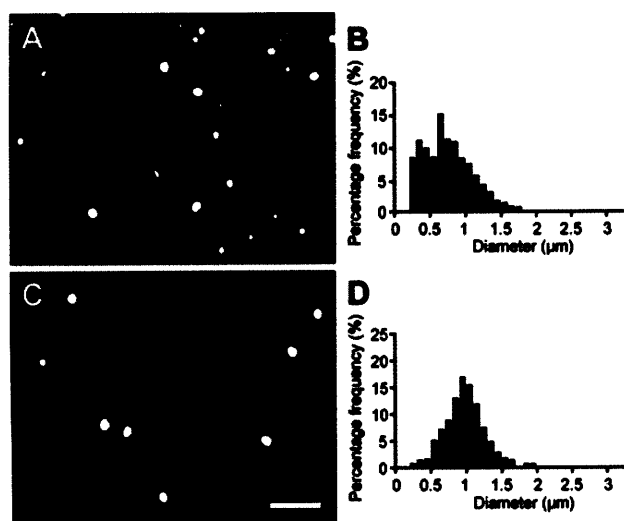


Figure II.3 Preparation of monodisperse POPC vesicles. (A) POPC vesicles (containing 2 mM HPTS, in 0.2 M Na-bicine, pH 8.5) after being extruded through 1- μ m-diameter pores, and (B) the corresponding size distribution, shown as percent per 0.1 μ m bin. (C) After 12 rounds of dialysis using membranes with 0.8- μ m-diameter pores, and (D) the corresponding size distribution. Scale bar, 5 μ m.

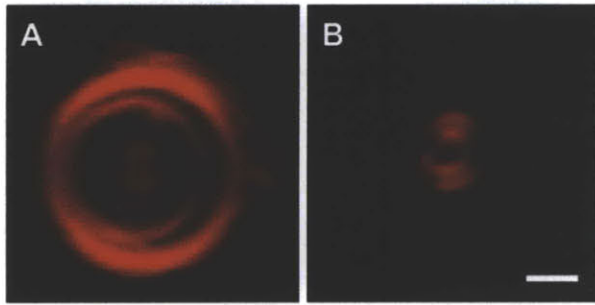


Figure II.4 Confocal images of oleate and POPC vesicles prepared by extrusion-dialysis.

(A) Confocal image of a multilamellar oleate vesicle after extrusion-dialysis (0.2 mol % Rh-DHPE, in 0.2 M Na-bicine, pH 8.5). (B) Confocal image of a multilamellar POPC vesicle after extrusion-dialysis (0.2 mol % Rh-DHPE, in 0.2 M Na-bicine, pH 8.5). Though the vesicle is small ($\sim 0.5 \mu\text{m}$ in radius, approaching the resolution limit of the confocal microscope), the image clearly indicates the presence of an internal membrane. Scale bar, $1 \mu\text{m}$.

References

Allen, T. M., and Cullis, P. R. (2004). Drug delivery systems: entering the mainstream. *Science* 303, 1818-1822.

Chen, I. A., Roberts, R. W., and Szostak, J. W. (2004). The emergence of competition between model protocells. *Science* 305, 1474-1476.

Chen, I. A., and Szostak, J. W. (2004a). A kinetic study of the growth of fatty acid vesicles. *Biophys J* 87, 988-998.

Chen, I. A., and Szostak, J. W. (2004b). Membrane growth can generate a transmembrane pH gradient in fatty acid vesicles. *Proc Natl Acad Sci USA* 101, 7965-7970.

Dhand, R. (2004). New frontiers in aerosol delivery during mechanical ventilation. *Respir Care* 49, 666-677.

Edwards, D. A., Ben-Jebria, A., and Langer, R. (1998). Recent advances in pulmonary drug delivery using large, porous inhaled particles. *J Appl Physiol* 85, 379-385.

Enoch, H. G., and Strittmatter, P. (1979). Formation and Properties of 1000-Å-Diameter, Single-Bilayer Phospholipid Vesicles. *Proceedings of the National Academy of Sciences of the United States of America* 76, 145-149.

Grabielle-Madelmont, C., Lesieur, S., and Ollivon, M. (2003). Characterization of loaded liposomes by size exclusion chromatography. *Journal of Biochemical and Biophysical Methods* 56, 189-217.

Hanczyc, M. M., Fujikawa, S. M., and Szostak, J. W. (2003). Experimental models of primitive cellular compartments: encapsulation, growth, and division. *Science* 302, 618-622.

Hargreaves, W. R., and Deamer, D. W. (1978). Liposomes from ionic, single-chain amphiphiles. *Biochemistry* 17, 3759-3768.

Hope, M. J., Bally, M. B., Webb, G., and Cullis, P. R. (1985). Production of Large Unilamellar Vesicles by a Rapid Extrusion Procedure - Characterization of Size Distribution, Trapped Volume and Ability to Maintain a Membrane-Potential. *Biochimica Et Biophysica Acta* 812, 55-65.

Knight, V., Koshkina, N. V., Waldrep, J. C., Giovanella, B. C., and Gilbert, B. E. (1999). Anticancer effect of 9-nitrocamptothecin liposome aerosol on human cancer xenografts in nude mice. *Cancer Chemother Pharmacol* 44, 177-186.

Korgel, B. A., van Zanten, J. H., and Monbouquette, H. G. (1998). Vesicle size distributions measured by flow field-flow fractionation coupled with multiangle light scattering. *Biophysical Journal* 74, 3264-3272.

Liu, D., Mori, A., and Huang, L. (1992). Role of liposome size and RES blockade in controlling biodistribution and tumor uptake of GM1-containing liposomes. *Biochim Biophys Acta* 1104, 95-101.

Lorceau, E., Utada, A. S., Link, D. R., Cristobal, G., Joanicot, M., and Weitz, D. A. (2005). Generation of polymerosomes from double-emulsions. *Langmuir* 21, 9183-9186.

Nagayasu, A., Shimooka, T., and Kiwada, H. (1995). Effect of vesicle size on in vivo release of daunorubicin from hydrogenated egg phosphatidylcholine-based liposomes into blood circulation. *Biol Pharm Bull* 18, 1020-1023.

Nagayasu, A., Uchiyama, K., and Kiwada, H. (1999). The size of liposomes: a factor which affects their targeting efficiency to tumors and therapeutic activity of liposomal antitumor drugs. *Adv Drug Deliv Rev* 40, 75-87.

Olson, F., Hunt, C. A., Szoka, F. C., Vail, W. J., and Papahadjopoulos, D. (1979). Preparation of Liposomes of Defined Size Distribution by Extrusion through Polycarbonate Membranes. *Biochimica Et Biophysica Acta* 557, 9-23.

Patty, P. J., and Frisken, B. J. (2003). The pressure-dependence of the size of extruded vesicles. *Biophysical Journal* 85, 996-1004.

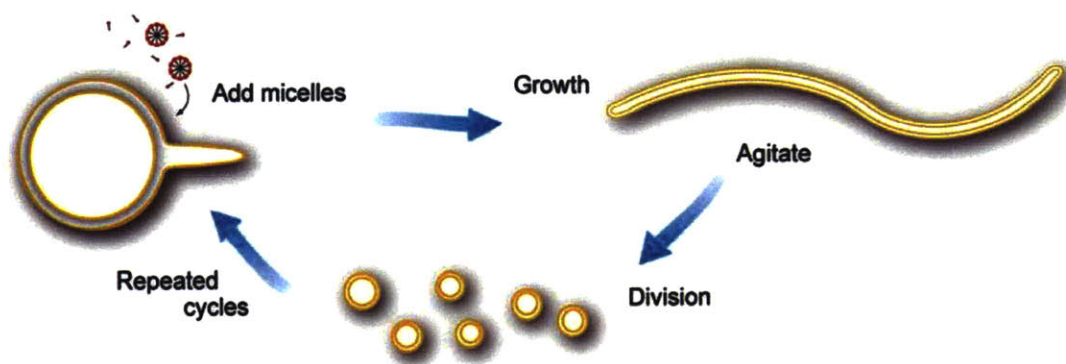
Sugiura, S., Kuroiwa, T., Kagota, T., Nakajima, M., Sato, S., Mukataka, S., Walde, P., and Ichikawa, S. (2008). Novel method for obtaining homogeneous giant vesicles from a monodisperse water-in-oil emulsion prepared with a microfluidic device. *Langmuir* 24, 4581-4588.

Szostak, J. W., Bartel, D. P., and Luisi, P. L. (2001). Synthesizing life. *Nature* 409, 387-390.

Utada, A. S., Lorceau, E., Link, D. R., Kaplan, P. D., Stone, H. A., and Weitz, D. A. (2005). Monodisperse double emulsions generated from a microcapillary device. *Science* 308, 537-541.

Verschraegen, C. F., Gilbert, B. E., Loyer, E., Huaranga, A., Walsh, G., Newman, R. A., and Knight, V. (2004). Clinical evaluation of the delivery and safety of aerosolized liposomal 9-nitro-20(s)-camptothecin in patients with advanced pulmonary malignancies. *Clin Cancer Res* 10, 2319-2326.

Coupled Growth and Division of Model Protocell Membranes



A portion of this chapter has been published in the *Journal of the American Chemical Society*.

Summary

The generation of synthetic forms of cellular life requires solutions to the problem of how biological processes such as cyclic growth and division could emerge from purely physical and chemical systems. Small unilamellar fatty acid vesicles grow when fed with fatty acid micelles, and can be forced to divide by extrusion, but this artificial division process results in significant loss of protocell contents during each division cycle. Here we describe a simple and efficient pathway for model protocell membrane growth and division. The growth of large multilamellar fatty acid vesicles fed with fatty acid micelles, in a solution where solute permeation across the membranes is slow, results in the transformation of initially spherical vesicles into long thread-like vesicles, a process driven by the transient imbalance between surface area and volume growth. Modest shear forces are then sufficient to cause the thread-like vesicles to divide into multiple daughter vesicles without loss of internal contents. In an environment of gentle shear, protocell growth and division are thus coupled processes. We show that model protocells can proceed through multiple cycles of reproduction. Encapsulated RNA molecules, representing a primitive genome, are distributed to the daughter vesicles. Our observations bring us closer to the laboratory synthesis of a complete protocell consisting of a self-replicating genome and a self-replicating membrane compartment. In addition, the robustness and simplicity of this pathway suggests that similar processes might have occurred under the prebiotic conditions of the early Earth.

Introduction

One of the major challenges confronting attempts to synthesize artificial forms of life is understanding how a structurally simple protocell could accomplish the apparently complex, biological function of self-replication in the absence of evolved biological machinery (Szostak et al., 2001). A self-replicating protocell requires, minimally, two essential components: a self-replicating genome such as an RNA polymerase ribozyme (Johnston et al., 2001) or a chemically replicating nucleic acid, and a membrane compartment that can grow and divide (Hanczyc et al., 2003; Hanczyc and Szostak, 2004). We have recently demonstrated the spontaneous copying of a vesicle-encapsulated genetic template (Mansy et al., 2008), and the thermal strand separation of an encapsulated DNA duplex (Mansy and Szostak, 2008), suggesting that the spontaneous replication of encapsulated genetic polymers may be possible. Here we describe simple processes that lead to the efficient growth and division of model protocell membranes.

Fatty acid vesicles have long been studied as a model system for protocell membranes (Gebicki and Hicks, 1973; Hanczyc et al., 2003; Hargreaves and Deamer, 1978; Mansy et al., 2008; Walde et al., 1994), as fatty acids and similar membrane-forming amphiphilic molecules have been isolated from meteorites and synthesized under simulated prebiotic conditions (Deamer, 1985; Deamer and Pashley, 1989; McCollom et al., 1999; Naraoka et al., 1999; Nooner et al., 1976; Rushdi and Simoneit, 2001; Yuen and Kvenvold, 1973). The physical properties of small (typically 100 nm in diameter) unilamellar fatty acid vesicles have been studied in depth (Chen et al., 2004; Chen and Szostak, 2004a; Chen and Szostak, 2004b; Hanczyc et al., 2003; Mansy et al., 2008; Mansy and Szostak, 2008; Sacerdote and Szostak, 2005). For a population of vesicles to grow, fresh lipid molecules must be supplied. Pioneering studies in the laboratory of

P. L. Luisi showed that when vesicles in a buffered solution are fed with alkaline fatty acid micelles (which become thermodynamically unstable at lower pH), the lipid molecules can either be incorporated into pre-existing membranes (leading to growth) (Berclaz et al., 2001; Chen and Szostak, 2004a; Hanczyc et al., 2003), or self-assemble into new vesicles (Berclaz et al., 2001; Blochliger et al., 1998; Luisi et al., 2004; Rasi et al., 2003; Rasi et al., 2004). While vesicle growth by feeding with fatty acid micelles can be very efficient (Hanczyc et al., 2003), vesicle division by extrusion through small pores results in the loss of a substantial fraction of the encapsulated vesicle contents to the environment (Hanczyc et al., 2003; Hanczyc and Szostak, 2004).

Furthermore, it is unlikely for an analogous vesicle extrusion process to occur in a prebiotic scenario on the early Earth, because vesicle extrusion by flowing suspended vesicles through a porous rock would require both the absence of any large pores or channels, and a very high pressure gradient. For extrusion to occur by flowing suspended vesicles through a porous rock, the rock must not have any large pores. Since the resistance to a laminar flow through a pore, as described by the Hagen-Poiseuille law, is inversely proportional to the fourth power of the radius of the pore, larger pores would have much less resistance and allow virtually all of the fluid volume to flow through. For instance, a large pore with 1 mm diameter is 10^{10} times less resistant to flow than a 2- μm -diameter pore, and would allow most of the vesicles to flow through without being extruded. To test this theory, we compared the extrusion of large ($\sim 4 \mu\text{m}$ in diameter) oleate vesicles (containing 2 mM HPTS) through membrane filters (with 2- μm -diameter pores) with or without a punctured 1-mm-diameter pore. Using the vesicle counting assay, we found that such a 1-mm-diameter pore completely prevented vesicle division from occurring. For the same reason, flowing vesicles through an open channel (e.g., a stream) would

allow virtually all of the vesicles to escape extrusion. Another important constraint is that the pressure gradient required for extrusion is immense. In the laboratory extrusion procedure (Hanczyc et al., 2003), the pressure gradient applied across the membrane filter is estimated to be greater than 100 atm/cm (the membrane filter used is only $\sim 10 \mu\text{m}$ in thickness). As the required pressure difference increases with the thickness of the porous rock, the rock must either be very thin (e.g., of several microns), or subjected to a high pressure difference (100 atm for 1 cm thickness) to allow for extrusion. Moreover, for multiple cycles of growth and division to occur, the vesicle suspension must be repeatedly recycled through the porous rock. It is unlikely for all these stringent conditions to be satisfied in a natural environment, and thus unlikely for an analogous vesicle extrusion process to occur in a prebiotic scenario on the early Earth. The possible spontaneous division of small unilamellar vesicles after micelle addition has been discussed (Luisi, 2006; Luisi et al., 2004), and electron microscopy has revealed structures that are possible intermediates of growth and division (Stano et al., 2006). However, the inheritance of the contents and membranes of parental vesicles by the newly formed vesicles has not been experimentally confirmed.

In contrast to the small unilamellar vesicles discussed above, fatty acid vesicles that form spontaneously by the rehydration of dry fatty acid films, or by the acidification of concentrated solutions of micelles, tend to be large (several microns in diameter) and multilamellar (Hanczyc et al., 2003; Hargreaves and Deamer, 1978). Until recently, we have avoided using multilamellar vesicles for laboratory studies, because populations of such vesicles are so heterogeneous that quantitative studies of growth and division are difficult. To address this problem, we developed a simple procedure for the preparation of large ($\sim 4 \mu\text{m}$ in diameter) monodisperse multilamellar vesicles by large-pore dialysis (Zhu and Szostak, 2009). This gentle procedure preserves the

original physical properties (e.g., multilamellar structure, volume, and osmolarity) of the large multilamellar vesicles. When we added fatty acid micelles to large monodisperse multilamellar vesicles prepared in this manner, we were able to directly observe a novel and unexpected mode of vesicle growth that allows for efficient division under modest shear forces.

Methods

Preparation of large monodisperse multilamellar vesicles. Fatty acids and fatty acid derivatives were obtained from Nu-chek Prep (Elysian, MN). Fluorescent dyes were obtained from Molecular Probes, Inc. (Eugene, OR). Oleate vesicles were prepared by resuspending a dried film of oleic acid in 0.2 M Na-bicine (Sigma-Aldrich, St. Louis, MO) containing 2-10 mM HPTS at pH 8.5, to a final concentration of 10 mM oleic acid. The vesicle suspension was vortexed briefly, and tumbled overnight. Dilutions of vesicles were made using buffers containing fatty acids above the critical aggregate concentration (cac; $\sim 80 \mu\text{M}$ for oleic acid, $\sim 4 \text{ mM}$ for myristoleic acid, and $\sim 30 \text{ mM}$ for decanoic acid), to avoid vesicle dissolution. The method for the preparation of large ($\sim 4 \mu\text{m}$ in diameter) monodisperse multilamellar vesicles by extrusion and large-pore dialysis has been described (Zhu and Szostak, 2009). Briefly, extrusion of polydisperse vesicles through 5- μm -diameter pores eliminates vesicles larger than 5 μm in diameter. Dialysis of extruded vesicles against 3- μm -pore-size polycarbonate membranes eliminates vesicles smaller than 3 μm in diameter, leaving behind a population of monodisperse vesicles with a mean diameter of $\sim 4 \mu\text{m}$. The wash buffer for the dialysis of fatty acid vesicles was prepared by resuspending 10 mM oleic acid in 0.2 M Na-bicine buffer at pH 8.5 but without fluorescent dye, to maintain the lipid concentration above the cac and avoid vesicle dissolution during dialysis. Thus the resultant vesicle population contained large monodisperse vesicles encapsulating fluorescent dye and smaller ones that were dye-free (since they are not fluorescent, their presence does not affect the imaging and the counting of large dye-labeled vesicles by fluorescence microscopy). Oleate vesicles in 0.2 M ammonium acetate or 0.2 M Na-glycine were prepared and dialyzed using the same method. Decanoate vesicles were prepared and dialyzed in a water bath above the melting temperature of decanoic acid, at 50 °C. Vesicles encapsulating

fluorescently-tagged RNA, 5'-DY547-AAA AAA AAA A-3' (Dharmacon, Chicago, IL), were prepared by dissolving 0.5 mM of the fluorescently-tagged RNA in 0.2 M Na-bicine buffer at pH 8.5, followed by the vesicle preparation and dialysis procedures described above. Dialysis was conducted under argon to avoid oxidation of dye-labeled RNA, and RNase-free reagents were used in all steps prior to dialysis (once formed, fatty acid membranes act as a barrier to RNase).

Adding micelles and imaging. To prepare fatty acid micelle solutions, fatty acids were dissolved in 1 equivalent of NaOH (final pH > 10), vortexed briefly, and agitated overnight under argon (Hanczyc et al., 2003). For the vesicle growth experiment in ammonium acetate, fatty acid micelle solutions were prepared by dissolving the fatty acid in 2 equivalents of NH₄OH. Large (~4 μm in diameter) multilamellar oleate vesicles (containing 2 mM HPTS) were prepared by large-pore dialysis, diluted 1:10 with the same buffer containing 0.8 mM oleic acid (to a final concentration of ~1 mM oleic acid), and stored in an eppendorf tube. For the vesicle growth experiment, 5 equivalents of oleate micelles were added to pre-formed vesicles, mixed, and then quickly pipetted into a disposable hemacytometer (Incyto, South Korea). These disposable hemacytometers are plastic microfluidic channels with small openings on the edge for sample loading. This design effectively prevents water evaporation and other perturbations during imaging. The addition of smaller quantities (1 equivalent) of oleate micelles was performed using the same method. Vesicles with encapsulated fluorescent dyes were imaged using a Nikon TE2000S inverted epifluorescence microscope with extra long working distance (ELWD) objective lenses. The illumination source was a metal halide lamp (EXFO, Canada) with a 480±20 nm (for HPTS) or a 546±5 nm (for DY547) optical filter (Chroma, Rockingham, VT). The illumination intensity was kept low enough to avoid photobleaching using a set of two neutral density filters on the microscope. The images and movies were recorded using a digital

camera (Hamamatsu Photonics, Japan) and post-processed using Phylum Live software (Improvision, Lexington, MA). Confocal images were taken using a Leica SP5 AOBS scanning laser confocal microscope with Leica acquisition software (Leica, Germany). All images were cropped using Photoshop CS2 (Adobe Systems, San Jose, CA), with linear adjustments of brightness and contrast. All imaging studies were performed at room temperature, except for the studies on decanoate vesicles, which were performed at 50 °C.

Vesicle growth and division. Large (~4 μm in diameter) multilamellar oleate vesicles (containing 2 mM HPTS) were prepared by the methods described above, diluted 1:300 with the same buffer (total oleic acid at ~1 mM). 5 equivalents of oleate micelles were added to the pre-formed vesicles, mixed, and then quickly pipetted into a depression on a cell-culture glass slide (Erie, Portsmouth, NH). The depression on the glass slide helps to hold the small volume of fluid and increase its stability during the imaging. The slide was covered by a home-made black-cardboard cover to avoid perturbations and evaporation during vesicle growth. After 20-25 min of imaging, we removed the cover and started to blow air briefly, at intervals, using a compressed air canister (Fisher, Hampton, NH) from 0.5 m away, until vesicle division occurred. Movies were recorded, processed, and exported using Phylum Live software. By cropping the images, we eliminated vesicle drifting within the ~25 min period, for a better presentation of the main phenomenon.

Geometry model for vesicle shape transformations. Assuming that vesicle elongation results from increased surface area while vesicle volume is conserved, and that a cylindrical shape is most favorable, the lengths of the thread-like vesicles formed after growth are easily

calculated. Here we show that the predicted vesicle length agrees with the experimentally determined lengths.

Suppose that a spherical vesicle has a radius of r_1 . Its surface area is

$$S_1 = 4\pi r_1^2 \quad [1]$$

and its volume is

$$V_1 = 4/3\pi r_1^3 \quad [2]$$

Suppose that after micelle addition, this spherical vesicle has elongated to a thread-like vesicle (simplified as a cylinder, including the branched vesicles) with a radius (or average radius of all branches in a branched vesicle) of r_2 and length (or total length of all branches for a branched vesicle) of l . Neglecting the cylindrical end caps, its surface area is approximately

$$S_2 = 2\pi r_2 l \quad [3]$$

and its volume is

$$V_2 = \pi r_2^2 l \quad [4]$$

Consider that the encapsulated volume of a vesicle is unchanged,

$$V_1 = V_2 \quad [5]$$

From [2], [4], and [5], we get

$$4/3 \pi r_1^3 = \pi r_2^2 l \quad [6]$$

Multiply both sides by $12\pi r_1$, we get

$$16 \pi^2 r_1^4 = 12 \pi^2 r_2^2 l r_1 \quad [7]$$

That is

$$(4\pi r_1^2)^2 = 3(2\pi r_2 l)^2 r_1 / l \quad [8]$$

Substitute $4\pi r_1^2$ with S_1 , and $2\pi r_2 l$ with S_2 , we get

$$l/r_1 = 3(S_2/S_1)^2 \quad [9]$$

Under similar conditions of micelle addition, the efficiency of micelle incorporation is ~50%, as measured in previous studies (Chen and Szostak, 2004a). Therefore, when 5 equivalents of oleate micelles are added to a vesicle suspension containing ~1 mM oleic acid, the increase of surface area should be ~3.5-fold. In our experiment, as measured in Figure III.2 (A), the average surface area increase was ~3.7-fold (assuming that all membrane layers increase by the same proportion after reaching the steady state), which corresponds to a efficiency of micelle incorporation of 54%. According to formula [9], a spherical vesicle with an original radius of 2 μm , after a surface area increase of 3.7-fold ($S_2/S_1 = 3.7$), should have a length of ~82 μm . In comparison, the vesicle shown in Figure III.2 (A) is ~94 μm in length. The vesicles in Figure III.1 (B) average 96 ± 15 μm ($n = 10$) in length (branched vesicles were measured by summing up the total lengths of all branches using Phylum Live software).

Vesicle counting. An imaging assay was developed to count the total number of dye- or RNA-containing vesicles. A sample of 12 μl vesicle suspension was loaded into a disposable hemacytometer, which has a confined channel depth of 20 μm , and the total number of dye- or RNA-containing vesicles was counted from 20 non-overlapping, randomly taken images. A Nikon TE2000S inverted epifluorescence microscope with 10X CFI Plan Fluor ELWD DM objective lens was used for imaging. New vesicles that form *de novo* following micelle addition

do not contain fluorescent dye or RNA, and since they cannot be observed by fluorescence microscopy, their formation does not affect the counting of the fluorescently labeled vesicles.

FRET assay. The use of a FRET assay to measure surface area increase has been reported previously (Chen et al., 2004; Chen and Szostak, 2004a; Hanczyc et al., 2003). The assay measures the distance-dependent energy transfer between two fluorescent phospholipids anchored on the fatty acid vesicle membrane. As the membrane surface area increases by incorporating additional lipid molecules supplied as micelles, the FRET efficiency decreases, measured as an increase of donor fluorescence. FRET-dye-labeled vesicles were prepared by co-dissolving oleic acid, 0.2 mol % NBD-PE (N-(7-nitrobenz-2-oxa-1,3-diazol-4-yl)-1,2-dihexadecanoyl-*sn*-glycero-3-phosphoethanolamine; excitation at 430 nm, emission at 530 nm), and 0.2 mol % Rh-DHPE (LissamineTM rhodamine B 1,2-dihexadecanoyl-*sn*-glycero-3-phosphoethanolamine; emission at 586 nm) in methanol before rotary evaporation and resuspension in buffer. The vesicle suspension was treated as described above for the preparation of large monodisperse vesicles. Large (~4 μm in diameter) multilamellar FRET-dye-labeled vesicles were diluted 1:10 with the same buffer containing 0.8 mM oleic acid, to a final concentration of ~1 mM oleic acid, and loaded into a measuring cuvette in a Cary Eclipse fluorimeter (Varian, Australia). Oleate micelles (5 equivalents) were added to the cuvette 5 min after the recording had started. Immediately after adding micelles, a small volume of the vesicle suspension was removed from the cuvette, loaded into a disposable hemacytometer for microscopic observation, and incubated in parallel with the vesicles in the cuvette. After incubating for 30 min, the vesicle suspension in the cuvette was agitated using a pipette tip (instead of removing the cuvette for shaking), and allowed to stabilize for another 5 min before the second cycle of micelle addition. The addition of micelles and agitation causes artifactual

intensity spikes, which were eliminated and replaced with break signs in Figure III.2 (A). (The increasingly noisy relative surface area curve towards the end of the second cycle indicates that the measurement with the FRET assay is becoming less sensitive to the surface area changes at that range.) The control experiment of adding 5 equivalents of NaOH (i.e., 5 mM final NaOH, which does not perturb the pH significantly due to the 0.2 M bicine buffer) was performed as described above. The increase of surface area of decanoate:decanol (2:1) vesicles during growth was measured using the same method. In this experiment, 2 equivalents of decanoate micelles and 1 equivalent of decanol emulsion were added to the decanoate:decanol (2:1) vesicles (in 0.2 M Na-bicine, pH 8.5, at room temperature, ~20 mM initial amphiphile concentration). The decanol emulsion was made by dispersing decanol (with 1 mol % decanoate added) into 1 equivalent of NaOH solution, followed by sonication. This method produced small droplets of relatively stable decanol emulsion (validated by microscopy; data not shown); without the addition of 1 mol % decanoate, the decanol droplets were much less stable, owing to inter-droplet fusion.

Preparation of unilamellar fatty acid vesicles. The dehydration/rehydration method has been used for preparing unilamellar phospholipid vesicles (Karlsson et al., 2001; Karlsson et al., 2000; Karlsson et al., 2002), and was adapted here for preparing unilamellar fatty acid vesicles. Oleate vesicles (in 0.2 M Na-bicine, pH 8.5, 5 mM oleic acid concentration with 0.2 mol % Rh-DHPE) were extruded through a polycarbonate membrane with 100-nm-diameter pores. A sample of 5 μ l of the vesicle suspension was placed on a glass slide (VWR, West Chester, PA) and allowed to spread into a thin film (~2-cm-diameter area), and vacuum dried overnight. After 10-15 min, 25 μ l of buffer (0.2 M Na-bicine, pH 8.5; resulting in a final oleic acid concentration of ~1 mM) was placed on the glass slide, large unilamellar oleate vesicles formed.

Quantifying the critical shear rate for vesicle division. Though wide-bore pipette tips were used to avoid excessive fluid shear, pipetting a vesicle suspension resulted in enough shear stress for some of the thread-like vesicles to divide, giving false positive results in vesicle counting. Therefore, we used the complete disappearance of the thread-like vesicles as an alternative indicator to confirm vesicle division. (In a control experiment where no fluid shear was applied, a large number of thread-like vesicles were present.) The disappearance of the thread-like vesicles is unlikely to be caused by lysis of vesicles as a result of shear stress, as the number of dye-labeled vesicles did indeed increase and no leakage of fluorescent dye was detected in these experiments. (Both the cone and plate of the viscometer are made of stainless steel, and thus unlikely to disrupt the vesicle membrane through surface interactions.) A sample of 500 μl of large ($\sim 4 \mu\text{m}$ in diameter) multilamellar oleate vesicles (containing 2 mM HPTS) was loaded into a cone-plate viscometer (Brookfield, Middleboro, MA), and 5 equivalents of oleate micelles were added. After incubating for 30 min to allow for vesicle growth, the viscometer was started at a designated spinning speed (increased in successive trials) for 30 sec. A sample was taken out from the vesicle suspension and loaded into a disposable hemacytometer to monitor vesicle division.

Cycles of vesicle growth and division. In each cycle, 5 equivalents of oleate micelles were added to large ($\sim 4 \mu\text{m}$ in diameter) multilamellar oleate vesicles (containing 10 mM HPTS, in 0.2 M Na-glycine, pH 8.5, $\sim 1 \text{ mM}$ initial oleic acid) in an eppendorf tube. After micelle addition, a small aliquot of vesicles was loaded into a disposable hemacytometer for microscopic observation, and incubated in parallel with the vesicles in the eppendorf tube. After 30 min, the eppendorf tube was agitated briefly (by inverting the tube 6 times), and the vesicle shapes and

sizes were monitored. A portion of the sample was then diluted 1:10 with buffer to a final concentration of ~1 mM oleic acid to maintain this total oleic acid concentration at the beginning of each cycle. Before starting the second cycle, 5 equivalents of oleate micelles were added to the vesicles, allowing the vesicles to increase in volume and grow back to their original sizes in the absence of agitation for 24 hrs. The increase of vesicle volume dilutes the encapsulated fluorescent dye, and thus the contrast of the images in the second row of Figure III.2 (B) has been enhanced (the unenhanced original images are shown in Figure III.9, B). To quantify the number of dye-labeled vesicles and monitor the exponential increase of vesicle population, we repeated the growth and division of large (~4 μm in diameter) multilamellar oleate vesicles (containing 10 mM HPTS, in 0.2 M Na-bicine, pH 8.5, ~1 mM initial oleic acid) in 3 cycles, but without allowing vesicle volume to increase (since the dilution of fluorescent dye would make such vesicles too dim for counting). Similarly to the procedures described above, the sample was diluted 1:10 with buffer to a final concentration of ~1 mM oleic acid to maintain this total oleic acid concentration at the beginning of each cycle, and this dilution factor was later used to adjust the total vesicle count.

Measuring RNA leakage. A small fraction of the vesicle suspension (less than 3% of the sample volume, to avoid vesicle disruption) was separated from intact vesicles by ultrafiltration in microcentrifuge tubes with 10 kDa cutoff filters. The fluorescence of 5'-DY547-labeled RNA (excitation at 557 nm, emission at 574 nm) was determined using a Cary Eclipse fluorimeter. RNA concentration levels of 0% and 100% were measured using vesicles before division, and vesicles after the addition of 1% Triton X-100, respectively.

Results

Vesicle growth and division. To observe the growth of multilamellar vesicles in real time, we prepared large monodisperse oleate (C18:1) vesicles (~1 mM initial oleic acid concentration) containing 2 mM encapsulated HPTS (8-hydroxypyrene-1,3,6-trisulfonic acid trisodium salt, a water-soluble, membrane-impermeable fluorescent dye). After the addition of 5 equivalents (i.e., 5 times the initial amount of amphiphiles) of oleate micelles, a series of dramatic shape transformations occurred. The initially spherical vesicles first began to form thin tails that were only faintly fluorescent (Figure III.1, A). Over time, the spherical vesicles shrank and the tails grew in length and width as progressively more of the aqueous contents (labeled by fluorescent dye) migrated from the spherical vesicles into the tails. After ~30 min, the initially spherical vesicles had completely transformed into long thread-like vesicles with the dye-labeled aqueous contents more or less evenly distributed along the length of the filament (Figure III.1, B). No further shape transformation was observed for up to 2 hrs. Whether vesicles were free-floating, or attached to a glass or plastic slide surface, we observed similar vesicle shape transformations. The shape transformations observed during growth were not altered by labeling the aqueous contents with a different fluorescent dye, calcein (Bis[*N,N*-bis(carboxymethyl)aminomethyl] fluorescein), or by labeling the membrane itself with a membrane-localized dye, Marina blue-DHPE (Marina Blue® 1,2-dihexadecanoyl-*sn*-glycero-3-phosphoethanolamine) or Rh-DHPE (LissamineTM rhodamine B 1,2-dihexadecanoyl-*sn*-glycero-3-phosphoethanolamine). Finally, we observed the same growth-associated shape transformations with oleate vesicles ranging from 0.5 to 10 μm in diameter.

The highly elongated shape of the thread-like vesicles suggested that they might be sufficiently fragile to divide in response to mild shear forces, thus avoiding membrane rupture and subsequent contents release. To test this idea experimentally, we loaded a sample of large multilamellar oleate vesicles (containing 2 mM HPTS, ~1 mM initial oleic acid) into a single-depression glass slide, added 5 equivalents of oleate micelles, and allowed ~25 min for the vesicles to grow into thread-like shapes (Figure III.1, D-F; Figure III.7, A, B). We then gently agitated the vesicle suspension by repeatedly blowing puffs of air onto the sample from a distance of about 0.5 m using a compressed air canister. We observed that the thread-like vesicles divided into multiple smaller spherical daughter vesicles (Figure III.1, G, H; Figure III.7, C, D). These daughter vesicles were distinctly separate from each other, gradually moving apart in random directions by Brownian motion. The daughter vesicles were brightly fluorescent, showing that most of the encapsulated contents were retained during division.

To quantify the fluid shear required for the division of thread-like vesicles, we used a cone-plate viscometer to measure the critical shear rate under controlled fluid shear. We determined that the critical shear rate for thread-like multilamellar vesicles to divide was 15 sec^{-1} , corresponding to a shear stress of 0.35 dynes/cm^2 (fluid viscosity measured 2.3 cP). Spherical multilamellar vesicles, prepared with the same fatty acid and buffer, remained undisrupted under the same or higher shear rates of up to $1,500 \text{ sec}^{-1}$ (the maximum shear rate measurable by our instrument). This suggests that the division of thread-like multilamellar vesicles is unlikely to be caused by simple membrane rupture, but rather through more complex mechanism (e.g., vesicle pearling under Plateau-Rayleigh instability, as previously observed with tubular phospholipid vesicles under surface tension induced by a laser tweezer (Bar-Ziv and Moses, 1994)). The mechanism of the division for thread-like multilamellar vesicles under modest shear forces

remains largely unclear and will require in-depth future studies. We also found that large unilamellar vesicles were very fragile. On exposure to gentle fluid shear (190 sec^{-1}), some of the vesicles were disrupted and a significant fraction of the encapsulated contents were released into the solution (Figure III.12). In addition, some of the originally unilamellar vesicles transformed into multilamellar vesicles, as observed by confocal microscopy (Figure III.5, H). How this occurred remains unclear, but may involve partial membrane fragmentation and reorganization in response to shear forces. In contrast, multilamellar vesicles can divide under a much high shear rates ($> 1,500 \text{ sec}^{-1}$) without disruption or loss of contents. In a prebiotic, wind-agitated pond, the shear rate induced by wind could easily exceed 15 sec^{-1} , and might often reach much higher values. Vesicles that could divide robustly under a wide range of shear rates without membrane disruption would therefore have an advantage in terms of decreased loss of contents (including genetic polymers) to the environment. We can simplify the scenario of wind blowing over the surface of a prebiotic pond as a case of simple shear in laminar flow in water (a Newtonian fluid), where the shear rate can be expressed as a gradient of velocity. We assume that the velocity at the fluid surface is the same as the speed of a typical wind at 5 m/s ($\sim 11 \text{ mph}$), and the fluid at the bottom of the pond is static. The shear rate in such a body of fluid is a function of its depth: 5 sec^{-1} for a depth of 1 m , 50 sec^{-1} for a depth of 0.1 m , or 500 sec^{-1} for a depth of 1 cm . Thus the closer to the shore, the higher the shear rate. In reality, the presence of waves, vortices, and turbulent flow may produce complex flow fields with a wide range of shear rates.

Having observed efficient growth and division following the addition of 5 equivalents of fatty acid to pre-formed vesicles, we asked whether efficient division could still occur following a smaller extent of growth. When vesicles were fed with smaller quantities of micelles (1

equivalent), they grew to the sphere-tail intermediate stage, at which point gentle agitation was still able to induce division (Figure III.8). In contrast, without micelle addition, vesicles remained spherical and were unable to divide by gentle agitation alone (Figure III.8, I). Vesicle division at the sphere-tail intermediate stage did not occur by simple “tearing-off” of the tail, but rather through redistribution of the encapsulated contents into the widening tail portion, followed by division into multiple progeny vesicles (Figure III.8, B-E). As observed by confocal microscopy, the majority of daughter vesicles were multilamellar after division. Hence, when only small quantities of micelles are added, and fluid agitation is present at the sphere-tail intermediate state of growth, vesicles can still divide into multiple progeny.

We determined the efficiency of fatty acid incorporation into growing vesicles by measuring the increase in vesicle surface area by two independent methods. First, we measured the surface area of individual vesicles before and after growth by analyzing high-resolution images; the results are approximate but suggest an increase of surface area by ~4-fold following the addition of 5 equivalents of oleate micelles to oleate vesicles. Before growth, the vesicle diameter measured $\sim 3.1 \mu\text{m}$, which corresponds to a surface area of $\sim 30.2 \mu\text{m}^2$ and a volume of $\sim 15.6 \mu\text{m}^3$. After growth, the thread-like vesicle length measured $\sim 81.1 \mu\text{m}$ and the width measured $0.49 \pm 0.02 \mu\text{m}$ (this scale is close to the resolution limit of optical microscopy, and results in larger measurement error), which corresponds to an estimated surface area of $\sim 124.8 \pm 5.1 \mu\text{m}^2$ (~4-fold increase from that before growth) and an estimated volume of $\sim 15.3 \pm 0.6 \mu\text{m}^3$. We then used a fluorescence assay based on Förster resonance energy transfer (FRET) to monitor the growth of oleate vesicles labeled by donor and acceptor membrane dyes (Chen and Szostak, 2004a; Chen and Szostak, 2004b; Hanczyc et al., 2003). After the addition of 5 equivalents of oleate micelles, we took a small sample out of the measuring cuvette, and observed the vesicles

growing into thread-like shapes on a glass slide (Figure III.2, A, micrographs). Meanwhile, we observed increasing donor fluorescence, corresponding to increasing membrane surface area, in the remainder of the sample. The membrane surface area increased by ~3.7-fold at 25 min after the addition of 5 equivalents of oleate micelles (Figure III.2, A). Thus both microscopic and FRET data suggest a 50-60% efficiency of incorporation of added fatty acid into pre-formed vesicles by this growth pathway, which is consistent with the results from previous studies (Chen and Szostak, 2004a).

Cycles of growth and division. Having demonstrated both growth and division of large multilamellar vesicles, we proceeded to examine multiple cycles of vesicle growth and division. First, we monitored 2 rounds of oleate vesicle growth and division using the FRET assay to confirm the increase in membrane surface area in both growth phases, and microscopy to monitor the shape transformations and division in both cycles (Figure III.2, A, micrographs). We then tested complete cycles of vesicle growth and division in a more prebiotically plausible buffer: glycine, the most abundant of the many amino acids found in a wide range of Miller-Urey-type prebiotic synthesis experiments (Miller, 1953; Miller and Urey, 1959). We monitored 2 cycles of vesicle growth and division, and observed that in each cycle, oleate vesicles (containing 10 mM HPTS, in 0.2 M Na-glycine, pH 8.5, ~1 mM initial oleic acid) grew into thread-like shapes after the addition of 5 equivalents of oleate micelles, and divided into spherical progeny after agitation (Figure III.2, B). Between each cycle, after the addition of 5 equivalents of micelles and in the absence of agitation for 24 hrs, the slowly permeable solute, glycine, equilibrates across the vesicle membranes, allowing the vesicles to increase in volume (Figure III.2, B; Figure III.9). In a true protocell containing a replicating genome, the replication of the genome could also contribute to the osmotically driven volume recovery between cycles

of growth and division (Chen et al., 2004). Finally, we used an imaging assay to count the number of daughter vesicles containing fluorescent dye, in order to monitor the vesicle population over 3 cycles of growth and division in bicine (*N,N*-Bis(2-hydroxyethyl)glycine) buffer (without volume recovery, which would dilute the fluorescent dye and compromise the counting assay). We found that the vesicle count increased exponentially ($r^2 > 0.99$) (Figure III.10), as would be expected if the efficiency of growth and division was constant in each cycle.

We were interested in whether the protocell growth and division cycle described above might also function in a more prebiotically plausible chemical environment, and this might represent a possible pathway for the reproduction of early protocells. We therefore prepared oleate vesicles (containing 2 mM HPTS, ~1 mM initial oleic acid) in a mixture of amino acids (60 mM glycine, 30 mM alanine, 10 mM aspartate, and 10 mM glutamate, pH 8.5) that partially mimics the outcome of Miller-Urey-type experiments (Miller, 1953; Miller and Urey, 1959), as well as amino acids found in carbonaceous chondrite meteorites (Kvenvolden et al., 1970). (Volatile compounds such as ammonia and acetic acid cannot accumulate to high concentrations.) We observed similar growth and division of vesicles in this mixed amino acid solution (Figure III.4, A, E). We also observed similar growth and division of oleate vesicles in glycine buffer and in Tris buffer (both at pH 8.5; data not shown), which, together with the previously described results, indicates that vesicle growth and division can occur under a variety of solution conditions.

Growth and division of RNA-containing model protocells. To mimic protocells containing a nucleic acid genome and test the redistribution of encapsulated genetic molecules into daughter vesicles after division, we prepared oleate vesicles containing encapsulated RNA molecules

(DY547-A₁₀, dye-labeled polyadenylic acid, 0.5 mM). We then repeated the vesicle growth experiment by adding 5 equivalents of oleate micelles to the pre-formed oleate vesicles, and observed the same vesicle shape transformations as previously seen with dye-labeled vesicles (Figure III.3, A, B). We next monitored vesicle division with redistribution of encapsulated RNA molecules into progeny using the vesicle counting assay. After inducing division by agitation, we observed a ~6-fold increase in vesicle count (Figure III.3, C), just as seen previously with dye-labeled vesicles. After division, only a trace amount of RNA leakage from vesicles was detected (Figure III.3, D). In contrast, the artificial means of vesicle division by extrusion is much less efficient in that ~40% of the encapsulated RNA leaked out.

Prebiotically plausible protocell membranes. Although oleate vesicles are an excellent model system for the study of protocell membranes (Chen et al., 2004; Chen and Szostak, 2004b; Hanczyc et al., 2003; Walde et al., 1994), shorter-chain, saturated fatty acids are more likely components of prebiotic membranes. We therefore examined the growth and division of multilamellar vesicles composed of two shorter-chain fatty acids: myristoleic (C14:1) and decanoic (C10:0) acids. After the addition of 5 equivalents of the corresponding fatty acid micelles, these vesicles grew into thread-like shapes (Figure III.4, B, C). They also divided, as expected, upon gentle agitation (Figure III.4, F, G).

Prebiotic vesicles were most likely composed of mixtures of amphiphiles. Notably, many such mixtures, such as decanoate:decanol (2:1), generate vesicles that are stable under a wider range of pH and ionic conditions, and are more permeable to nutrient molecules than pure fatty acid vesicles (Chen et al., 2004; Mansy et al., 2008). However, a 2:1 decanoate:decanol mixture does not form micelles at high pH, and it was therefore necessary to investigate alternative

means of feeding such vesicles. We found that a combination of decanoate micelles and decanol emulsion led to efficient growth of 2:1 decanoate:decanol vesicles (Figure III.4, D; Figure III.11), which were able to divide and redistribute the encapsulated RNA molecules into daughter vesicles without significant leakage (Figure III.3, E, F). Finally, when we added oleate micelles to POPC (1-palmitoyl-2-oleoyl-*sn*-glycero-3-phosphocholine) vesicles, which are more closely related to modern cell membranes and can maintain a pH gradient across the membrane (Chen and Szostak, 2004b), they also went through similar shape transformations. These observations suggest that the growth of multilamellar vesicles through a series of shape transformations is a phenomenon that occurs with vesicles composed of a wide variety of lipids and lipid mixtures.

Mechanism of initiation of filamentous vesicle growth. The increased vesicle surface area that follows the addition of micelles must, in the absence of a corresponding volume increase, lead to a change in vesicle shape. As shown above, when micelles are added quickly to pre-formed vesicles, vesicle surface area increases rapidly (Figure III.2, A). Since the buffer solutes (e.g., bicine, glycine or other amino acids) are impermeable to oleate membranes on this timescale (Chen and Szostak, 2004b), the vesicle volume cannot increase through the equilibration of external and internal solutes. Estimates of vesicle volume derived from the analysis of high-resolution optical images are consistent with this prediction. In comparison, previous studies of reduced volume (e.g., sub-spherical) phospholipid vesicles have shown that a wide variety of shapes can be generated, such as vesicles with bead-like protrusions (Bozic et al., 2002), as summarized in shape versus volume phase diagrams (Dobereiner, 2000a; Dobereiner, 2000b). However, none of these forms resembles the growth intermediate of a spherical vesicle decorated with one or two thin tail-like protrusions that we have observed.

To account for the unusual growth mode that we observed, we hypothesized that during the early stages of vesicle growth, the added fatty acid molecules first encounter the outermost membrane, which therefore grows faster than the inner membrane layers. Since the volume between the outermost membrane and the inner membrane layers (inter-membrane volume) is small, and cannot increase on the time-scale of membrane surface growth, the outermost membrane can only grow by forming protrusions (Figure III.5, A). At later times, the inner membrane layers may also grow and spread throughout the growing thread-like vesicle. To test this idea, we first asked whether the multilamellar structure of vesicles was essential for the formation of thin tail-like protrusions during growth. We began by examining our initial spherical vesicles and sphere-tail growth intermediates by confocal microscopy, using a membrane-localized fluorescent dye to image the vesicle membranes. The initially spherical vesicles were clearly multilamellar (Figure III.5, B). At ~10 min after micelle addition, one or a few of the outer membrane layers formed a tail-like protrusion, while the inner membrane layers remained spherical (Figure III.5, C). After division, the daughter vesicles remained multilamellar, allowing for subsequent cycles of efficient growth and division to occur with the multilamellar progeny (Figure III.5, D). To directly test the hypothesis that the multilamellar structure of vesicles played an important role in their shape transformations following micelle addition, we prepared unilamellar oleate vesicles by a modified dehydration/rehydration method (Karlsson et al., 2001; Karlsson et al., 2000). We observed that, in contrast to the growth of multilamellar vesicles, unilamellar vesicles elongated symmetrically into tubular shapes without forming tails during growth (Figure III.5, G).

Finally, we further tested the hypothesis that the vesicle shape transformation through sphere-tail growth intermediates is a consequence of volume conservation, due to the slow permeability of buffer solutes. We prepared large multilamellar oleate vesicles in ammonium acetate (0.2 M, pH 8.5) buffer, a solute that is highly permeable to vesicle membranes as a result of its equilibrium with ammonia (NH_3) and acetic acid (CH_3COOH) (Figure III.6, A). The rapid permeation of these neutral species allows vesicle volume to increase significantly during growth, resulting in maintenance of spherical vesicle shapes and the complete absence of formation of sphere-tail intermediates. By confocal microscopy, we observed that the growth of the outermost membrane had indeed outpaced that of the inner membrane layers, such that the inter-membrane volume increased significantly (Figure III.6, C). When multilamellar oleate vesicles containing 2 mM HPTS (a membrane-impermeable dye) grew in ammonium acetate buffer, the fluorescence intensity in the inter-membrane space decreased due to the dilution of the fluorescent dye, reflecting the influx of solutes and water into the inter-membrane space (Figure III.6, E).

Discussion

The pathway for protocell growth and division that we have described is robust, in that it operates over a wide range of lipid compositions, solutes, shear rates, and vesicle sizes. This allows for considerable flexibility in the design of more complete or sophisticated protocell models involving the integration of replicating membrane and genetic systems. In this new pathway, growth and division are naturally coupled, in that growth leads to the formation of fragile thread-like vesicles that are predisposed to divide. In a fluid environment of modest shear forces, growth inevitably leads to division, so that no additional built-in mechanism is needed to coordinate growth and division. Such coupling of growth and division constitutes a significant simplification for efforts to map out a pathway for the synthesis of artificial forms of cellular life. On the other hand, many of the physical properties of model protocell membranes such as permeability (Mansy et al., 2008; Sacerdote and Szostak, 2005), thermostability (Mansy and Szostak, 2008), and competition (Chen et al., 2004) have so far been examined only with small unilamellar vesicles, and thus we are currently re-examining these properties in the context of large multilamellar vesicles.

A population of growing and dividing vesicles, while reminiscent of a population of growing and dividing cells, cannot evolve to the greater complexity required for adaptation to a changing environment without some form of heritable genetic information. A complete model of a simple protocell therefore requires the addition of a genome that can replicate within the membrane-bound compartment and be inherited by daughter protocells. The pathway for protocell growth and division shown here allows short RNA strands dissolved in the aqueous contents of parental vesicles to be randomly redistributed into their daughter vesicles in amounts proportional to their

volume, without significant leakage. This pathway is compatible with several distinct models of protocell genome replication, such as ribozyme catalyzed RNA replication (Johnston et al., 2001), or spontaneous chemical replication (Mansy et al., 2008), where short strands of RNA, DNA, or perhaps some other genetic polymer constitute the genome. Any catalytically or structurally useful genetic polymer that promoted faster protocell self-replication would tend to increase in frequency within a population of growing and dividing vesicles, providing a possible route for the emergence of Darwinian evolutionary behavior among protocells (Chen et al., 2004; Szostak et al., 2001).

We suggest that the simplicity of the conditions required for artificial protocell growth and division makes it plausible that similar processes might have occurred on the early Earth. Repeated cycles of growth and division, in which both the parental membrane material and aqueous contents are transmitted to progeny, could have been a common phenomenon in environments providing an episodic source of fatty acids to an aqueous reservoir. The energy source for the division of thread-like vesicles is simply the kinetic energy of mildly agitated liquid water which is common in many natural environments. These conditions are far simpler than might have been expected in view of the remarkable complexity of modern cellular growth and division, and are simpler than those proposed in previous models (Hanczyc et al., 2003; Hanczyc and Szostak, 2004; Szostak et al., 2001). While specific scenarios are easy to imagine (vesicles in a wind-agitated pond, fed with fatty acid micelles from an alkaline hot spring source of fatty acids synthesized by Fischer-Tropsch type chemistry at depth), they are poorly constrained due to our lack of detailed knowledge of plausible pathways for prebiotic fatty acid synthesis, which should be a priority for future studies in prebiotic chemistry.

Our experiments lead to a series of intriguing questions concerning protocell membranes, e.g., why only one or two tail-like protrusions emerge from a growing vesicle, and what forces drive the transfer of fatty acids from the outermost to inner membrane layers at the later stage of vesicle growth, resulting in their elongation into thread-like shapes. With respect to division, it is important to determine the mechanism of the shear-induced division of thread-like vesicles, e.g., whether the tension-induced pearling instability (Bar-Ziv and Moses, 1994) plays a role (Figure III.7, C). A better understanding of the underlying mechanisms will facilitate the design of artificial living systems, and may also lead to greater insight into the origin of cellular life.

Figures

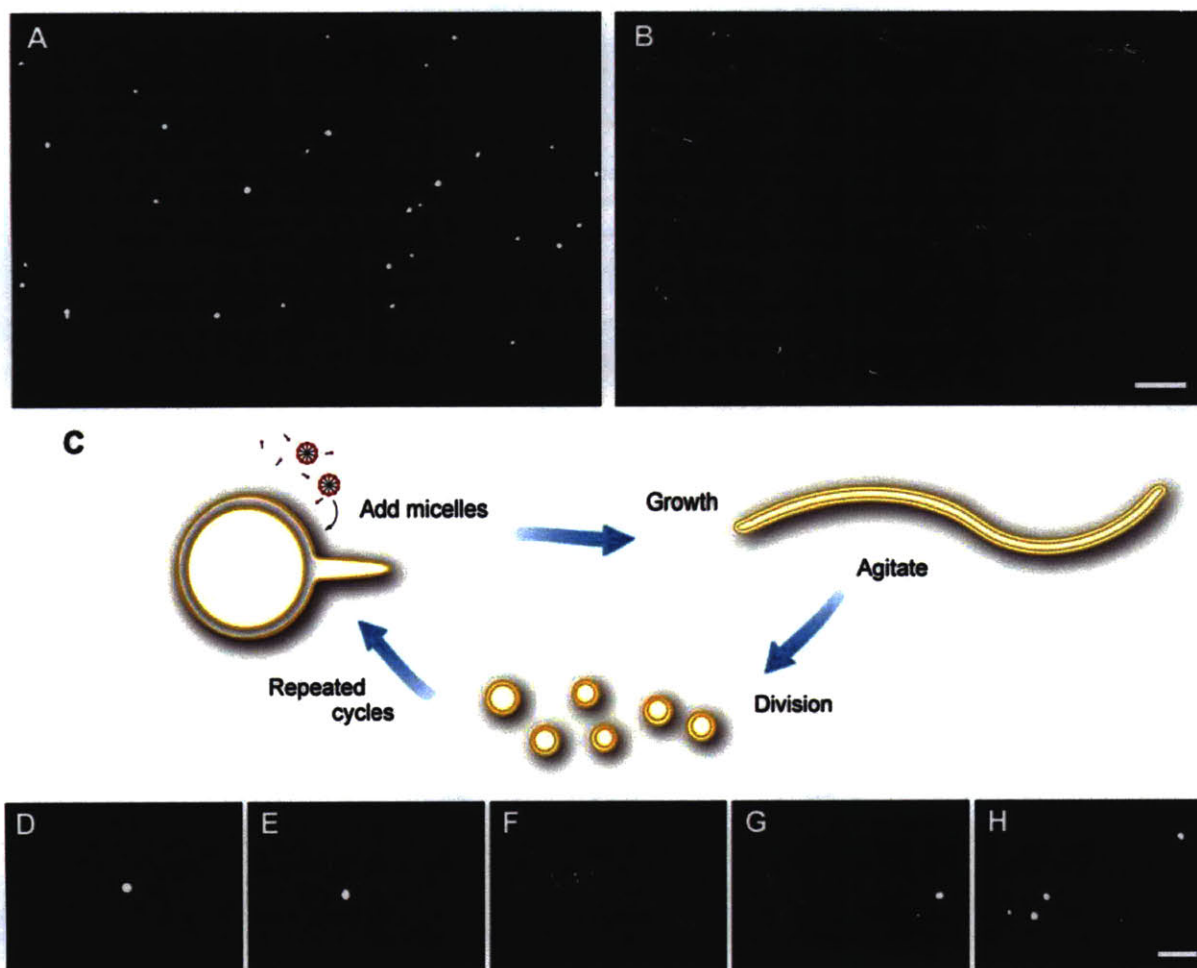


Figure III.1 Vesicle growth and division. (A, B) Epifluorescence micrographs of vesicle shape transformations during growth, 10 min and 30 min after the addition of 5 equivalents of oleate micelles to multilamellar oleate vesicles (in 0.2 M Na-bicine, pH 8.5, ~1 mM initial oleic acid), respectively. All vesicles were labeled with 2 mM encapsulated HPTS, a water-soluble fluorescent dye, in their internal aqueous space. Scale bar, 50 μm . (C) Schematic diagram of cyclic multilamellar vesicle growth and division: vesicles remain multilamellar before and after division (shown as, but not limited to two layers). (D-F) Growth of a single multilamellar oleate vesicle, 3 min, 10 min, and 25 min after the addition of 5 equivalents of oleate micelles,

respectively. (G, H) In response to mild fluid agitation, this thread-like vesicle divided into multiple smaller daughter vesicles. Scale bar for (D-H), 20 μm .

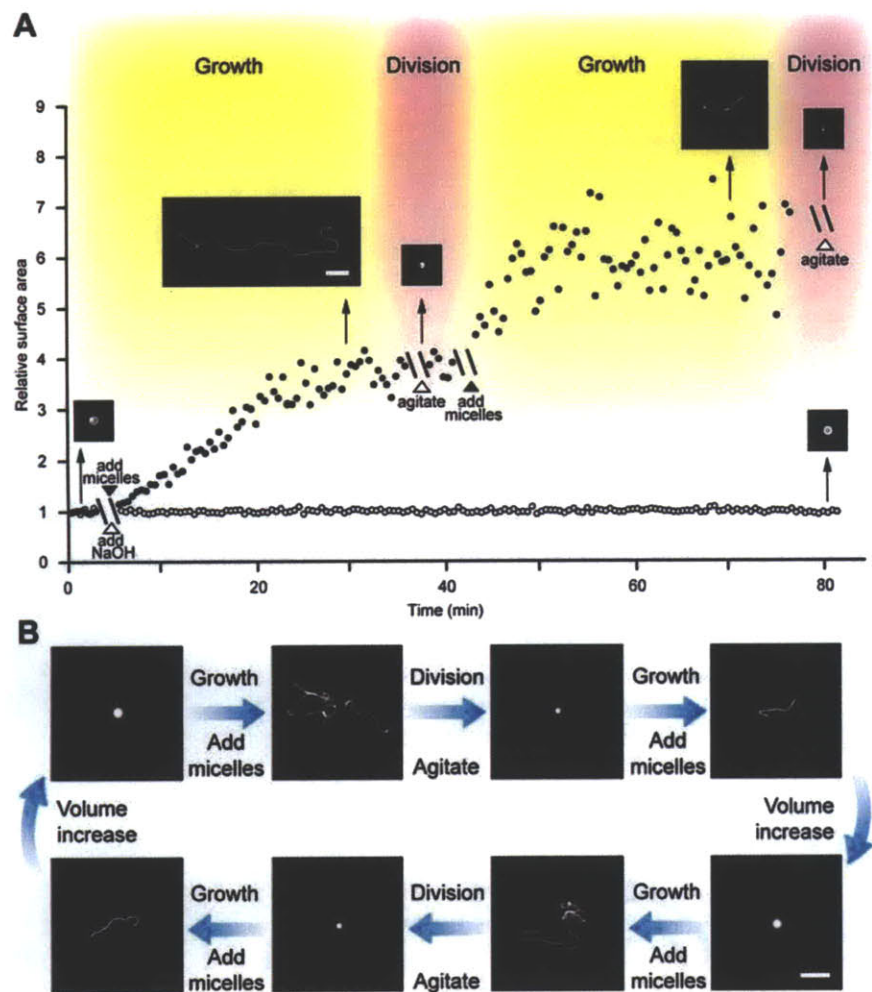


Figure III.2 Cycles of vesicle growth and division. (A) Relative surface area after two cycles of addition of 5 equivalents of oleate micelles (solid circles) or 5 equivalents of NaOH (open circles) to oleate vesicles, each followed by agitation. Inset micrographs show vesicle shapes at indicated times. Scale bar, 10 μm . (B) Vesicle shapes during cycles of growth and division in a model prebiotic buffer (0.2 M Na-glycine, pH 8.5, ~ 1 mM initial oleic acid, vesicles contain 10 mM HPTS for fluorescence imaging). Scale bar, 20 μm .

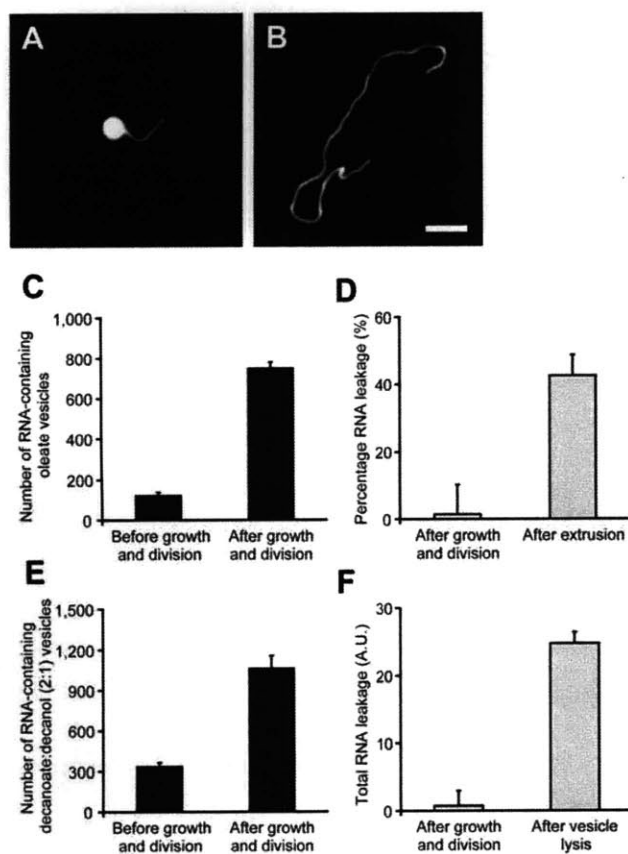


Figure III.3 Growth of vesicles containing encapsulated RNA, and redistribution of RNA molecules into daughter vesicles. (A, B) Oleate vesicle (in 0.2 M Na-bicine, pH 8.5, ~1 mM initial oleic acid) containing 5'-DY547-labeled RNA (DY547-A₁₀, 0.5 mM) at 10 min and 30 min after the addition of 5 equivalents of oleate micelles, respectively. Scale bar, 10 μ m. (C) Number of RNA-containing oleate vesicles before and after division, n = 3. (D) Percentage RNA leakage after the division of thread-like oleate vesicles by agitation, versus the leakage from 4- μ m-diameter vesicles extruded through 2 μ m pores, n = 3. (E) Number of RNA-containing decanoate:decanol (2:1) vesicles (in 0.2 M Na-bicine, pH 8.5, at room temperature, ~20 mM initial amphiphile concentration) before and after division, n = 3. (F) Total amount of RNA leakage from decanoate:decanol (2:1) vesicles after division, versus the leakage from vesicles lysed by adding 1% Triton X-100, n = 3.

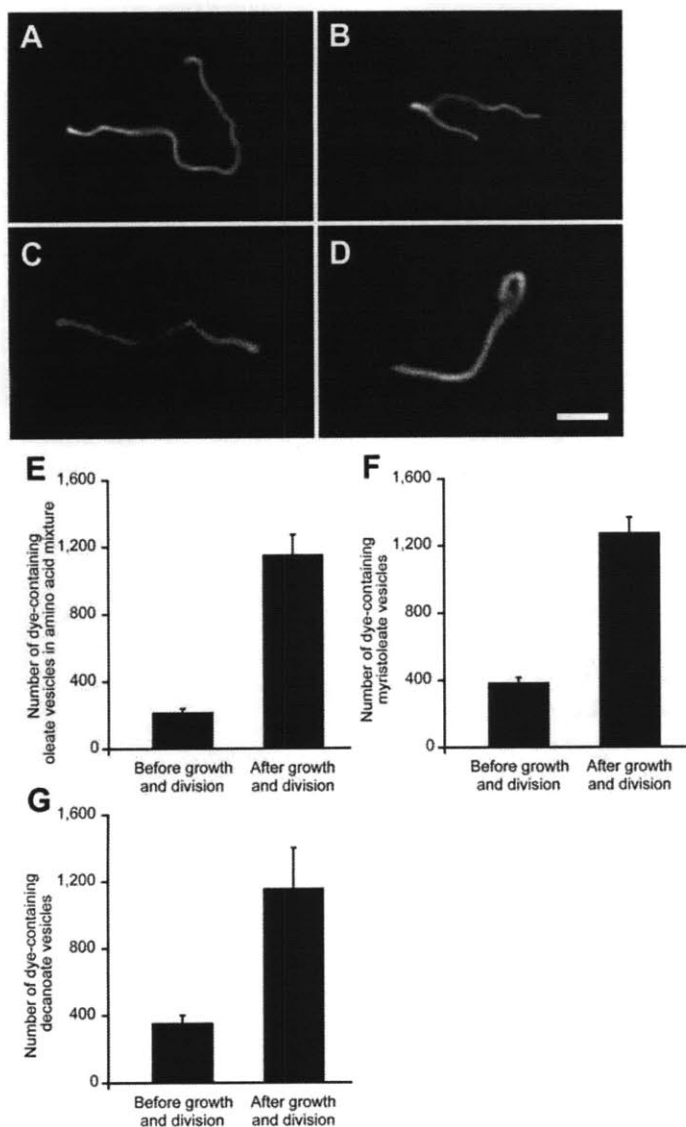


Figure III.4 Vesicle growth and division in various buffers and with various lipid

compositions. (A) Oleate vesicle (containing 2 mM HPTS, in 60 mM Na-glycine, 30 mM Na-alanine, 10 mM Na-aspartate, and 10 mM Na-glutamate, pH 8.5, ~1 mM initial oleic acid) at 30 min after the addition of 5 equivalents of oleate micelles. (B) Myristoleate vesicle (containing 2 mM HPTS, in 0.2 M Na-bicine, pH 8.5, ~4 mM initial myristoleic acid) at 30 min after the addition of 5 equivalents of myristoleate micelles. (C) Decanoate vesicle (containing 2 mM HPTS, in 0.2 M Na-bicine, pH 7.4, at 50 °C, ~60 mM initial decanoic acid) at 30 min after the addition of 1.7 equivalents of decanoate micelles. (D) Decanoate:decanol (2:1) vesicle

(containing 2 mM HPTS, in 0.2 M Na-bicine, pH 8.5, at room temperature, ~20 mM initial amphiphile concentration) at 30 min after the addition of 2 equivalents of decanoate micelles and 1 equivalent of decanol emulsion. Scale bar for (A-D), 10 μ m. (E) Number of dye-containing oleate vesicles in a mixed amino acid solution (conditions as above) before and after growth and division, n = 3. (F) Number of dye-containing myristoleate vesicles (conditions as above) before and after growth and division, n = 3. (G) Number of dye-containing decanoate vesicles (conditions as above) before and after growth and division, n = 3.

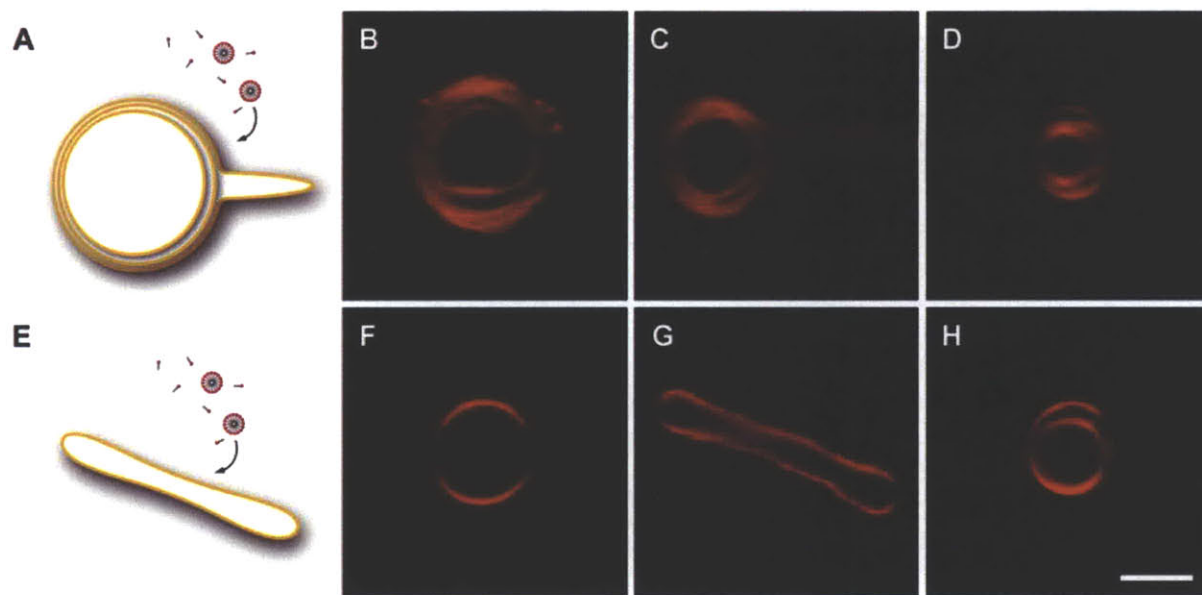


Figure III.5 Growth of multilamellar versus unilamellar vesicles. (A) Schematic diagram of incorporation of micelles into a multilamellar vesicle: the outermost membrane grows faster than the inner membrane layers. (B, C) Confocal images of multilamellar oleate vesicle (0.2 mol % Rh-DHPE, in 0.2 M Na-bicine, pH 8.5, ~1 mM initial oleic acid) before, and 10 min after the addition of 1 equivalent of oleate micelles, respectively. (D) Confocal image of multilamellar vesicle after division. (E) Schematic diagram of incorporation of micelles into a unilamellar vesicle. (F, G) Confocal images of unilamellar oleate vesicle (conditions as above) before, and 10 min after the addition of 1 equivalent of oleate micelles, respectively. (H) Confocal image of a multilamellar vesicle formed after the agitation of elongated unilamellar vesicles. Scale bar for (B-D; F-H), 2 μm .

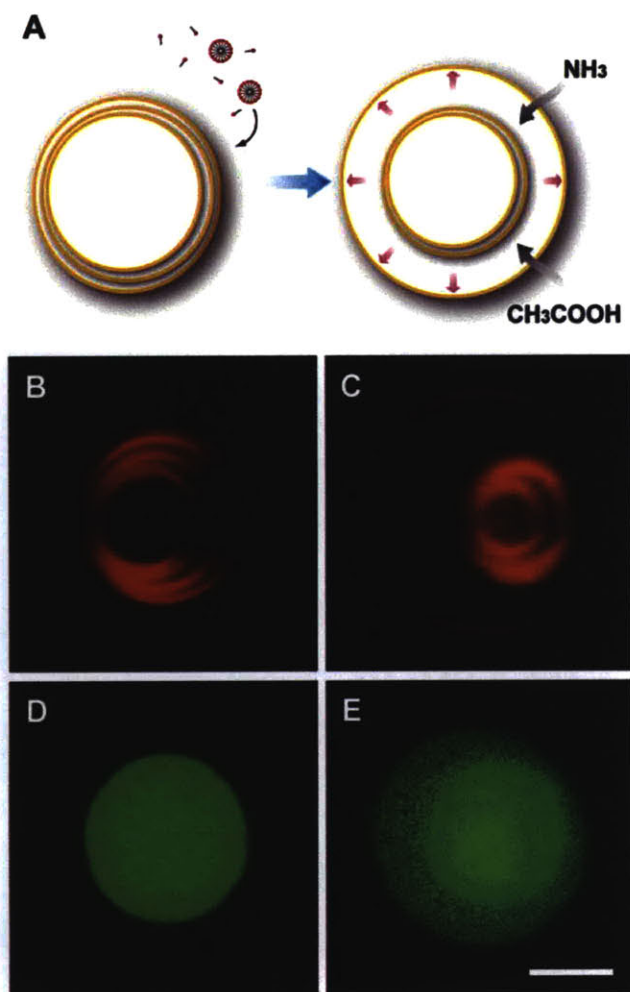


Figure III.6 Vesicle growth in a highly permeable buffer. (A) Schematic diagram of growth of a multilamellar vesicle in ammonium acetate: as the surface area of the outermost membrane increases, the solutes in their neutral forms (NH_3 and CH_3COOH) permeate the membrane, allowing the internal volume to increase. (B, C) Confocal images of multilamellar oleate vesicle (0.2 mol % Rh-DHPE, in 0.2 M ammonium acetate, pH 8.5, ~ 1 mM initial oleic acid) before, and 10 min after the addition of 1 equivalent of oleate micelles, respectively. (D, E) Confocal images of multilamellar oleate vesicle (containing 2 mM HPTS, in 0.2 M ammonium acetate, pH 8.5, ~ 1 mM initial oleic acid) before, and 10 min after the addition of 1 equivalent of oleate micelles, respectively. Scale bar for (B-E), 2 μm .

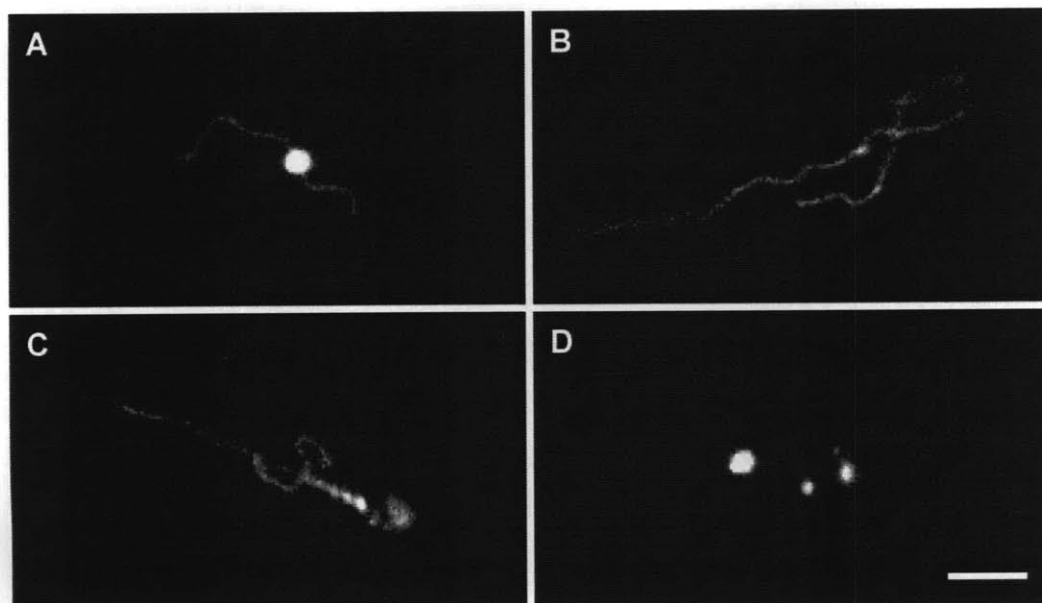


Figure III.7 An additional example of vesicle growth and division. Conditions as in Figure III.1, D-H. (A, B) Oleate vesicle growth at 10 min and 30 min after the addition of 5 equivalents of oleate micelles, respectively. (C, D) Under mild fluid agitation, this thread-like vesicle divided into multiple smaller daughter vesicles. Scale bar, 10 μm .

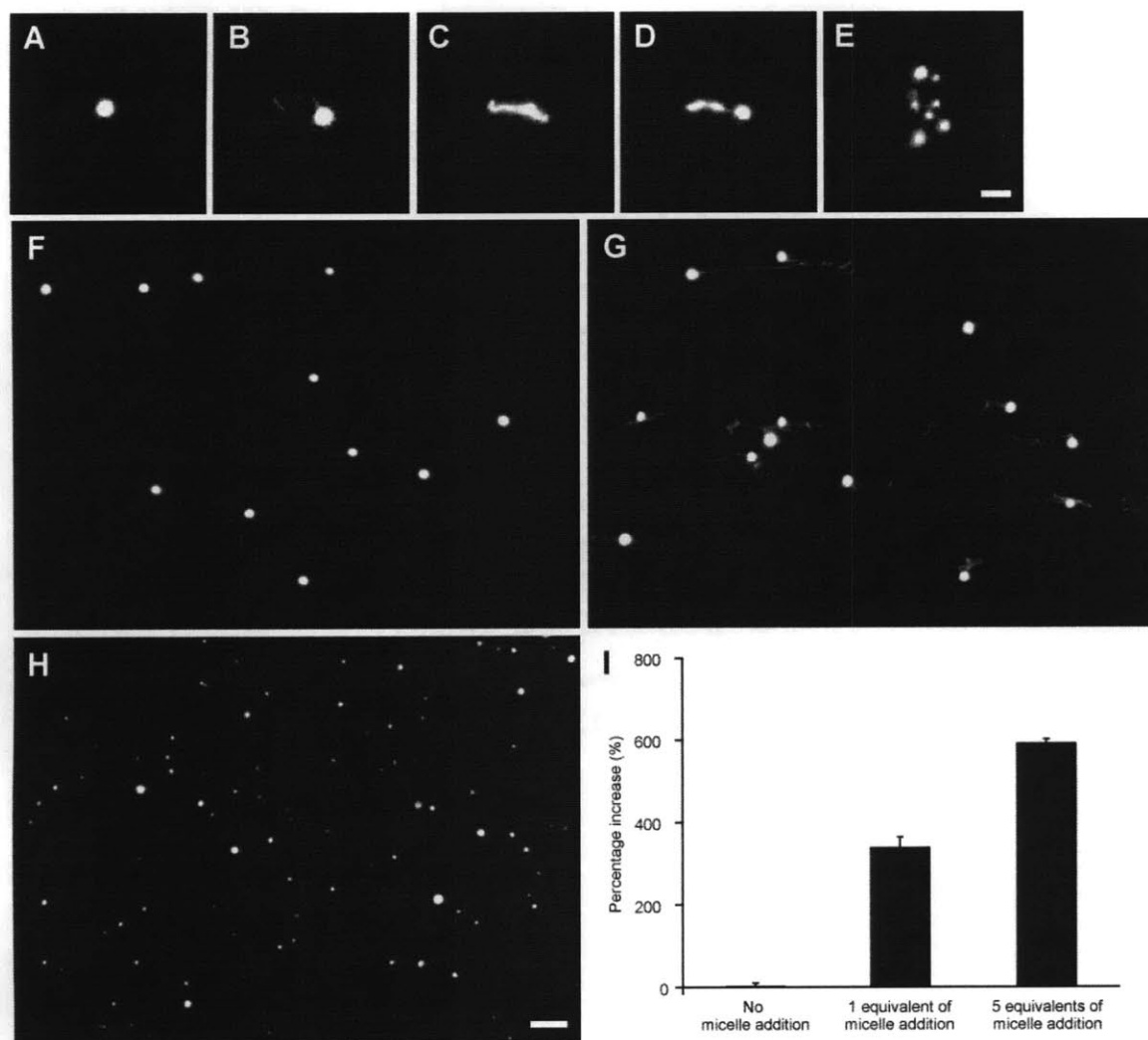


Figure III.8 Vesicle growth and division after the addition of small quantities of micelles.

(A, B) Oleate vesicle (containing 2 mM HPTS, in 0.2 M Na-bicine, pH 8.5, ~1 mM initial oleic acid) immediately, and 10 min after the addition of 1 equivalent of oleate micelles, respectively.

(C-E) In response to mild fluid agitation, this thread-like vesicle divided into multiple smaller daughter vesicles. Scale bar for (A-E), 10 μm . (F) Image for vesicle counting before growth and division.

(G) Vesicle shapes at 30 min after the addition of 1 equivalent of oleate micelles (no further shape transformation was observed after 30 min, up to 2 hrs), and (H) image for vesicle counting after agitation, 30 min after the addition of micelles.

(I) Percentage increases in the number of oleate vesicles from a baseline count after brief agitation, 30 min after the addition of

0, 1, and 5 equivalents of oleate micelles, respectively, suggesting that the efficiency of vesicle growth and division is influenced by the amount of fatty acid micelles added, $n = 3$. Scale bar for (F-H), 20 μm .

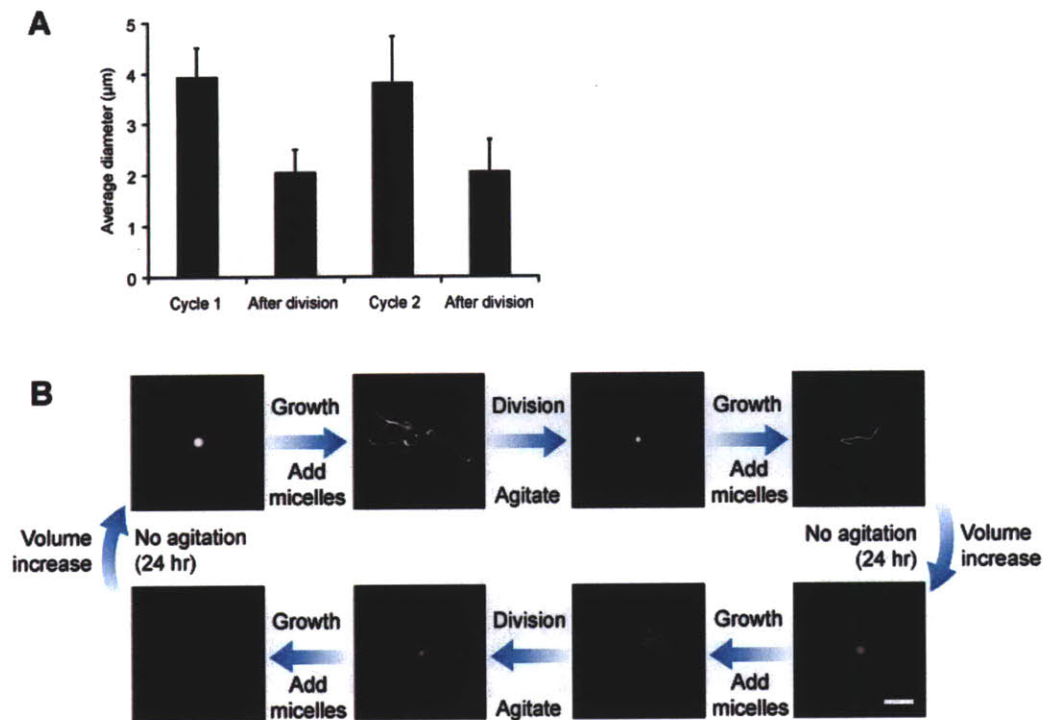


Figure III.9 Vesicle shapes during cycles of growth and division in a model prebiotic

buffer. (A) Average vesicle diameters before and after division in 2 cycles, $n = 10$. (B) Vesicle shapes in cycles of growth and division (in 0.2 M Na-glycine, pH 8.5, ~1 mM initial oleic acid, vesicles contain 10 mM HPTS for fluorescence imaging). Dimmer images in the second row reflect the dilution of the encapsulated fluorescent dye during vesicle volume increase. (Same images with enhanced contrast are shown in Figure III.2, B.) Scale bar, 20 μm .

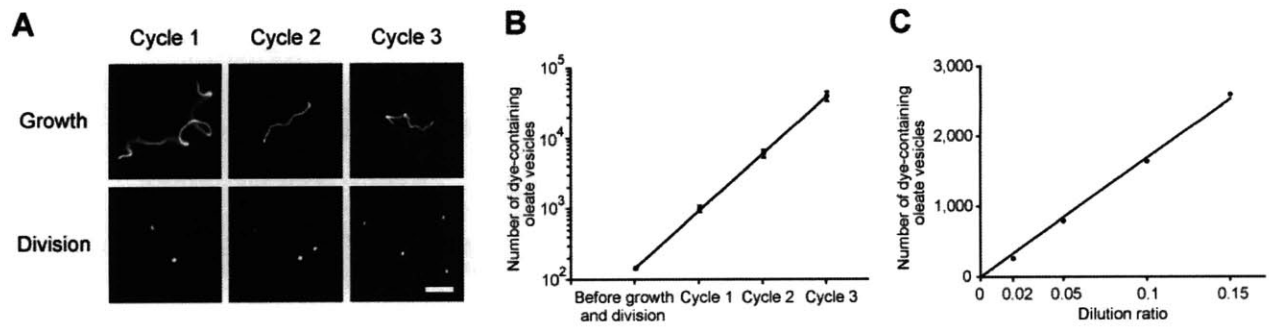


Figure III.10 Three sequential cycles of vesicle growth and division. (A) Vesicle shapes in cycles of growth and division (containing 10 mM HPTS, in 0.2 M Na-bicine, pH 8.5, ~1 mM initial oleic acid). Scale bar, 10 μ m. (B) Total number of dye-labeled oleate vesicles (conditions as above) during 3 cycles of growth and division. The total vesicle count increased exponentially ($r^2 > 0.99$), $n = 3$. (C) Validating the vesicle counting assay. The counted number of dye-labeled oleate vesicles is proportional to the total number of dye-labeled vesicles in the vesicle suspension ($r^2 > 0.99$).

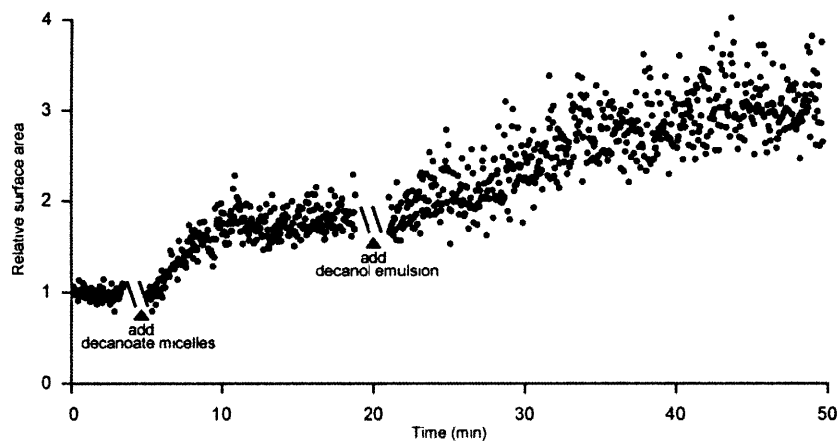


Figure III.11 Growth of decanoate:decanol (2:1) vesicles. Relative surface area (solid circles), measured using a FRET assay after the addition of 2 equivalents of decanoate micelles and 1 equivalent of decanol emulsion. Both decanoate micelles and decanol emulsion can be incorporated into the decanoate:decanol (2:1) vesicles (in 0.2 M Na-bicine, pH 8.5, at room temperature, ~20 mM initial amphiphile concentration).

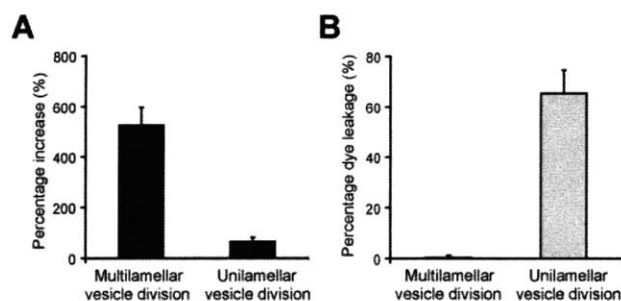


Figure III.12 Division of multilamellar versus unilamellar vesicles. (A) Percentage increase in the number of dye-labeled oleate vesicles from baseline count, after growth and division, comparing multilamellar with unilamellar vesicles (both containing 10 mM HPTS, in 0.2 M Na-bicine, pH 8.5, ~1 mM initial oleic acid, briefly agitated at 30 min after the addition of 5 equivalents of oleate micelles), n = 3. (B) Percentage dye leakage from vesicles after division, comparing multilamellar with unilamellar vesicles, n = 3.

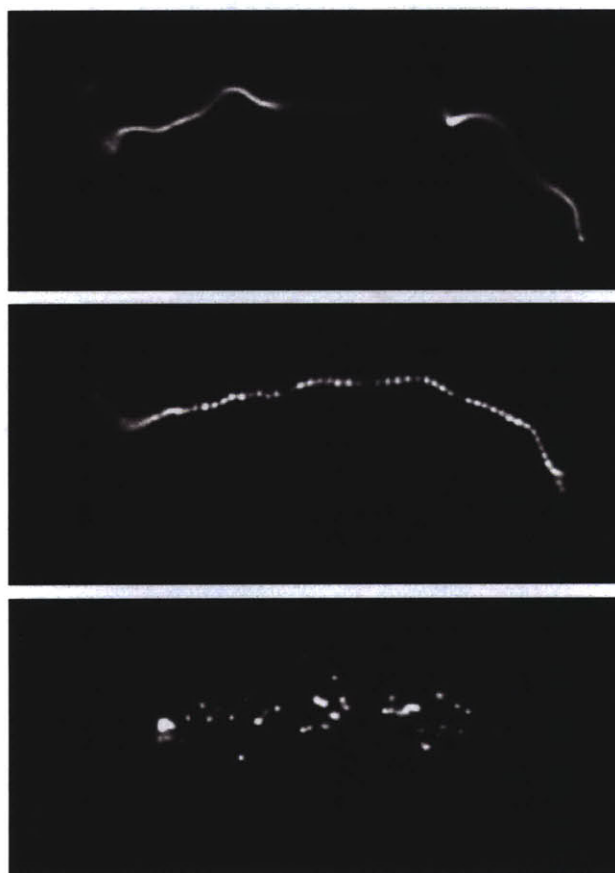
References

- Bar-Ziv, R., and Moses, E. (1994). Instability and "pearling" states produced in tubular membranes by competition of curvature and tension. *Phys Rev Lett* *73*, 1392-1395.
- Berclaz, N., Muller, M., Walde, P., and Luisi, P. L. (2001). Growth and transformation of vesicles studied by ferritin labeling and cryotransmission electron microscopy. *J Phys Chem B* *105*, 1056-1064.
- Blochliker, E., Blocher, M., Walde, P., and Luisi, P. L. (1998). Matrix effect in the size distribution of fatty acid vesicles. *J Phys Chem B* *102*, 10383-10390.
- Bozic, B., Gomiscek, G., Kralj-Iglic, V., Svetina, S., and Zeks, B. (2002). Shapes of phospholipid vesicles with beadlike protrusions. *Eur Biophys J* *31*, 487-496.
- Chen, I. A., Roberts, R. W., and Szostak, J. W. (2004). The emergence of competition between model protocells. *Science* *305*, 1474-1476.
- Chen, I. A., and Szostak, J. W. (2004a). A kinetic study of the growth of fatty acid vesicles. *Biophys J* *87*, 988-998.
- Chen, I. A., and Szostak, J. W. (2004b). Membrane growth can generate a transmembrane pH gradient in fatty acid vesicles. *Proc Natl Acad Sci USA* *101*, 7965-7970.
- Deamer, D. W. (1985). Boundary structures are formed by organic-components of the Murchison carbonaceous chondrite. *Nature* *317*, 792-794.
- Deamer, D. W., and Pashley, R. M. (1989). Amphiphilic components of the Murchison carbonaceous chondrite: surface properties and membrane formation. *Orig Life Evol Biosph* *19*, 21-38.
- Dobereiner, H. G. (2000a). in *Giant Vesicles* (New York).
- Dobereiner, H. G. (2000b). Properties of giant vesicles. *Curr Opin Colloid Interface Sci* *5*, 256-263.
- Gebicki, J. M., and Hicks, M. (1973). Ufasomes are stable particles surrounded by unsaturated fatty acid membranes. *Nature* *243*, 232-234.
- Hanczyc, M. M., Fujikawa, S. M., and Szostak, J. W. (2003). Experimental models of primitive cellular compartments: encapsulation, growth, and division. *Science* *302*, 618-622.

- Hanczyc, M. M., and Szostak, J. W. (2004). Replicating vesicles as models of primitive cell growth and division. *Curr Opin Chem Biol* 8, 660-664.
- Hargreaves, W. R., and Deamer, D. W. (1978). Liposomes from ionic, single-chain amphiphiles. *Biochemistry* 17, 3759-3768.
- Johnston, W. K., Unrau, P. J., Lawrence, M. S., Glasner, M. E., and Bartel, D. P. (2001). RNA-catalyzed RNA polymerization: accurate and general RNA-templated primer extension. *Science* 292, 1319-1325.
- Karlsson, A., Karlsson, R., Karlsson, M., Cans, A. S., Stromberg, A., Ryttsen, F., and Orwar, O. (2001). Networks of nanotubes and containers. *Nature* 409, 150-152.
- Karlsson, M., Nolkranz, K., Davidson, M. J., Stromberg, A., Ryttsen, F., Akerman, B., and Orwar, O. (2000). Electroinjection of colloid particles and biopolymers into single unilamellar liposomes and cells for bioanalytical applications. *Anal Chem* 72, 5857-5862.
- Karlsson, M., Sott, K., Davidson, M., Cans, A. S., Linderholm, P., Chiu, D., and Orwar, O. (2002). Formation of geometrically complex lipid nanotube-vesicle networks of higher-order topologies. *Proc Natl Acad Sci USA* 99, 11573-11578.
- Kvenvolden, K., Lawless, J., Pering, K., Peterson, E., Flores, J., Ponnamperna, C., Kaplan, I. R., and Moore, C. (1970). Evidence for extraterrestrial amino-acids and hydrocarbons in the Murchison meteorite. *Nature* 228, 923-926.
- Luisi, P. L. (2006). *The emergence of life: from chemical origins to synthetic biology* (Cambridge: Cambridge University Press).
- Luisi, P. L., Stano, P., Rasi, S., and Mavelli, F. (2004). A possible route to prebiotic vesicle reproduction. *Artif Life* 10, 297-308.
- Mansy, S. S., Schrum, J. P., Krishnamurthy, M., Tobe, S., Treco, D. A., and Szostak, J. W. (2008). Template-directed synthesis of a genetic polymer in a model protocell. *Nature* 454, 122-125.
- Mansy, S. S., and Szostak, J. W. (2008). Thermostability of model protocell membranes. *Proc Natl Acad Sci USA* 105, 13351-13355.
- McCollom, T. M., Ritter, G., and Simoneit, B. R. (1999). Lipid synthesis under hydrothermal conditions by Fischer-Tropsch-type reactions. *Orig Life Evol Biosph* 29, 153-166.
- Miller, S. L. (1953). A production of amino acids under possible primitive earth conditions. *Science* 117, 528-529.

- Miller, S. L., and Urey, H. C. (1959). Organic compound synthesis on the primitive earth. *Science* *130*, 245-251.
- Naraoka, H., Shimoyama, A., and Harada, K. (1999). Molecular distribution of monocarboxylic acids in Asuka carbonaceous chondrites from Antarctica. *Orig Life Evol Biosph* *29*, 187-201.
- Nooner, D. W., Gibert, J. M., Gelpi, E., and Oro, J. (1976). Closed system Fischer-Tropsch synthesis over meteoritic iron, iron-ore and nickel-iron alloy. *Geochim Cosmochim Acta* *40*, 915-924.
- Rasi, S., Mavelli, F., and Luisi, P. L. (2003). Cooperative micelle binding and matrix effect in oleate vesicle formation. *J Phys Chem B* *107*, 14068-14076.
- Rasi, S., Mavelli, F., and Luisi, P. L. (2004). Matrix effect in oleate micelles-vesicles transformation. *Orig Life Evol Biosph* *34*, 215-224.
- Rushdi, A. I., and Simoneit, B. R. (2001). Lipid formation by aqueous Fischer-Tropsch-type synthesis over a temperature range of 100 to 400 degrees C. *Orig Life Evol Biosph* *31*, 103-118.
- Sacerdote, M. G., and Szostak, J. W. (2005). Semipermeable lipid bilayers exhibit diastereoselectivity favoring ribose. *Proc Natl Acad Sci USA* *102*, 6004-6008.
- Stano, P., Wehrli, E., and Luisi, P. L. (2006). Insights into the self-reproduction of oleate vesicles. *J Phys: Condens Matter* *18*, S2231-S2238.
- Szostak, J. W., Bartel, D. P., and Luisi, P. L. (2001). Synthesizing life. *Nature* *409*, 387-390.
- Walde, P., Wick, R., Fresta, M., Mangone, A., and Luisi, P. L. (1994). Autopoietic self-reproduction of fatty acid vesicles. *J Am Chem Soc* *116*, 11649-11654.
- Yuen, G. U., and Kvenvold, K. A. (1973). Monocarboxylic acids in Murray and Murchison carbonaceous meteorites. *Nature* *246*, 301-302.
- Zhu, T. F., and Szostak, J. W. (2009). Preparation of large monodisperse vesicles. *PLoS ONE* *4*, e5009.

Vesicle Pearling and Division



Summary

In the previous chapter, we demonstrated a pathway for fatty acid vesicle growth: vesicles fed with fatty acid micelles can go through a series of transformations into long thread-like shapes. We also showed that these long thread-like vesicles can divide under gentle fluid shear forces—a simple but efficient pathway for vesicle division. Here we describe another pathway by which long thread-like vesicles can divide into multiple progeny. We show that long thread-like fatty acid vesicles containing a fluorescent dye, with dithiothreitol (DTT) or other thiols in the solution, and under intense illumination, can rapidly (< 1 sec) go through pearling and subsequent division. The mechanisms for such a process are not entirely clear, but are likely due to the oxidation of thiol groups by reactive oxygen species (ROS), creating surface tension in long thread-like vesicles and thence pearling and division.

Introduction

The coupled pathway for vesicle growth and division described in Chapter III has provided important insights into the mechanisms by which a primitive cell could grow and divide in the absence of any biological machinery (Zhu and Szostak, 2009a). We have shown that feeding a large multilamellar fatty acid vesicle with a pulse of fatty acid micelles results in a remarkable series of shape transformations, beginning with the emergence of a thin membranous filament from the side of the initially spherical vesicle. The filament grows and gradually incorporates the contents and membranes of the parental vesicle, which is transformed into a long thread-like vesicle. Under modest shear forces, the thread-like vesicle divides into multiple daughter vesicles. Our imaging studies of vesicle growth and division were affected by an unexpected artifact: long thread-like oleate vesicles containing a fluorescent dye can, under intense illumination, round up into large spherical vesicles, possibly due to radical-mediated oxidation of the internal buffer solute (since most fluorescent dyes can generate ROS under illumination). We therefore attempted to prevent this artifact by adding 10 mM dithiothreitol (DTT), a reducing agent. To our surprise, with 10 mM DTT in the solution and under intense illumination, long thread-like fatty acid vesicles went through spontaneous pearling and subsequent division.

Methods

Fatty acids and fatty acid derivatives were obtained from Nu-chek Prep (Elysian, MN). Fluorescent dyes were obtained from Molecular Probes, Inc. (Eugene, OR). Dithiothreitol, 3-mercaptopropionic acid, 3-mercapto-1-propanol, 1-mercapto-2-propanol, and 3-mercapto-1,2,4-triazole were purchased from Sigma-Aldrich (St. Louis, MO). Oleate vesicles were prepared by resuspending a dried film of oleic acid in 0.2 M Na-bicine (Sigma-Aldrich, St. Louis, MO) containing 10 mM HPTS at pH 8.5, to a final concentration of 10 mM oleic acid. The vesicle suspension was vortexed briefly and then tumbled overnight. Dilutions of vesicles were made using buffers containing fatty acids above the critical aggregate concentration (cac; $\sim 80 \mu\text{M}$ for oleic acid), to avoid vesicle dissolution. The method for the preparation of large ($\sim 4 \mu\text{m}$ in diameter) monodisperse multilamellar vesicles by extrusion and large-pore dialysis has been described (Zhu and Szostak, 2009b). Briefly, extrusion of polydisperse vesicles through 5- μm -diameter pores eliminates vesicles larger than 5 μm in diameter. Dialysis of extruded vesicles against 3- μm -pore-size polycarbonate membranes then eliminates vesicles smaller than 3 μm in diameter, leaving behind a population of monodisperse vesicles with a mean diameter of $\sim 4 \mu\text{m}$. Oleate vesicles in 0.2 M glycine hydrochloride were prepared and dialyzed using the same method.

Methods for studying vesicle growth have been previously described (Zhu and Szostak, 2009a). In the current study, vesicle growth experiments were performed in a buffer solution containing DTT, 3-mercaptopropionic acid, 3-mercapto-1-propanol, 1-mercapto-2-propanol, or 3-mercapto-1,2,4-triazole. To prepare fatty acid micelle solutions for vesicle growth, fatty acids were dissolved in 1 equivalent of NaOH (final pH > 10), vortexed briefly, and agitated overnight

under argon (Hanczyc et al., 2003). Large ($\sim 4 \mu\text{m}$ in diameter) multilamellar oleate vesicles (containing 2 mM HPTS) were prepared by large-pore dialysis, diluted 1:10 with the same buffer containing 0.8 mM oleic acid (to a final concentration of ~ 1 mM oleic acid), and stored in an eppendorf tube. For observing vesicle growth, 5 equivalents of oleate micelles were added to pre-formed vesicles, mixed, and then quickly pipetted into a disposable hemacytometer (Incyto, South Korea). The addition of smaller quantities (1 equivalent) of oleate micelles was performed using the same method. Vesicles with encapsulated fluorescent dyes were imaged using a Nikon TE2000S inverted epifluorescence microscope with extra long working distance (ELWD) objective lenses. The illumination source was a metal halide lamp (EXFO, Canada) with a 480 ± 20 nm (for HPTS) or a 546 ± 5 nm (for Rh-DHPE) optical filter (Chroma, Rockingham, VT). The illumination intensity was controlled using a set of two neutral density filters on the microscope. The images and movies were recorded using a digital camera (Hamamatsu Photonics, Japan) and post-processed using Phylum Live software (Improvision, Lexington, MA). All images were cropped using Photoshop CS2 (Adobe Systems, San Jose, CA), with linear adjustments of brightness and contrast.

Results

Our imaging studies of vesicle growth and division were affected by a surprising artifact that caused long thread-like oleate vesicles containing a fluorescent dye (in 0.2 M Na-bicine, pH 8.5) to round up into large spherical vesicles under intense illumination (Figure IV.4). To prevent this artifact, we added 10 mM DTT to the vesicle suspension (oleate vesicles containing 2 mM HPTS, in 0.2 M Na-bicine, pH 8.5, 30 min after the addition of 5 equivalents of oleate micelles). To our surprise, with 10 mM DTT in the solution and under intense illumination, long thread-like fatty acid vesicles went through pearling and subsequent division, in both bicine and glycinamide buffers (Figure IV.1): the long tubular membrane first transformed into a periodic string of smaller ellipsoidal vesicles connected by narrow necks, and the smaller vesicles eventually broke apart into independent vesicles. Oleate vesicles, when fed with small quantities of micelles (1 equivalent), can transform into sphere-tail shapes, and divide under gentle fluid shear forces (Zhu and Szostak, 2009a). We tested whether the addition of DTT could also cause oleate vesicles at sphere-tail stages (containing 2 mM HPTS, in 0.2 M Na-bicine, pH 8.5, 30 min after the addition of 1 equivalent of oleate micelles) to divide without requiring external mechanical forces. With 10 mM DTT in the solution, under intense illumination, pearling and division of the filamentous portion was indeed observed (Figure IV.2, A, B).

To understand the mechanisms that lead to the pearling and division of long thread-like fatty acid vesicles, we tested oleate vesicles (in 0.2 M Na-bicine, pH 8.5, 10 mM DTT, 30 min after the addition of 5 equivalents of oleate micelles) labeled with a different internal fluorescent dye, 2 mM calcein (Bis[*N,N*-bis(carboxymethyl)aminomethyl] fluorescein). Vesicle pearling and division were also observed. In contrast, we found that long thread-like oleate vesicles labeled

with a membrane-localized dye (0.5 mol % Rh-DHPE (LissamineTMrhodamine B 1,2-dihexadecanoyl-*sn*-glycero-3-phosphoethanolamine), in 0.2 M Na-bicine, pH 8.5, 10 mM DTT, 30 min after the addition of 5 equivalents of oleate micelles) did not go through pearling and division. Thus it is crucial that the vesicles are labeled with a water-soluble fluorescent dye in their internal aqueous space, as opposed to being labeled with a membrane-localized dye. This is likely because there are fewer dye molecules associated with the vesicles in the latter case; as in a control experiment where the encapsulated water-soluble fluorescent dye was adjusted to a lower concentration (0.05 mM) comparable to that of the membrane dye used, no vesicle pearling and division was observed.

We have shown that fatty acid vesicles of other lipid compositions, such as decanoate:decanol (2:1) vesicles (as model prebiotic vesicles), can grow into long thread-like shapes when fed with 2 equivalents of decanoate micelles and 1 equivalent of decanol emulsion (Zhu and Szostak, 2009a). With 10 mM DTT in the solution (vesicles containing 2 mM HPTS, in 0.2 M Na-bicine, pH 8.5), vesicle pearling and division were also observed (Figure IV.2, C, D). Since both decanoic acid and decanol have saturated hydrocarbon chains that are unlikely to react with ROS or DTT, the mechanisms of vesicle pearling and division are unlikely to be caused by reactions with the hydrocarbon chain, and are more likely due to physico-chemical interactions with the fatty acid head groups. We also tested whether phospholipid vesicles can also go through pearling and division with DTT in the solution. We observed that POPC (1-palmitoyl-2-oleoyl-*sn*-glycero-3-phosphocholine) vesicles (containing 2 mM HPTS, in 0.2 M Na-bicine, pH 8.5, 10 mM DTT), after the addition of 0.2 M sucrose (to produce thread-like vesicles) and under intense illumination, did not go through pearling and division as fatty acid

vesicles did (data not shown). This experiment further indicates that physico-chemical interactions between ROS, DTT, and the carboxylate groups may be responsible for the pearling and division of long thread-like fatty acid vesicles.

To further understand the effect of thiols on vesicle pearling and division, we tested whether other thiols can also cause this phenomenon. We show that thiols such as 3-mercaptopropionic acid (10 mM), 3-mercapto-1-propanol (50 mM), 1-mercapto-2-propanol (50 mM), and 3-mercapto-1,2,4-triazole (50 mM), can also cause long thread-like oleate vesicles (containing 2 mM HPTS, in 0.2 M Na-bicine, pH 8.5, 30 min after the addition of 5 equivalents of oleate micelles) to undergo pearling and division (Figure IV.3). At lower thiol concentrations (2 mM 3-mercaptopropionic acid, 10 mM 3-mercapto-1-propanol, 10 mM 1-mercapto-2-propanol, and 10 mM 3-mercapto-1,2,4-triazole, vesicle pearling was observed but without division.

Discussion

The phenomenon of vesicle pearling has been experimentally demonstrated by various methods, such as using a laser tweezer to induce vesicle surface tension and Rayleigh instability in membranes (Bar-Ziv and Moses, 1994). Recent experiments have also shown that encapsulated cationic nanoparticles can induce vesicle pearling (Yu and Granick, 2009). However, to the best of our knowledge, this is the first time that photoactivated vesicle pearling and division in a highly controlled manner has been reported. While the mechanisms leading to vesicle pearling and division in our study are not entirely clear, our experiments suggest that the oxidation of thiol groups, possibly by creating surface tension through interactions with the carboxylic head groups on fatty acids, might be responsible for the vesicle pearling and division we observed. Future experiments to address the mechanisms of this phenomenon should focus on how the oxidation of thiols can lead to increased vesicle surface tension.

Our discovery that thiols facilitate vesicle pearling and division may also have implications for understanding the environment for life's origins. Deep ocean hydrothermal vents, where extremophile biospheres that do not require solar power were found (Gold, 1992), are conceivable locations for the origin of life. Thiols, abundant in such environments (Schulte and Rogers, 2004), may play a role in the division process of early primitive cells (however, how ROS can be generated in such an environment should be evaluated). On the other hand, a recent paper has shown that a wall-deficient form (L-form) of *Bacillus subtilis* can proliferate without requiring the FtsZ machinery (while the wild-type cannot reproduce without FtsZ) (Leaver et al., 2009). Remarkably, the morphology of L-form *Bacillus subtilis* growth and division closely resembles what we observed here (Figure IV.2). How could two entirely different models, one

attempting to build an artificial cell from the bottom up, another trying to strip down existing bacteria, result in such remarkably similar morphologies in growth and division? The answer to this question could lead us to deeper understandings of the division machinery of bacteria and of how early forms of life could have emerged and evolved.

Figures

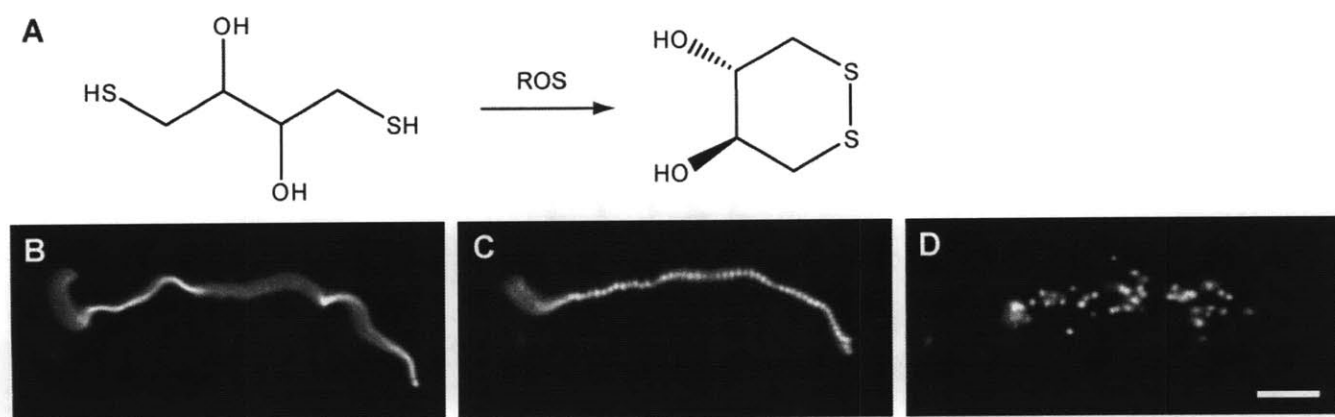


Figure IV.1 Oleate vesicle pearlying and division. (A) Radical-mediated oxidation of DTT. (B) An oleate vesicle (containing 2 mM HPTS, in 0.2 M Na-glycinamide, pH 8.5, 10 mM DTT), 30 min after the addition of 5 equivalents of oleate micelles. (C, D) Under intense illumination, the long thread-like vesicle went through pearlying and division. Scale bar, 10 μm .

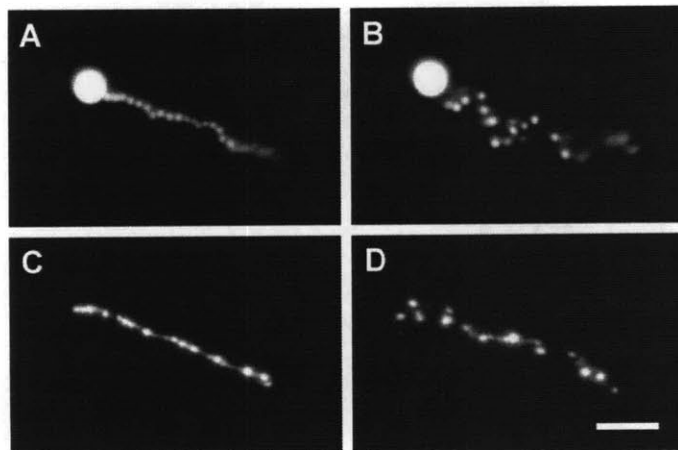


Figure IV.2 Vesicle pearling and division under various conditions. (A, B) An oleate vesicle (containing 2 mM HPTS, in 0.2 M Na-bicine, pH 8.5, 10 mM DTT) 30 min after the addition of 1 equivalent of oleate micelles. Under intense illumination, the filamentous portion of the vesicle went through pearling and division. (C, D) A decanoate:decanol (2:1) vesicle (in 0.2 M Na-bicine, pH 8.5, 30 min after the addition of 2 equivalents of decanoate micelles and 1 equivalent of decanol emulsion), went through pearling and division under intense illumination. Scale bar, 10 μm .

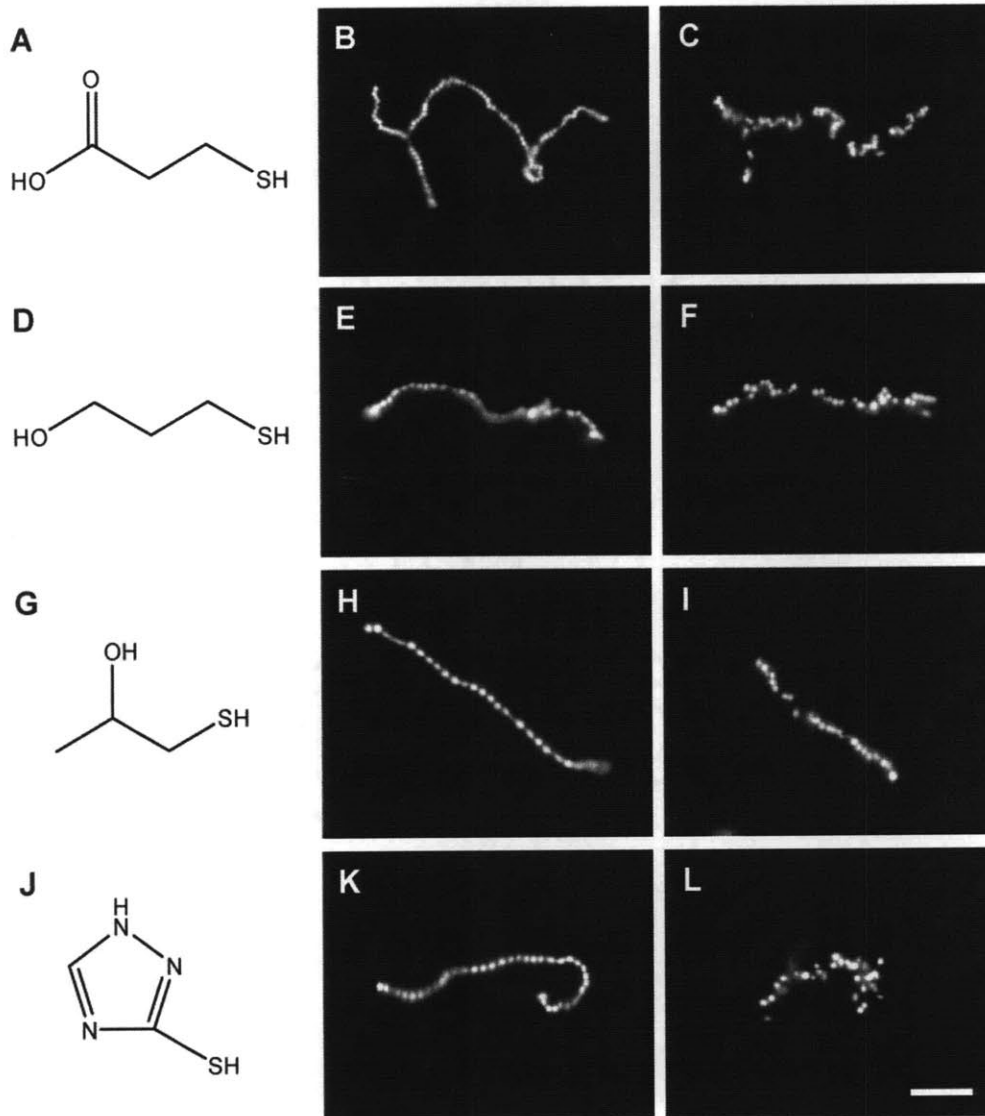


Figure IV.3 Oleate vesicle pearling and division with various thiols in the solution. (A)

Structure of 3-mercaptopropionic acid. (B, C) An oleate vesicle (containing 2 mM HPTS, in 0.2 M Na-bicine, pH 8.5, 10 mM 3-mercaptopropionic acid, 30 min after the addition of 5 equivalents of oleate micelles), went through pearling and division under intense illumination.

(D) Structure of 3-mercapto-1-propanol. (E, F) An oleate vesicle (containing 2 mM HPTS, in 0.2 M Na-bicine, pH 8.5, 50 mM 3-mercapto-1-propanol, 30 min after the addition of 5 equivalents of oleate micelles), went through pearling and division under intense illumination. (G) Structure

of 1-mercapto-2-propanol. (H, I) An oleate vesicle (containing 2 mM HPTS, in 0.2 M Na-bicine, pH 8.5, 50 mM 1-mercapto-2-propanol, 30 min after the addition of 5 equivalents of oleate micelles), went through pearling and division under intense illumination. (J) Structure of 3-mercapto-1,2,4-triazole. (K, L) An oleate vesicle (containing 2 mM HPTS, in 0.2 M Na-bicine, pH 8.5, 50 mM 3-mercapto-1,2,4-triazole, 30 min after the addition of 5 equivalents of oleate micelles), went through pearling and division under intense illumination. Scale bar, 20 μm .

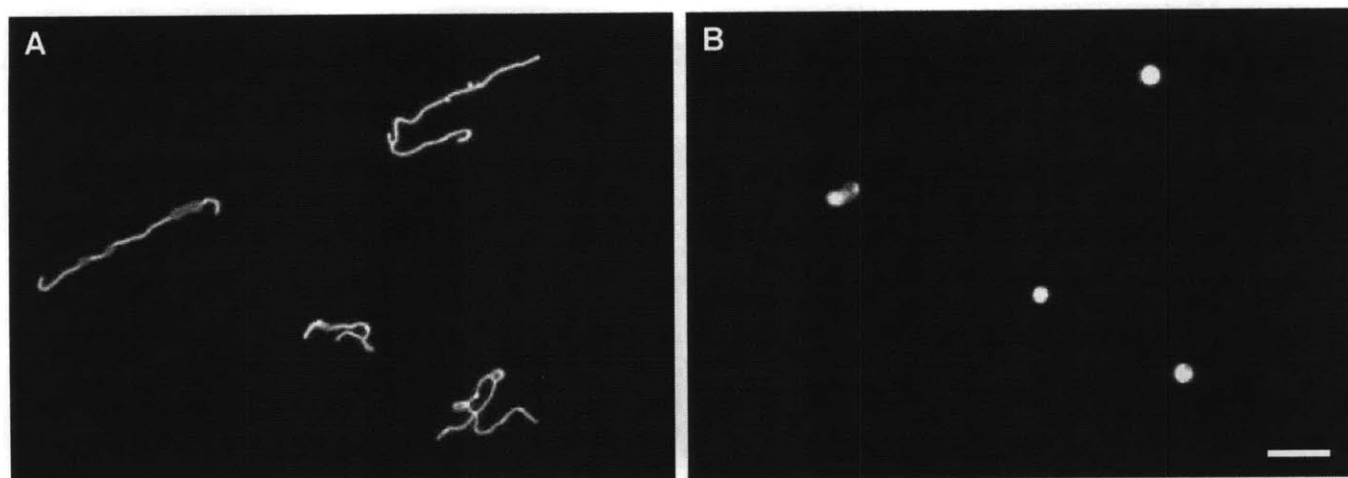


Figure IV.4 Long thread-like oleate vesicles round up into large spherical vesicles. (A)

Oleate vesicles (containing 2 mM HPTS, in 0.2 M Na-bicine, pH 8.5, 10 mM DTT), 30 min after the addition of 5 equivalents of oleate micelles. (B) The long thread-like oleate vesicles rapidly (< 5 sec) round up into large spherical vesicles under intense illumination. Scale bar, 20 μm .

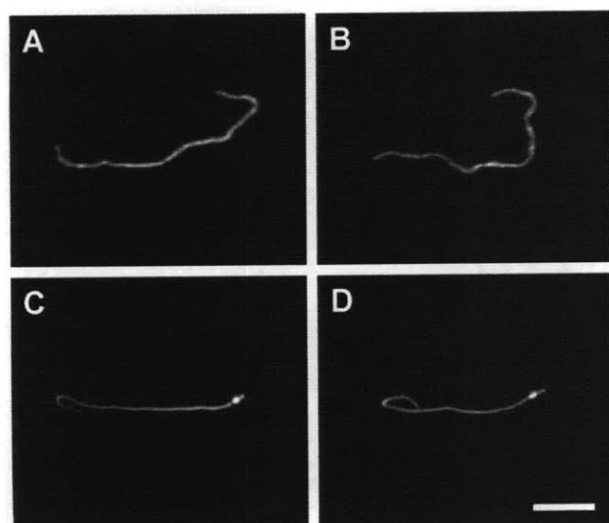
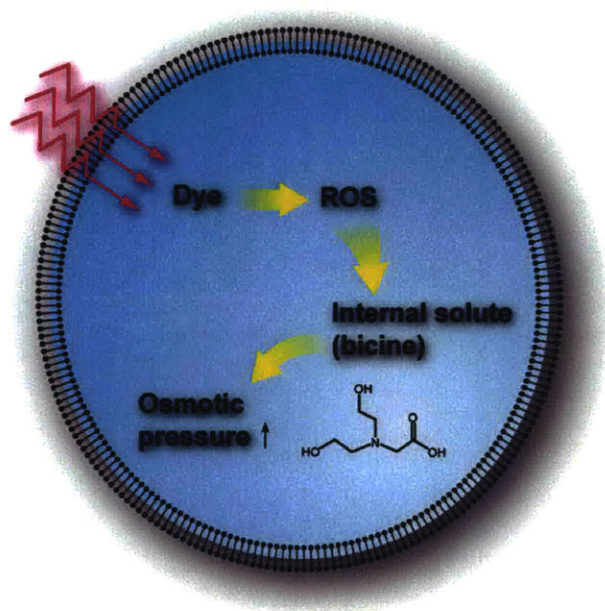


Figure IV.5 Membrane dye labeled oleate vesicles and POPC vesicles did not go through pearling and division. (A, B) A long thread-like oleate vesicle labeled with a membrane-localized dye (0.5 mol % Rh-DHPE, in 0.2 M Na-bicine, pH 8.5, 10 mM DTT, 30 min after the addition of 5 equivalents of oleate micelles), under intense illumination for 10 sec, did not go through pearling and division. (C, D) A long thread-like POPC vesicle (containing 2 mM HPTS, in 0.2 M Na-bicine, pH 8.5, 10 mM DTT), under intense illumination for 10 sec, did not go through pearling and division. Scale bar, 20 μm .

References

- Bar-Ziv, R., and Moses, E. (1994). Instability and "pearling" states produced in tubular membranes by competition of curvature and tension. *Phys Rev Lett* *73*, 1392-1395.
- Gold, T. (1992). The deep, hot biosphere. *Proc Natl Acad Sci U S A* *89*, 6045-6049.
- Hanczyc, M. M., Fujikawa, S. M., and Szostak, J. W. (2003). Experimental models of primitive cellular compartments: encapsulation, growth, and division. *Science* *302*, 618-622.
- Leaver, M., Dominguez-Cuevas, P., Coxhead, J. M., Daniel, R. A., and Errington, J. (2009). Life without a wall or division machine in *Bacillus subtilis*. *Nature* *457*, 849-853.
- Schulte, M. D., and Rogers, K. L. (2004). Thiols in hydrothermal solution: standard partial molal properties and their role in the organic geochemistry of hydrothermal environments. *Geochimica et Cosmochimica Acta* *68*, 1087-1097.
- Yu, Y., and Granick, S. (2009). Pearling of lipid vesicles induced by nanoparticles. *J Am Chem Soc* *131*, 14158-14159.
- Zhu, T. F., and Szostak, J. W. (2009a). Coupled growth and division of model protocell membranes. *J Am Chem Soc* *131*, 5705-5713.
- Zhu, T. F., and Szostak, J. W. (2009b). Preparation of large monodisperse vesicles. *PLoS ONE* *4*, e5009.

Exploding Vesicles



Summary

In the course of studying fatty acid vesicles, we have discovered a striking phenomenon: intense illumination causes dye-containing vesicles of a few microns in diameter to explode, rapidly (< 0.5 sec) and locally (within a few microns) releasing the encapsulated contents. Further studies show that such vesicle explosions are caused by increasing internal osmotic pressure, resulting from the decomposition of an internal solute (bicine) mediated by reactive oxygen species (ROS) generated by dye excitation in the presence of dioxygen. The localized, rapid release of substances from photoactivated exploding vesicles suggests potential applications of this phenomenon in many areas across disciplines, such as delivering drugs to target cancer cells and releasing functionalized nanoparticles in microfluidic channels.

Introduction

Explosions are remarkable phenomena characterized by rapid increase in pressure and volume and sudden release of energy in an extreme manner. Recently, we have developed a method for preparing large ($\sim 4 \mu\text{m}$ in diameter) monodisperse (uniform-sized) vesicles by adapting the traditional dialysis and vesicle extrusion methods (Zhu and Szostak, 2009b). The development of this vesicle preparation method has led us to the discovery of a striking phenomenon: intense illumination causes dye-containing vesicles of a few microns in diameter to explode, rapidly ($< 0.5 \text{ sec}$) and locally (within a few microns) releasing the encapsulated contents.

The photoactivated release of substances from exploding vesicles in a highly spatio-temporally controlled manner suggests intriguing applications of this phenomenon in many areas across disciplines. For instance, controlled release of therapeutic agents from membrane-bound carriers is crucial to developing effective drug delivery systems. Various methods have been developed in attempts to localize drug release from vesicles, such as applying ultrasound sonoporation to disrupt the membrane (Marmottant and Hilgenfeldt, 2003) or using bacterial proteins to lyse drug delivery liposomes (Cheong et al., 2006). In a proof-of-principle experiment, we show that photoactivated exploding vesicles can be used to release chemotherapy drugs to kill cancer cells. We also demonstrate that exploding vesicles can be used to deliver functionalized nanoparticles to a specific area in a microfluidic channel.

Methods

Vesicle preparation. Fatty acids and fatty acid derivatives were obtained from Nu-chek Prep (Elysian, MN). Fluorescent dyes were obtained from Molecular Probes, Inc. (Eugene, OR). Dithiothreitol (DTT) was purchased from Sigma-Aldrich (St. Louis, MO). Oleate vesicles were prepared by resuspending a dried film of oleic acid in 0.2 M Na-bicine (Sigma-Aldrich, St. Louis, MO) containing 10 mM HPTS at pH 8.5, to a final concentration of 10 mM oleic acid (Zhu and Szostak, 2009a). The vesicle suspension was vortexed briefly and then tumbled overnight. Dilutions of vesicles were made using buffers containing fatty acids above the critical aggregate concentration (c_{ac} ; $\sim 80 \mu\text{M}$ for oleic acid), to avoid vesicle dissolution. The method for the preparation of large ($\sim 4 \mu\text{m}$ in diameter) monodisperse multilamellar vesicles by extrusion and large-pore dialysis has been described (Zhu and Szostak, 2009b). Briefly, extrusion of polydisperse vesicles through 5- μm -diameter pores eliminates vesicles larger than 5 μm in diameter. Dialysis of extruded vesicles against 3- μm -pore-size polycarbonate membranes then eliminates vesicles smaller than 3 μm in diameter, leaving behind a monodisperse population of vesicles with a mean diameter of $\sim 4 \mu\text{m}$.

Vesicle imaging. Vesicles with encapsulated fluorescent dyes were imaged using a Nikon TE2000S inverted epifluorescence microscope with extra long working distance (ELWD) and oil-immersion objective lenses. The illumination source was a metal halide lamp (EXFO, Canada) with a $360 \pm 20 \text{ nm}$ (UV), a $480 \pm 20 \text{ nm}$ (for HPTS), or a $546 \pm 5 \text{ nm}$ (for Rh-DHPE) optical filter (Chroma, Rockingham, VT). The illumination intensity was controlled using a set of two neutral density filters on the microscope. The images and movies were recorded using a digital camera (Hamamatsu Photonics, Japan) and post-processed using Phylum Live software

(Improvision, Lexington, MA). All images were cropped using Photoshop CS2 (Adobe Systems, San Jose, CA), with linear adjustments of brightness and contrast.

Estimation of temperature increases. MATLAB R2007a Pdetool (partial differential equation toolbox) (MathWorks, Natick, MA) was used to solve the thermal conduction equation in 2D. The boundary conditions were set so that the temperature at the edge of the slide was 0 °C (arbitrarily) and the heat flux at the membrane/water interface was equal to the total amount of heat being generated by the internal fluorescent dye (at steady state). Knowing the energy output of the lamp at wavelengths between 480 ± 20 nm, the efficiency of the optical filter, the extinction coefficient of HPTS (2×10^4 L mol⁻¹ cm⁻¹), and the cross-section area of a vesicle compared to that of the entire slide, we estimated that the total light energy being absorbed by the fluorescent dye inside a single vesicle was $\sim 1.2 \times 10^{-5}$ W.

Illumination and analysis of a bicine solution. A solution containing 100 μ l 0.2 M bicine (pH 8.5), 10 mM HPTS, and 0.1 M H₂O₂ in an eppendorf tube was mounted on a microscope and illuminated using the same illumination source that we used for imaging (with a 480 ± 20 nm filter). An Esquire6000 ion trap mass spectrometer with EsquireControl software (Bruker Daltonics, Billerica, MA) was used to analyze the solute before and after illumination. A vapor pressure osmometer (Wescor, Logan, UT) was used to measure the osmolarity changes before and after illumination. To measure the critical osmotic gradient for membrane rupture, a micropipette pulled from a thin-wall glass capillary tubing (Fisher Scientific, Pittsburgh, PA) was held in place by a three-axis oil hydraulic fine micromanipulator (Narishige, Japan). The micropipette was connected to a manual microsyringe pump (World Precision Instruments,

Sarasota, FL), which was used to push vesicles into a hypotonic solution in a depression on a cell-culture glass slide (Erie, Portsmouth, NH).

Photoactivated exploding vesicles for killing cancer cells. The A549 (human lung adenocarcinoma) cell line was obtained from ATCC (Manassas, VA). The cells were cultured in glass-bottom culture dishes (MatTek, Ashland, MA) using 1X F-12K Nutrient Mixture medium (Invitrogen, Carlsbad, CA) containing 10% FBS and 10 $\mu\text{g}/\text{ml}$ gentamycin. The cells were cultured for 9 days before use, with the cell culture medium changed every 3 days. POPC:oleate (4:1) vesicles containing cisplatin (*cis*-dichlorodiammine platinum(II)) or carboplatin (*cis*-diammine(1,1-cyclobutanedicarboxylato) platinum) (Sigma-Aldrich, St. Louis, MO) were prepared by rehydrating a dried lipid film containing 80% POPC and 20% oleic acid, in a solution that contained either 7 mM cisplatin or 27 mM carboplatin (in 15 mM HPTS, 0.2 M Na-ADA, pH 7.4), to a final concentration of 40 mM lipids. The vesicles were then extruded through 5- μm -diameter pores and dialyzed against 3- μm -pore-size polycarbonate membranes to remove the unencapsulated cisplatin or carboplatin and vesicles smaller than 3 μm in diameter. Aseptic 1X D-MEM/F-12 without phenol red (Invitrogen, Carlsbad, CA) containing 10 $\mu\text{g}/\text{ml}$ gentamycin was used as the wash buffer. To ensure that the remaining unencapsulated drugs after dialysis did not inhibit cell growth, the wash buffer was collected in the last round of dialysis (which contained the same concentration of unencapsulated drugs) for later use in culturing the control group. A small volume ($\sim 200 \mu\text{l}$) of the dialysed vesicle suspension was added to cancer cells in a glass-bottom culture dish, sealed by a coverslip on top to prevent evaporation. Photoactivation of exploding vesicles was achieved by illuminating the glass-bottom culture dish on a microscope through an oil-immersion lens, after which the cells were

cultured in the solution for 3 days before imaging and cell counting. Cell counting was performed in disposable hemacytometers (Incyto, South Korea). Control experiments included 1) culturing cells in the medium collected from the last round of dialysis, to show that the concentration of unencapsulated drug was not biologically significant, and 2) growing cells in a culture medium containing plain POPC:oleate (4:1) vesicles.

Nanoparticle release from exploding vesicles. To encapsulate nanoparticles in vesicles, oleate vesicles were prepared in a solution containing biotin-coated fluorescent nanoparticles (40 nm in diameter, 0.1% solid suspension) (Invitrogen, Carlsbad, CA), 10 mM HPTS, and 0.2 M Na-bicine (pH 8.5). The vesicles were extruded through 5- μ m-diameter pores and dialyzed against 3- μ m-pore-size polycarbonate membranes using the methods described above, to remove both the unencapsulated nanoparticles and vesicles smaller than 3 μ m in diameter. The streptavidin coating of glass coverslips was performed using methods described in the literature (Elenko et al., 2009). A simple PDMS (polydimethylsiloxane) microfluidic channel with an inlet and an outlet was designed using AutoCAD 2006 (Autodesk, San Rafael, CA) and fabricated by the Stanford University Microfluidics Foundry (Stanford, CA). The flow of nanoparticle-encapsulating vesicles was controlled by a manual microsyringe pump, and the vesicle explosions were triggered by full intensity illumination through a 480 \pm 20 nm filter and an oil-immersion lens.

***C. elegans* imaging.** Adult wild-type *C. elegans* were grown in a petri dish seeded with *E. coli* as the food source. A worm picker made by mounting a piece of 32-gauge platinum wire on the tip of a Pasteur pipette was used to pick up and move the animals. A drop of melted 4% agar

was placed onto a large glass coverslip until cooled. The animals were paralyzed in 10 mM sodium azide and placed on the agar, covered by another smaller coverslip. The animals were imaged by full intensity illumination through a 360 ± 20 nm (UV) filter and an oil-immersion lens.

Results

We prepared large ($\sim 4 \mu\text{m}$ in diameter) monodisperse oleate vesicles (containing 10 mM HPTS, in 0.2 M Na-bicine, pH 8.5) through a combination of vesicle extrusion and dialysis methods (Zhu and Szostak, 2009b). To our surprise, we observed that these oleate vesicles, shortly ($< 0.5 \text{ sec}$) after being exposed to intense illumination, exploded and released the encapsulated dye and smaller internal vesicles (Figure V.1, A, B). To confirm the rupture of vesicle membrane during the explosion, we labeled the vesicles with a membrane dye (Rh-DHPE (LissamineTM rhodamine B 1,2-dihexadecanoyl-*sn*-glycero-3-phosphoethanolamine); excited at a different emission wavelength from HPTS), and observed that the vesicle membrane burst open on one side and then quickly shrank (Figure V.1, C-F). We also tested vesicles containing different internal fluorescent dyes, such as calcein (bis[*N,N*-bis(carboxymethyl)aminomethyl] fluorescein) and Rose Bengal (4,5,6,7-tetrachloro-2',4',5',7'-tetraiodofluorescein disodium salt; a photodynamic therapy drug currently in clinical trial), and observed similar vesicle explosions (data not shown).

One of the possible mechanisms for the vesicle explosion is that the internal fluorescent dye (the external dye has been eliminated through dialysis), under intense illumination, causes a temperature increase in the vesicle and expansion of the internal volume. We tested this hypothesis using a numerical method: knowing the total energy input, derived from the illumination intensity and the molar extinction coefficient of the fluorescent dye ($2 \times 10^4 \text{ L mol}^{-1} \text{ cm}^{-1}$ for HPTS), and assuming that the majority of the energy input ($1.2 \times 10^{-5} \text{ W}$) was converted into heat, we estimated the maximum temperature increase in a vesicle that could be created by this mechanism. Solving the thermal conduction equation in 2D using MATLAB (Figure V.4),

we estimated that the maximum temperature increase in the vesicle was $< 1\text{ }^{\circ}\text{C}$, which is likely insufficient to cause vesicle explosions. (In a control experiment where we diluted vesicles into buffer solutions at lower temperatures, no membrane rupture was observed.)

Another possible mechanism is that most fluorescent dyes such as HPTS can generate oxidative free radicals under illumination (Kochevar and Redmond, 2000), which may react with certain components of the vesicle and cause explosion. We tested this theory through several experiments. First, we added 10 mM DTT (dithiothreitol, a reducing agent) to the vesicle suspension, and no vesicle explosion was observed under full intensity illumination. This experiment, together with the MATLAB simulation, suggests that ROS-mediated oxidation, instead of temperature increase, is responsible for the vesicle explosions. We then examined whether the unsaturated membrane lipid (oleic acid) or the internal solute (bicine, (*N,N*-bis(2-hydroxyethyl)glycine)) participates in the ROS-mediated oxidation. Replacing the unsaturated membrane lipid (oleic acid) with a saturated fatty acid and fatty alcohol that are unlikely to be oxidized (decanoate:decanol (2:1) vesicles containing 10 mM HPTS, in 0.2 M bicine, pH 8.5), vesicle explosions were again observed (data not shown). Replacing the internal solute (bicine) with glycineamide (oleate vesicles containing 10 mM HPTS, in 0.2 M Na-glycineamide, pH 8.5), however, no vesicle explosion was observed (data not shown). These two experiments suggest that the ROS-mediated oxidation of bicine, as opposed to the oxidation of the membrane lipid, might be the cause for the vesicle explosions. To further test this hypothesis, we put equal concentrations of fluorescent dye (10 mM HPTS) inside and outside the membrane (in 0.2 M Na-bicine, pH 8.5; vesicles were labeled and visualized by a membrane dye, Rh-DHPE); in this case, the vesicle membranes remained intact after full intensity illumination for 10 sec (Figure V.5).

This experiment further indicates that a reaction with the internal buffer solute as opposed to the direct oxidation of the membrane is likely responsible for vesicle explosions. We then performed cross-mixing experiments by diluting vesicles made in 0.2 M bicine buffer (containing 10 mM HPTS, pH 8.5) into 0.2 M glycine buffer (pH 8.5), and vice versa, and observed vesicle explosions only in the former case, which further suggests that the internal solute, bicine, is critical to vesicle explosions.

We next investigated the mechanism of the ROS-mediated oxidation of bicine, and how such reactions could lead to vesicle explosions. It has previously been shown that in the presence of ROS, bicine can be degraded into diethanolamine and acetic acid (Horikoshi et al., 2001), a process that could increase the internal osmotic pressure of a vesicle and rupture the membrane (Figure V.2, A, C). To test this theory, we prepared a 100 μ l solution containing 0.2 M bicine (pH 8.5), 10 mM HPTS, and 0.1 M H₂O₂ in an eppendorf tube, and illuminated the sample using the same illumination source as we used for vesicle imaging. We analyzed the sample before and after illumination by mass spectrometry and identified diethanolamine after illumination, one of the decomposition products of bicine (whereas acetic acid, with its smaller molecular weight, is harder to detect by mass spectrometry) (Figure V.2, D). We also measured the osmolarity of the samples using a vapor pressure osmometer and found a \sim 60 mOsm/L osmolarity increase after illumination (Figure V.2, B), corresponding to the decomposition of \sim 30% of the bicine molecules (no significant pH change in the solution was measured as the remaining bicine acted as a strong buffer). We then examined whether this osmotic gradient is sufficient to cause vesicle membrane rupture. In the experiment, instead of increasing the internal osmolarity, which is difficult to control and measure, we lowered the external osmolarity by diluting vesicles into a

hypotonic solution through a micropipette (under low intensity illumination) (Figure V.6). We found that a ~ 20 mOsm/L osmotic gradient is required to rupture the outer membranes of oleate vesicles of ~ 4 μm in diameter. According to the Young–Laplace equation, we estimated that the rupture surface tension for oleate membrane is ~ 11 dyn/cm, matching the results reported in previous studies (Chen et al., 2004). Also according to the Young–Laplace equation, for a given cross-membrane osmotic gradient, larger vesicles are expected to be subject to greater surface tension. Thus, larger vesicles are expected to explode more easily than smaller ones under the same illumination intensity. To test this model, we prepared a population of polydisperse oleate vesicles (containing 10 mM HPTS, in 0.2 M Na-bicine, pH 8.5), and observed that the larger (> 3 μm in diameter) vesicles exploded under full intensity illumination while the smaller vesicles remained intact as the encapsulated HPTS gradually became photobleached (Figure V.7).

Understanding the mechanisms responsible for vesicle explosion helps us to explore the practical applications of exploding vesicles, taking advantage of their ability to release substances in a rapid, spatio-temporally controlled manner. A major question in treating cancer is how to target and localize cytotoxic drugs to tumors and reduce systemic toxicity. By delivering a cargo drug such as a chemotherapeutic agent through photoactivation, exploding vesicles may be used to localize the drug release and strengthen the effectiveness of cancer treatments (Figure V.3, A). As an initial step towards translating the exploding vesicle system into a photoactivated drug delivery system, we modified the membrane compositions and the internal buffer solute. Since fatty acids bind to albumin in blood, pure fatty acid vesicles are not stable in the blood stream. Therefore, for the photoactivated drug delivery vesicle system, we used POPC:oleate (4:1) vesicles instead. (Adding 20% oleate to the membrane helped to reduce the rupture surface

tension and increase the efficiency of membrane rupture, because pure POPC vesicles require 2.5 times higher osmotic gradient to rupture than oleate vesicles (Chen et al., 2004.) Bicine, with a pKa at ~8.3, cannot be photodegraded efficiently at pH 7.4 (possibly because the tertiary amine groups are protected when protonated), and thus vesicles containing bicine cannot explode efficiently under physiological conditions. We instead used ADA (*N*-(2-acetamido)iminodiacetic acid) buffer as the internal solute, which has a similar structure to bicine (but with a pKa at ~6.9) and allows vesicles to explode efficiently at pH 7.4.

In a proof-of-principle experiment, we used an in-vitro cell culture system to test the effectiveness of this experimental photoactivated drug delivery system. Since the oxidation of cargo drugs by ROS is a concern, we used platinum-based chemotherapy drugs such as cisplatin (*cis*-dichlorodiammine platinum(II)) and carboplatin (*cis*-diammine(1,1-cyclobutanedicarboxylato) platinum) as model cargo drugs. Cisplatin and carboplatin cause DNA crosslinks, leading to cancer cell apoptosis (Knox et al., 1986). The metal-coordinated ammonia molecules on these drugs are less likely to be oxidized than the tertiary amine groups on bicine or ADA, protecting the drugs from immediate ROS oxidation. Human lung adenocarcinoma (A549) cells were cultured in glass-bottom culture dishes and treated by photoactivated exploding vesicles releasing cisplatin or carboplatin (Figure V.3, C, D). We show that the treated cells have approximately 90% and 80% (respectively) lower survival rates than those in the control group (Figure V.3, E). In the control group, cells cultured in the medium collected from the last round of dialysis grew normally, showing that there was no biologically significant concentration of unencapsulated drugs in the solution (Figure V.3, B). Similarly, cells

cultured in medium containing plain POPC:oleate (4:1) vesicles showed normal growth (data not shown).

We also show that exploding vesicles can be used to release functionalized nanoparticles (Figure V.8, A-C), for purposes such as modifying surfaces locally in a microfluidic channel. In a proof-of-principle experiment, we encapsulated biotin-coated fluorescent nanoparticles in vesicles, which were lysed under full intensity illumination in a microfluidic channel. This process allowed the released biotin-coated fluorescent nanoparticles to attach to the streptavidin-coated surface of a microfluidic channel within the illuminated region of $\sim 100 \mu\text{m}$ in length (Figure V.8, D).

Discussion

While light-triggered ruptures of dye-containing lysosomes have been observed *in vivo* (Brunk et al., 1997; Jaiswal et al., 2007), to the best of our knowledge, this is the first time that photoactivated vesicle explosions have been discovered in a well-controlled *in vitro* system. Understanding the mechanisms responsible for these exploding vesicles may help us to understand the light-triggered lysosome rupture *in vivo*. It has been shown that lysosomes stained by acridine orange in rat and human astrocytes could explode by laser excitation (Jaiswal et al., 2007). It has also been shown that acridine orange-stained lysosomes in human fibroblasts could rupture under intense illumination (Brunk et al., 1997). Additionally, we have observed the explosion of autofluorescent lysosomes (containing lipofuscin pigments (Clokey and Jacobson, 1986)) in *C. elegans* under intense UV (360 ± 20 nm) illumination (Figure V.9), suggesting that similar phenomena may exist in a variety of cells and animal models. Notably, oxidative stress has been known to play an important role in lysosome rupture in cells, leading to cell aging, apoptosis, and various lysosomal storage diseases (Kurz et al., 2008). The current theory suggests that the oxidation of lysosome membranes leads to their rupture, yet few experiments are available to support this model. Our mechanistic studies of an *in vitro* exploding vesicle system suggest another possible mechanism for oxidative stress-induced lysosome rupture: oxidation of internal solutes leading to increased osmotic pressure and ultimately membrane rupture. Future experiments to analyze the lysosomal internal solutes (e.g., various peptides) and to address how their oxidation may increase the internal osmolarity of lysosomes may help to elucidate the mechanisms for oxidative stress-induced lysosome rupture.

Several technical issues remain to be addressed in developing practical applications of the exploding vesicle system, particularly in cancer drug delivery. First, the excitation light for HPTS (blue light of ~480 nm wavelength) has a limited effective tissue penetration distance, whereas using red or infrared light to excite a photosensitizer with a longer excitation wavelength can help to achieve deeper tissue penetration of up to a few mm (Soler et al., 2000). Future improvements in this area may take advantage of the variety of ROS-generating photosensitizers being developed for photodynamic therapies (some of which are in clinical use or in clinical trials) (Dolmans et al., 2003; Triesscheijn et al., 2006). Second, ROS may oxidize the cargo drugs, limiting the variety of drugs to be delivered by this system (in the current study, we only used platinum-based chemotherapy drugs such as cisplatin and carboplatin). Using drug-conjugated nanoparticles (Sengupta et al., 2005) to carry and protect cargo drugs from ROS oxidation and applying photoactivated exploding vesicles to localize their release to tumors may help to resolve the oxidation issue. As an alternative strategy, since we understand that vesicle explosions are caused by increasing internal osmotic pressure as opposed to the direct oxidation of the membrane, it may be possible to design a different photochemical process that can increase the internal osmotic pressure and cause vesicle explosions without generating ROS. In-depth future studies on the mechanisms of the ROS-mediated decomposition of bicine and similar compounds (Horikoshi et al., 2001; Sorensen et al., 1998) may be helpful for designing such a photochemical process.

As we have shown in the two proof-of-principle experiments on the applications of the exploding vesicle system, the ability to release encapsulated substances such as a cargo drug or functionalized nanoparticles from membrane-bound carriers in a highly spatio-temporally

controlled manner may lead to many potential applications across disciplines. For example, patterns of functionalized surfaces can be produced in a microfluidic channel by coating the surface with functionalized nanoparticles, for a variety of applications such as in the imaging and sorting of *C. elegans* (Chung et al., 2008). Additionally, the exploding vesicle system may be used for studying bacterial chemotaxis and neurophysiology. In current studies on neuronal responses to neurotransmitters, photocleavable, caged neurotransmitters have been used for activating neurons (Harvey and Svoboda, 2007), yet the variety of available caged neurotransmitters for such studies is limited. Photoactivated release of vesicle-encapsulated signaling molecules extracellularly or intracellularly (by pre-injection or uptake of vesicles into the cell) may allow a wider variety of signaling molecules and their cellular actions to be studied. The development of these new applications may in turn lead us to exciting new discoveries in other disciplines.

Figures

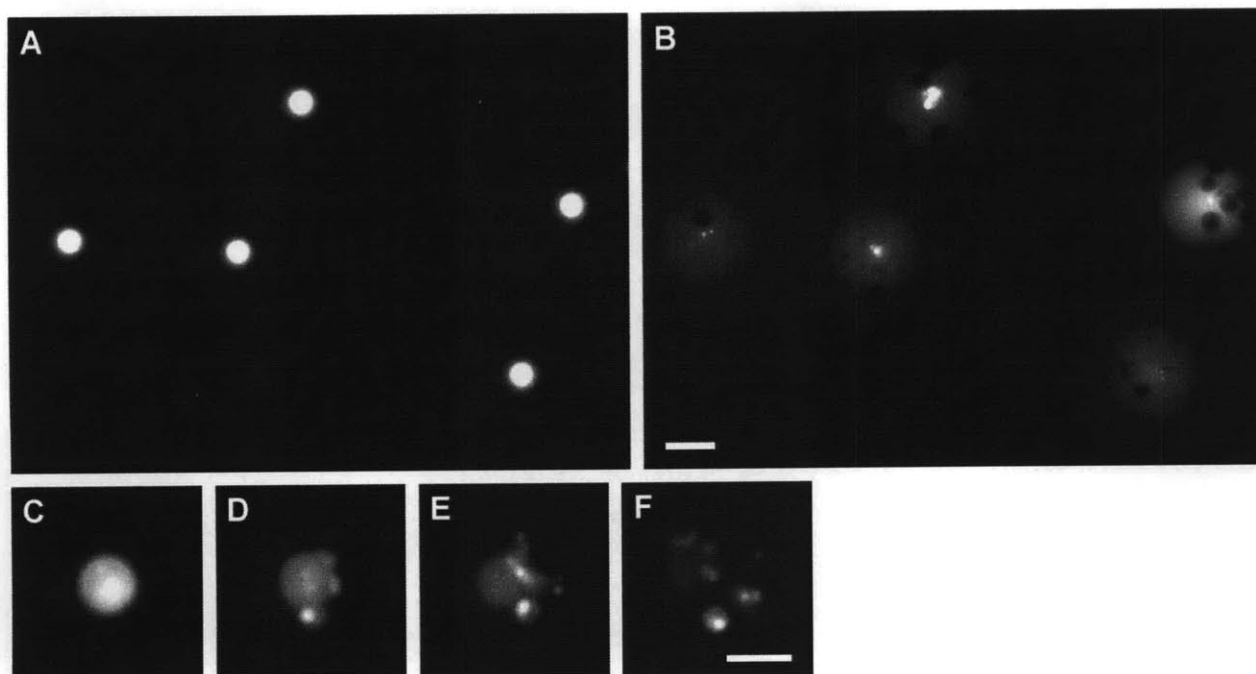


Figure V.1 Exploding vesicles. (A, B) Oleate vesicles (containing 10 mM HPTS, in 0.2 M Na-bicine, pH 8.5) exploded shortly (~ 0.5 sec) after being exposed to full intensity illumination. Scale bar for (A, B), 10 μm . (C-F) An oleate vesicle (containing 10 mM HPTS, in 0.2 M Na-bicine, pH 8.5), labeled by a membrane-localized dye (Rh-DHPE), exploded and ruptured the membrane under intense illumination at the excitation wavelength of HPTS. Scale bar for (C-F), 5 μm .

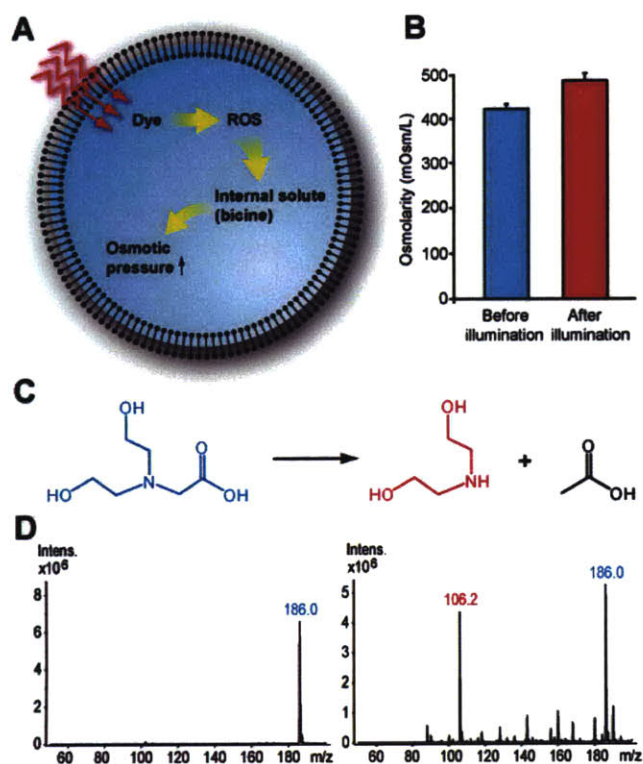


Figure V.2 Mechanisms for vesicle explosion. (A) Schematic diagram for ROS-mediated decomposition of bicine, leading to the increase of internal osmotic pressure in a vesicle. (B) Osmolarity of a bicine solution (containing 10 mM HPTS, 0.2 M bicine, and 0.1 M H₂O₂) before and after 30 min of illumination, n = 3. (C) Decomposition products of bicine: diethanolamine and acetic acid. (D) Mass spectrometry analysis of a bicine solution before (left) and after (right) illumination (bicine at m/z 186.0; diethanolamine at m/z 106.2).

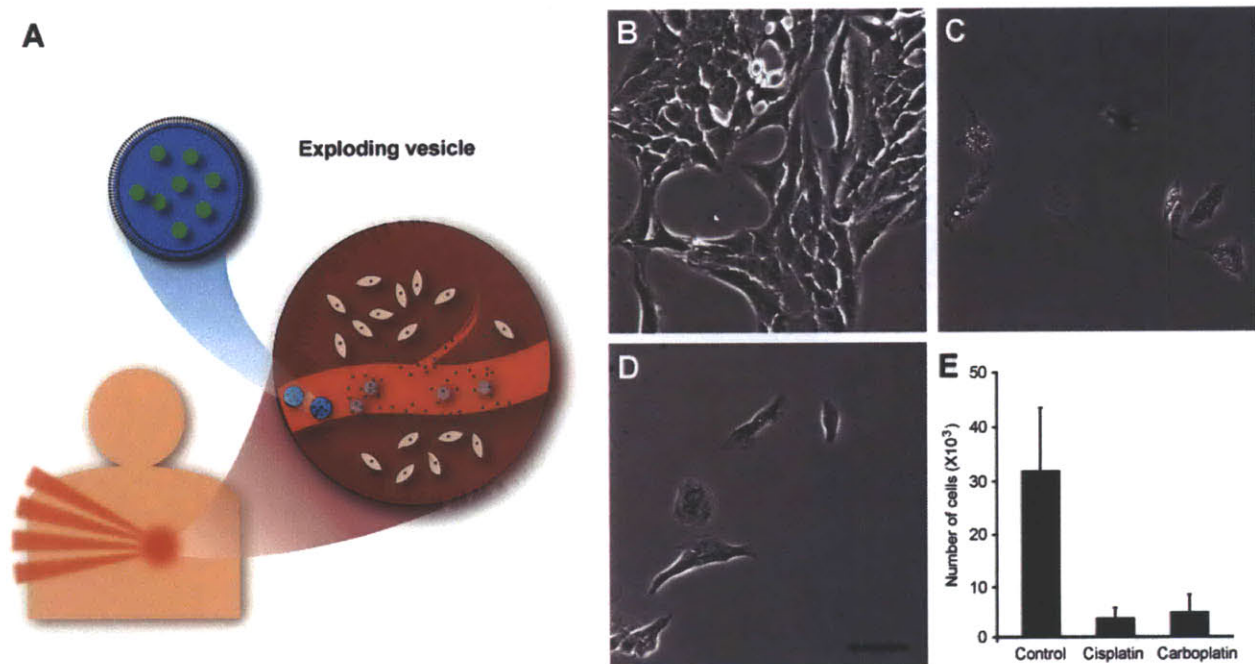


Figure V.3 Exploding vesicles for killing cancer cells. (A) Schematic diagram for a potential strategy to localize the release of chemotherapy drugs from exploding vesicles through photoactivation. (B) In the control group, human lung adenocarcinoma (A549) cells were cultured in the medium collected from the last round of dialysis. Cells were imaged using differential interference contrast microscopy (DIC). (C, D) Cells treated by cisplatin or carboplatin, respectively, released from photoactivated exploding vesicles. (E) Number of total viable cells after the treatment, $n = 3$. Scale bar, $50 \mu\text{m}$.

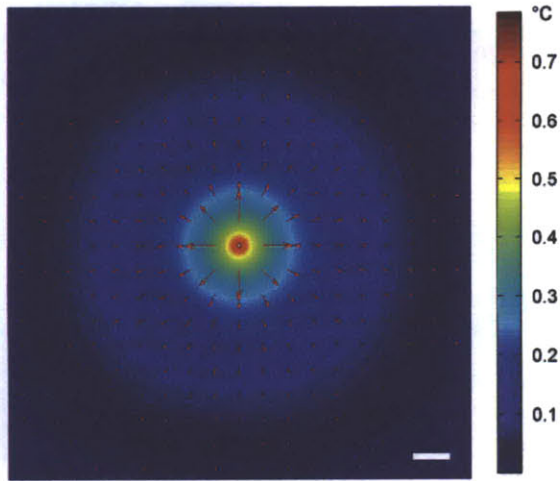


Figure V.4 Estimated temperature increases. Pseudo colors correspond to the temperature increases in water surrounding a vesicle with a constant heat input of 1.2×10^{-5} W, solved in 2D and plotted by MATLAB. The maximum temperature increase immediately outside the vesicle membrane (shown as a small white circle in the middle) was estimated < 1 °C. Heat flux vectors are shown in red arrows. Scale bar, 100 μm .

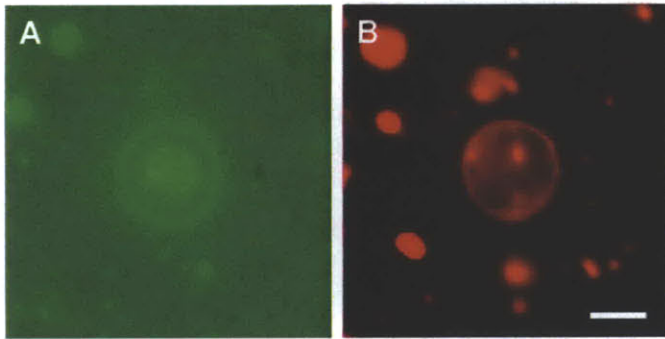


Figure V.5 Equal concentrations of fluorescent dye inside and outside the membrane. (A) A large vesicle (with 10 mM HPTS inside and outside the membrane, in 0.2 M Na-bicine, pH 8.5) remained intact after full intensity illumination for 10 sec. (B) The vesicle was labeled and visualized by a membrane dye (Rh-DHPE). Scale bar, 5 μm .

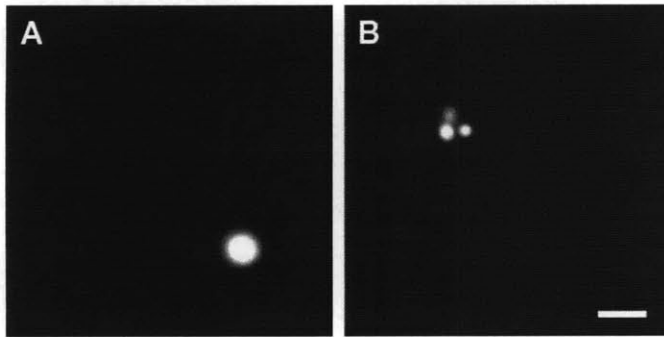


Figure V.6 Critical osmotic gradient for membrane rupture. (A) Diluting a vesicle into a hypotonic solution through a micropipette. (B) The membrane ruptured and released the smaller internal vesicles. Scale bar, 5 μm .

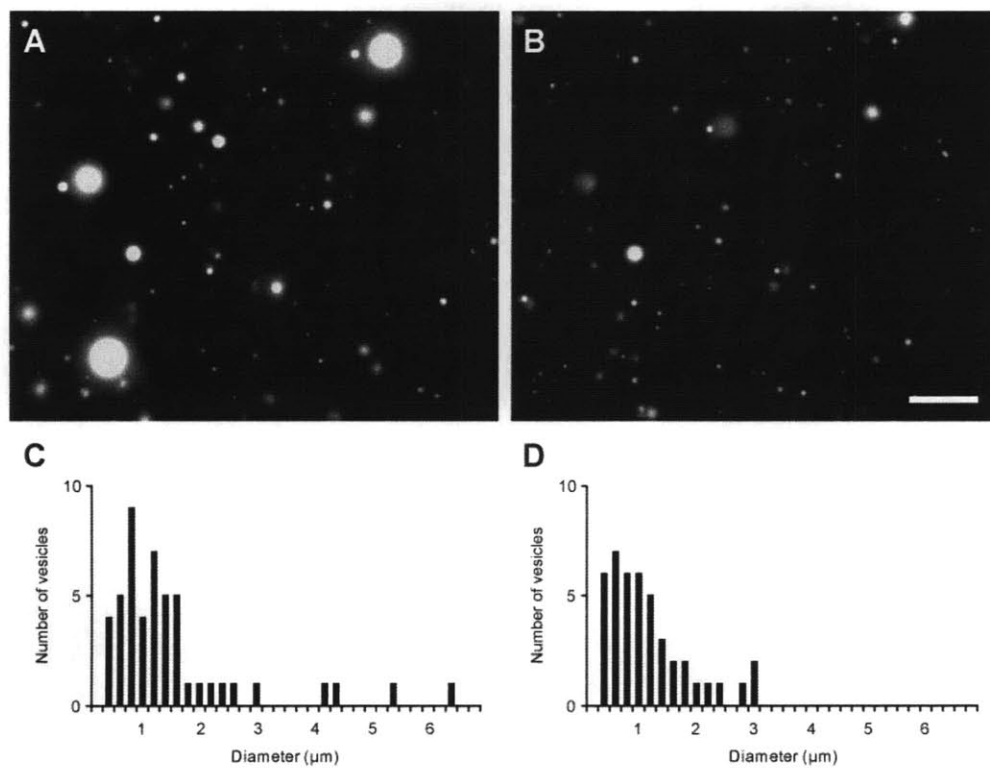


Figure V.7 Size dependency of vesicle explosions. (A, B) A population of polydisperse oleate vesicles (containing 10 mM HPTS, in 0.2 M Na-bicine, pH 8.5) before and after intense illumination for 5 sec. The corresponding size distributions before (C) and after (D) intense illumination, shown as number of vesicles per 0.2 μm bin (vesicles between 0-0.2 μm in diameter were not counted). Scale bar, 10 μm.

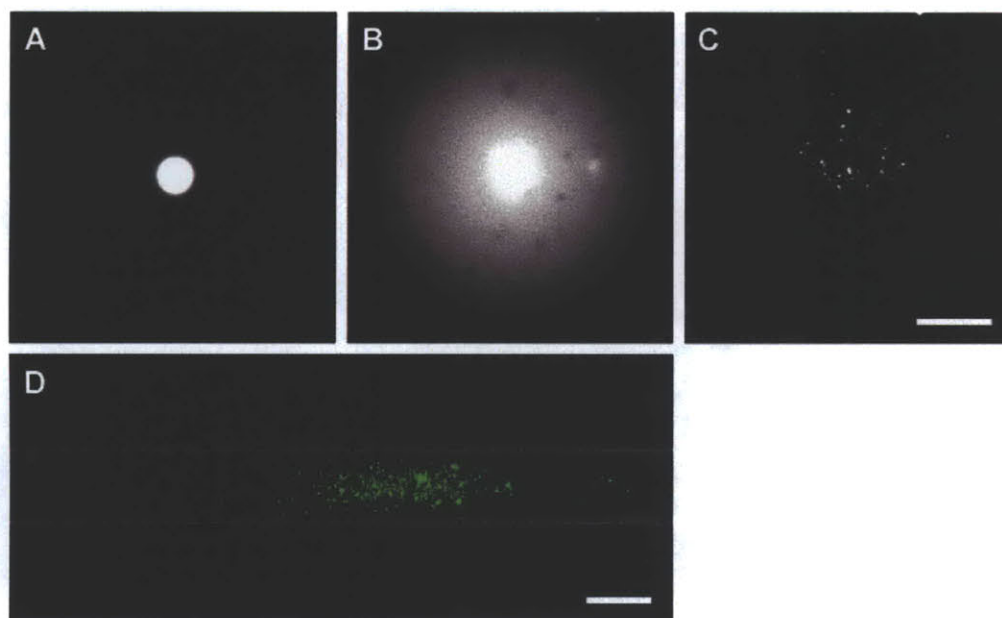


Figure V.8 Nanoparticle release from exploding vesicles. (A, B) An oleate vesicle (containing 10 mM HPTS, in 0.2 M Na-bicine, pH 8.5) encapsulating biotin-coated fluorescent nanoparticles explodes shortly after full intensity illumination, releasing the nanoparticles. (C) The nanoparticles attached to a streptavidin-coated glass surface. Scale bar for (A-C), 10 μm . (D) Using exploding vesicles to localize the release of nanoparticles to a specific area in a microfluidic channel. Scale bar for (D), 50 μm .

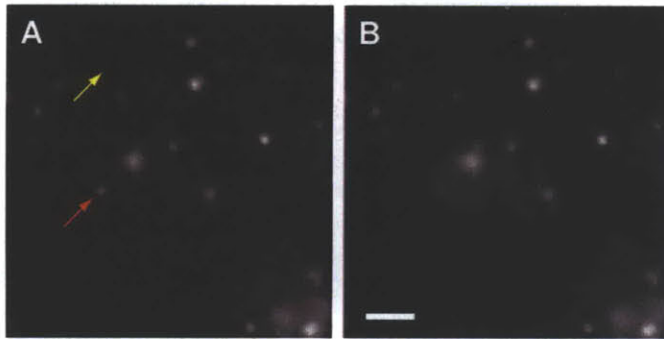


Figure V.9 Lysosome explosions in *C. elegans*. (A, B) Under full intensity UV (360 ± 20 nm) illumination, an autofluorescent lysosome (red arrow) exploded, releasing its contents. The cells shown were gut granule cells, with the yellow arrow pointing at the gut lumen. Scale bar, 5 μm .

References

Brunk, U. T., Dalen, H., Roberg, K., and Hellquist, H. B. (1997). Photo-oxidative disruption of lysosomal membranes causes apoptosis of cultured human fibroblasts. *Free Radic Biol Med* 23, 616-626.

Chen, I. A., Roberts, R. W., and Szostak, J. W. (2004). The emergence of competition between model protocells. *Science* 305, 1474-1476.

Cheong, I., Huang, X., Bettgowda, C., Diaz, L. A., Jr., Kinzler, K. W., Zhou, S., and Vogelstein, B. (2006). A bacterial protein enhances the release and efficacy of liposomal cancer drugs. *Science* 314, 1308-1311.

Chung, K., Crane, M. M., and Lu, H. (2008). Automated on-chip rapid microscopy, phenotyping and sorting of *C. elegans*. *Nat Methods* 5, 637-643.

Clokey, G. V., and Jacobson, L. A. (1986). The autofluorescent "lipofuscin granules" in the intestinal cells of *Caenorhabditis elegans* are secondary lysosomes. *Mech Ageing Dev* 35, 79-94.

Dolmans, D. E., Fukumura, D., and Jain, R. K. (2003). Photodynamic therapy for cancer. *Nat Rev Cancer* 3, 380-387.

Elenko, M. P., Szostak, J. W., and van Oijen, A. M. (2009). Single-molecule imaging of an in vitro-evolved RNA aptamer reveals homogeneous ligand binding kinetics. *J Am Chem Soc* 131, 9866-9867.

Harvey, C. D., and Svoboda, K. (2007). Locally dynamic synaptic learning rules in pyramidal neuron dendrites. *Nature* 450, 1195-1200.

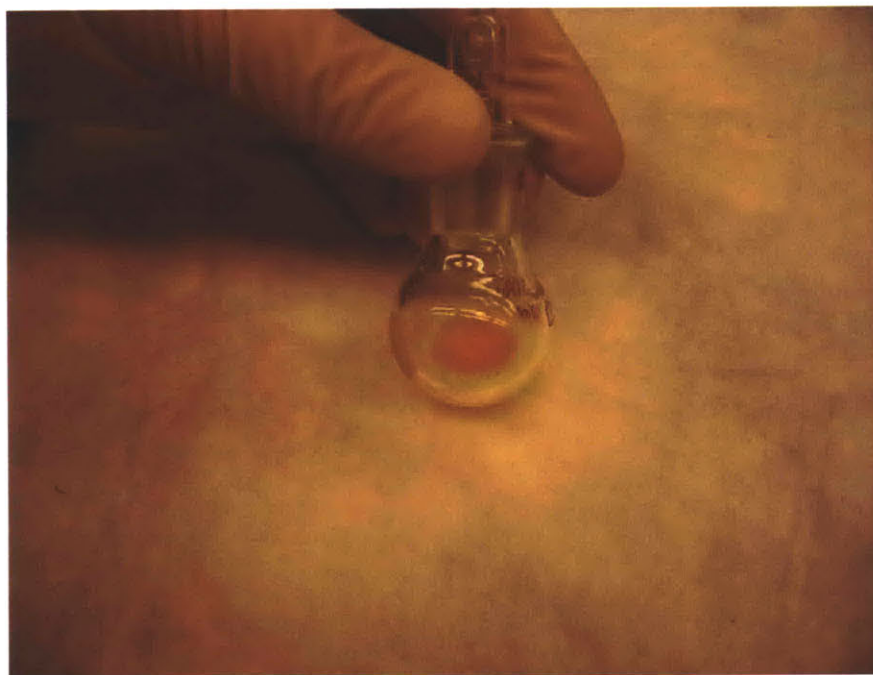
Horikoshi, S., Watanabe, N., Mukae, M., Hidaka, H., and Serpone, N. (2001). Mechanistic examination of the titania photocatalyzed oxidation of ethanolamines. *New Journal of Chemistry* 25, 999-1005.

Jaiswal, J. K., Fix, M., Takano, T., Nedergaard, M., and Simon, S. M. (2007). Resolving vesicle fusion from lysis to monitor calcium-triggered lysosomal exocytosis in astrocytes. *Proc Natl Acad Sci U S A* 104, 14151-14156.

Knox, R. J., Friedlos, F., Lydall, D. A., and Roberts, J. J. (1986). Mechanism of cytotoxicity of anticancer platinum drugs: evidence that cis-diamminedichloroplatinum(II) and cis-diammine-(1,1-cyclobutanedicarboxylato)platinum(II) differ only in the kinetics of their interaction with DNA. *Cancer Res* 46, 1972-1979.

- Kochevar, I. E., and Redmond, R. W. (2000). Photosensitized production of singlet oxygen. *Methods Enzymol* 319, 20-28.
- Kurz, T., Terman, A., Gustafsson, B., and Brunk, U. T. (2008). Lysosomes and oxidative stress in aging and apoptosis. *Biochim Biophys Acta* 1780, 1291-1303.
- Marmottant, P., and Hilgenfeldt, S. (2003). Controlled vesicle deformation and lysis by single oscillating bubbles. *Nature* 423, 153-156.
- Sengupta, S., Eavarone, D., Capila, I., Zhao, G., Watson, N., Kiziltepe, T., and Sasisekharan, R. (2005). Temporal targeting of tumour cells and neovasculature with a nanoscale delivery system. *Nature* 436, 568-572.
- Soler, A. M., Angell-Petersen, E., Warloe, T., Tausjo, J., Steen, H. B., Moan, J., and Giercksky, K. E. (2000). Photodynamic therapy of superficial basal cell carcinoma with 5-aminolevulinic acid with dimethylsulfoxide and ethylenediaminetetraacetic acid: a comparison of two light sources. *Photochem Photobiol* 71, 724-729.
- Sorensen, M., Zurell, S., and Frimmel, F. H. (1998). Degradation pathway of the photochemical oxidation of ethylenediaminetetraacetate (EDTA) in the UV/H₂O₂-process. *Acta Hydrochimica Et Hydrobiologica* 26, 109-115.
- Triesscheijn, M., Baas, P., Schellens, J. H. M., and Stewart, F. A. (2006). Photodynamic therapy in oncology. *Oncologist* 11, 1034-1044.
- Zhu, T. F., and Szostak, J. W. (2009a). Coupled growth and division of model protocell membranes. *J Am Chem Soc* 131, 5705-5713.
- Zhu, T. F., and Szostak, J. W. (2009b). Preparation of large monodisperse vesicles. *PLoS ONE* 4, e5009.

Preparation of Fatty Acid or Phospholipid Vesicles



Purpose

Preparation of polydisperse, multilamellar vesicles through the rehydration of a thin film of fatty acids or phospholipids.

Theory

The rehydration of a dry film of lipid(s) leads to the formation of vesicles. The lipid composition for the membranes can include phospholipids, single chain lipids (fatty acids, glycerol esters), sterols, or mixtures of various amphiphiles. For fatty acid vesicles, the buffer pH should be near the pKa of the bilayer-associated fatty acid (Cistola et al., 1988). The encapsulated contents of the vesicles are determined by the buffer used for the rehydration.

Equipment

Rotary evaporator

Glass 10 ml round-bottom flask with cap

Bench top rotary tumbler

Bench top vortex machine

pH meter

1.5 ml Eppendorf tubes

Materials

1-palmitoyl-2-oleoyl-*sn*-glycero-3-phosphocholine (POPC)

LissamineTMrhodamine B 1,2-dihexadecanoyl-*sn*-glycero-3-phosphoethanolamine (Rh-DHPE)

Oleic acid

Myristoleic acid

Glycerol monomyristoleate (GMM)

Bicine (or other buffer of choice, except borate or phosphate buffer, which produces leaky fatty acid vesicles)

8-hydroxypyrene-1,3,6-trisulfonic acid trisodium salt (HPTS, or other water-soluble fluorescent dye of choice)

NaOH

Chloroform

Methanol

Deionized water

Solutions and Preparation

Buffers

20 mM POPC, 10 mM oleic acid in chloroform

Component	Stock	Amount
20 mM POPC in chloroform	20 mM	1 ml
oleic acid (pure)	>99%	3.2 ul

10 mM oleic acid, 0.1 mM Rh-DHPE in chloroform

Component	Stock	Amount
chloroform	pure	1 ml

oleic acid (pure)	>99%	3.2 ul
-------------------	------	--------

Rh-DHPE in chloroform	10 mM	10 ul
-----------------------	-------	-------

20 mM myristoleic acid, 10 mM glycerol monomyristoleate in chloroform (or use methanol)

Component	Stock	Amount
-----------	-------	--------

chloroform	pure	1 ml
------------	------	------

myristoleic acid (pure)	>99%	5.6 ul
-------------------------	------	--------

glycerol	>99%	2.8 ul
----------	------	--------

monomyristoleate (pure)		
-------------------------	--	--

Na-bicine buffer (200 mM), 2 mM HPTS, pH 8.5

Component	Stock	Amount
-----------	-------	--------

Na-bicine	1 M	1 ml
-----------	-----	------

HPTS	100 mM	0.1 ml
------	--------	--------

Add water to 5 ml

Na-bicine buffer (200 mM), pH 8.5

Component	Stock	Amount
-----------	-------	--------

Na-bicine	1 M	1 ml
-----------	-----	------

Add water to 5 ml

Protocol

Duration

Preparation	about 10 minutes
-------------	------------------

Protocol	about 24 hour
----------	---------------

Preparation Prepare a solution containing the desired lipid composition for vesicles in a non-polar solvent (e.g. chloroform).

Caution *Work in a hood. All lipids should be stored at -20°C. Always use glass tips for pipetting chloroform.*

Step 1 Formation of a thin lipid film

Overview Formation of a thin layer of dry lipid film in a round-bottom flask.

Duration 30 min

1.1 Pipette the prepared solution of the desired lipids in a non-polar solvent into a 10 ml round-bottom flask. If fatty acid(s) are in the desired lipid composition, pipette the appropriate amount of pure fatty acid into the round-bottom flask first (Figure A.1)

Tip *Clean the round-bottom flask with methanol before the procedure.*

Tip *Avoid light by wrapping aluminum foil around the sample. Avoid oxygen by flushing the container with argon or nitrogen gas.*

1.2 Rotary evaporate the round-bottom flask to completely eliminate the chloroform in the sample (Figure A.2). Alternatively, dry the film under a stream of argon while manually rotating the flask (Figure A.3).

Tip To ensure all solvent is removed from the film, leave the flask under vacuum for 1 hour.

Tip If only fatty acids or glycerol esters are in the desired lipid composition, one can skip the step of desolving fatty acids into chloroform, and instead directly add neat fatty acids or glycerol esters to the buffer solution to make vesicles (Hanczyc et al., 2003).

Step 2 Rehydration of the thin lipid film

Overview Rehydration of the thin lipid film by adding buffer solution, leading to the formation of vesicles.

Duration 20 min

2.1 Add the prepared buffer solution to the round-bottom flask. Any solutes to be encapsulated should be included in the buffer.

2.2 Tightly cap the round-bottom flask, briefly vortex, and tumble for 10 min, until the thin lipid film at the bottom of the flask is completely dispersed in the buffer (Figure A.4).

2.3 Pipette the sample into a 1.5 ml Eppendorf tube, vortex briefly, and tumble overnight (Figure A.5).

Tip Multiple cycles of freezeing and thawing the vesicle sample may improve the encapsulation efficiency.

Tip A thin film of phospholipid(s), does not desolve well in a buffer solution without any metal ions (e.g., ammonium acetate solution without Na^+). In this case, adding a small amount of NaCl or NaOH helps to desolve the lipid.

Figures



Figure A.1 Pipette the prepared solution of the desired lipids in a non-polar solvent into the round-bottom flask.

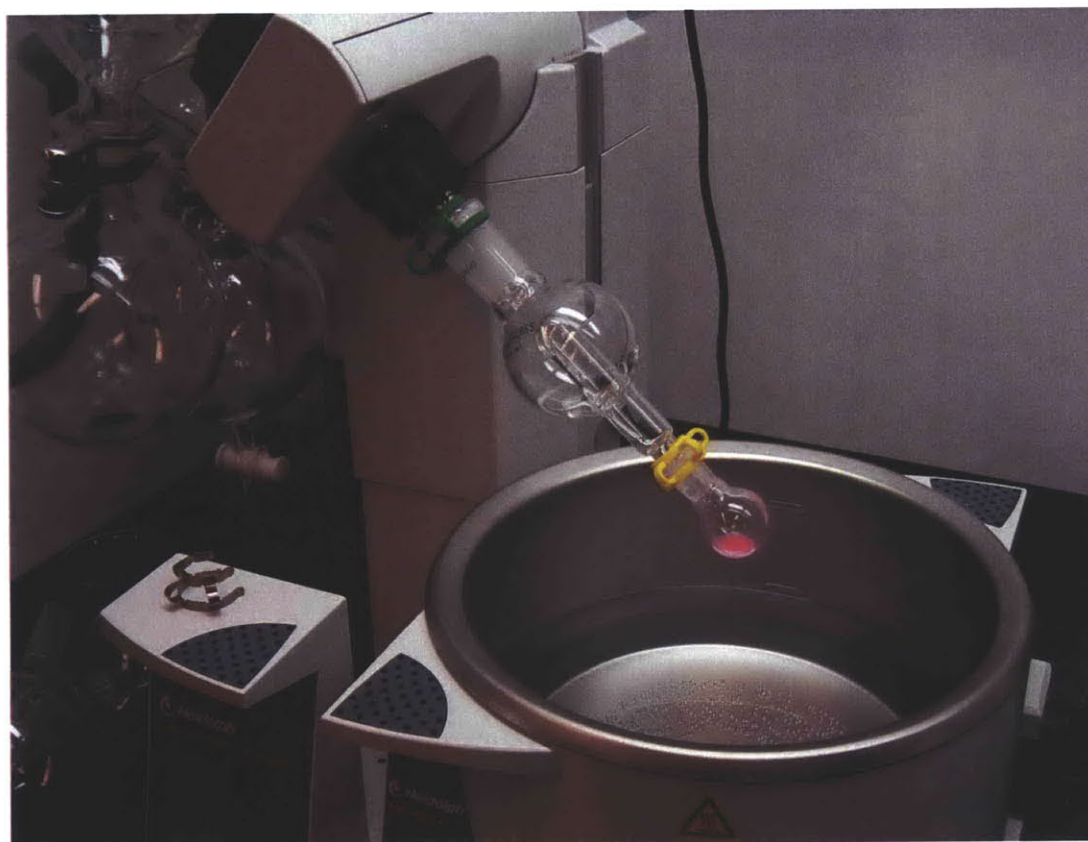


Figure A.2 Remove chloroform by rotary evaporation.

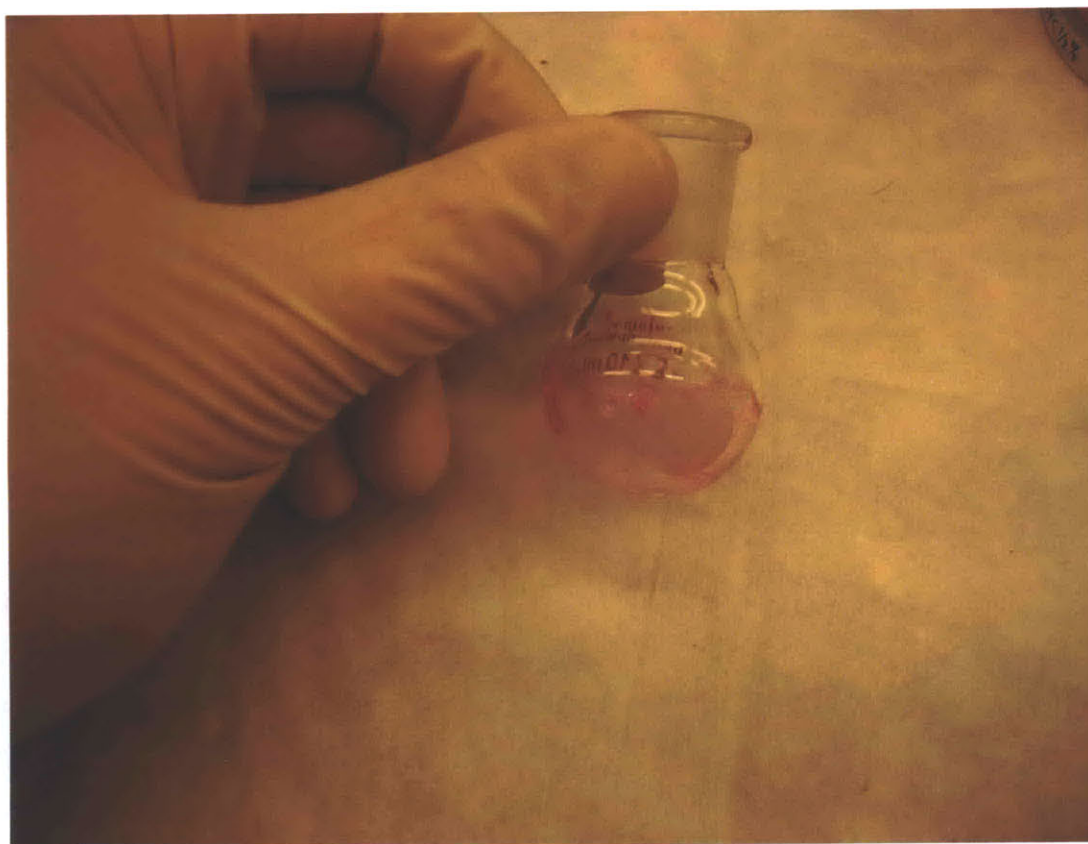


Figure A.3 Formation of a thin lipid film in a round-bottom flask.



Figure A.4 The thin lipid film (red) at the bottom of the flask is completely dispersed in the buffer containing 2 mM HPTS (green).

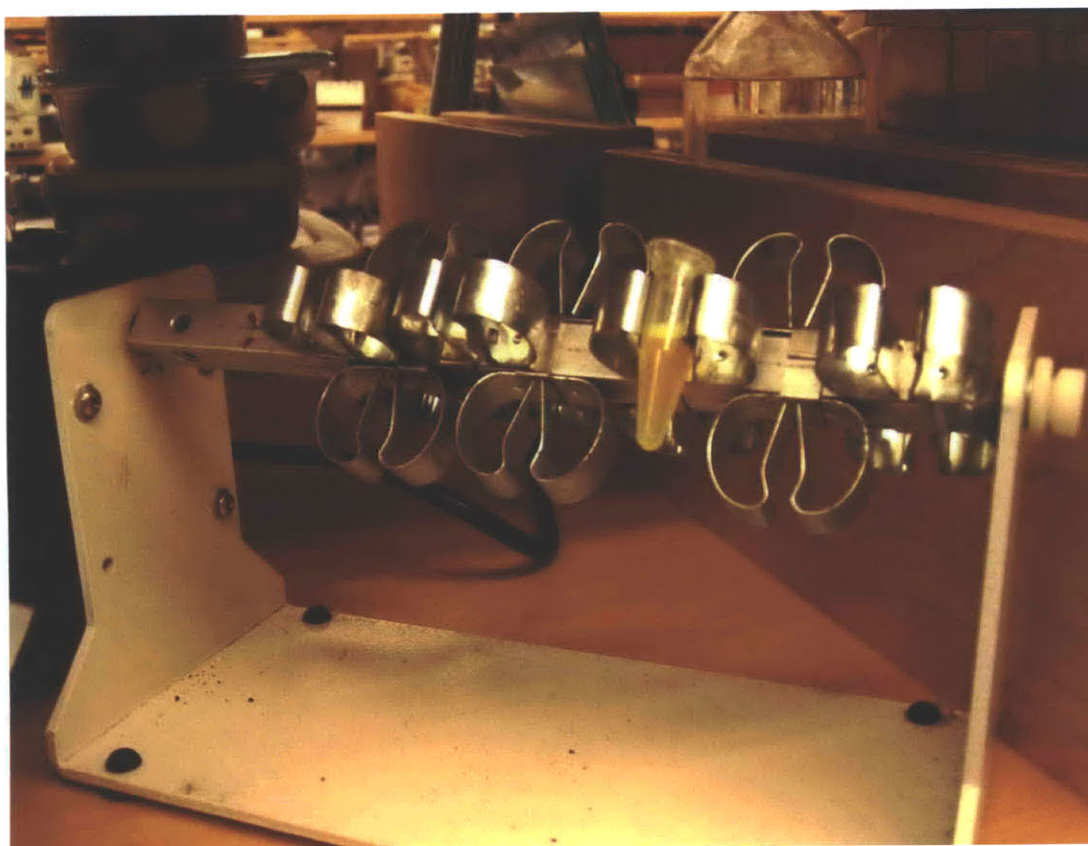


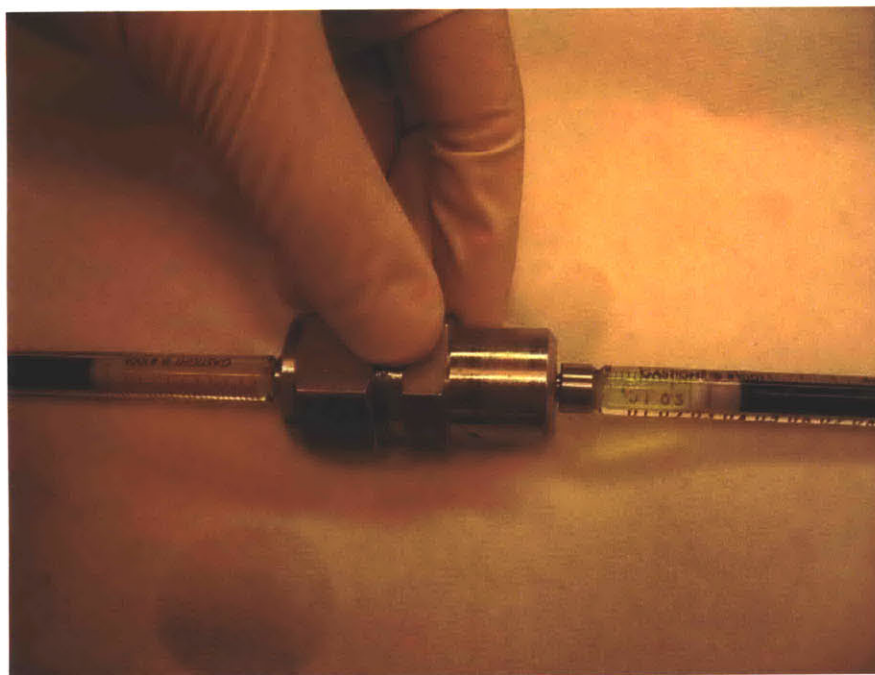
Figure A.5 Vesicle suspension in a 1.5 ml Eppendorf tube, on a bench top rotary tumbler.

References

Cistola, D. P., Hamilton, J. A., Jackson, D., and Small, D. M. (1988). Ionization and phase behavior of fatty acids in water: application of the Gibbs phase rule. *Biochemistry* 27, 1881-1888.

Hanczyc, M. M., Fujikawa, S. M., and Szostak, J. W. (2003). Experimental models of primitive cellular compartments: encapsulation, growth, and division. *Science* 302, 618-622.

Vesicle Extrusion through Track-etched Membranes



Purpose

The vesicle extrusion method is used for preparing small (e.g. 100 nm diameter) monodisperse (uniform-sized) vesicles. Polycarbonate track-etched membranes with pores generally ranging from 50 nm to 200 nm in diameter and a hand-held mini-extruder are used for such a procedure. Extrusion through small (100 nm in diameter or smaller) pores also ensures that the vesicle population is predominantly unilamellar.

Theory

The vesicle extrusion method takes advantage of the fact that when vesicles are forced through membrane pores smaller than their diameters, they break down into smaller vesicles closer to the pore size (Mayer et al., 1986). Vesicle extrusion has also been used as a laboratory method to induce protocell division (Hanczyc et al., 2003).

Equipment

Hand-held mini-extruder (<http://www.ncnr.nist.gov/userlab/pdf/E134extruder.pdf>)

Two gas-tight syringes (often come with extruder)

pH meter

1.5 ml Eppendorf tubes

Materials

Polycarbonate track-etched membranes, either 13 or 25 mm in diameter

(<http://www.whatman.com/NucleporeTrackEtchedMembranes.aspx>)

10 mm Filter Supports

(http://avantilipids.com/index.php?option=com_content&view=article&id=522&Itemid=293&categorynumber=610014)

1-palmitoyl-2-oleoyl-*sn*-glycero-3-phosphocholine (POPC)

(or any phospholipid of choice)

Oleic acid (or any fatty acid of choice)

LissamineTMrhodamine B 1,2-dihexadecanoyl-*sn*-glycero-3-phosphoethanolamine (Rh-DHPE)

(for fluorescent membrane labeling, if desired)

Bicine (or other buffer of choice, except borate or phosphate buffer, which produces leaky fatty acid vesicles)

8-hydroxypyrene-1,3,6-trisulfonic acid trisodium salt (HPTS, or other water-soluble fluorescent dye of choice)

NaOH

Chloroform

Methanol

Deionized water

Solutions and Preparation

Buffers

Na-bicine buffer (200 mM), 2 mM HPTS, pH 8.5

Component	Stock	Amount
-----------	-------	--------

Na-bicine	1 M	1 ml
HPTS	100 mM	0.1 ml
Add water to 5 ml		

Na-bicine buffer (200 mM), pH 8.5

Component	Stock	Amount
Na-bicine	1 M	1 ml
Add water to 5 ml		

Protocol

Duration

Preparation	about 1 day
Protocol	about 50 minutes

Preparation Prepare vesicles by suspending lipid(s) in a buffer solution.

Caution *If using photosensitive lipids, avoid light by wrapping aluminum foil around the flask containing the vesicles. Avoid oxygen by flushing the container with argon or nitrogen gas.*

Step 1 Assemble the extrusion apparatus

Overview Assemble the extrusion apparatus with the polycarbonate track-etched membranes and filter supports (Figure B.1)

Duration 5 min

1.1 Pre-wet the polycarbonate track-etched membranes of choice (e.g., with 100 nm diameter pores) and the filter supports.

Tip *Rinse the extruder parts with water before assembly.*

Tip *When pre-wetting the polycarbonate track-etched membranes and filter supports, rapidly dip the membranes or filter supports into the same buffer used for preparing vesicles.*

1.2 Put one filter support on each side of the two internal membrane support (white plastic parts), with the pre-wetted polycarbonate track-etched membrane on top. Assemble the rest of the parts (Figure B.2 and Figure B.3).

Tip *One can choose to double the polycarbonate track-etched membrane to prevent membrane rupture, especially when using high pressure for extrusion.*

Step 2 Load the gas-tight syringes

Overview Load the gas-tight syringes with vesicle sample.

Duration 5 min

- 2.1 Rinse the syringes with water and then the same buffer used for preparing vesicles.
- 2.2 Load one of the gas-tight syringes with the vesicle sample at a volume between 0.5 to 1 ml.

Step 3 Extrusion to yield monodisperse vesicles

Overview Force the vesicles in the two gas-tight syringes back and forth through the hand-held mini-extruder 11 times.

Duration 10 min

- 3.1 Lock the gas-tight syringes in place on the hand-held mini-extruder.
- 3.2 Slowly push one syringe, so that all the solution in it goes through the hand-held mini-extruder to the other side, into the other syringe (Figure B.4).

Tip *For larger pore sizes (> 100 nm), slowly push the syringe at a constant rate of 1 mL/min. Extrusion at higher flow rates may lead to excessive vesicle disruption (Hanczyc et al., 2003).*

- 3.3 Push from the other side using the other syringe. Repeat this 11 times through the filter, and collect the final product vesicles.

Tip *Make sure that the final product vesicles are collected from the non-starter syringe.*

Figures



Figure B.1 Hand-held mini-extruder with two gas-tight syringes.

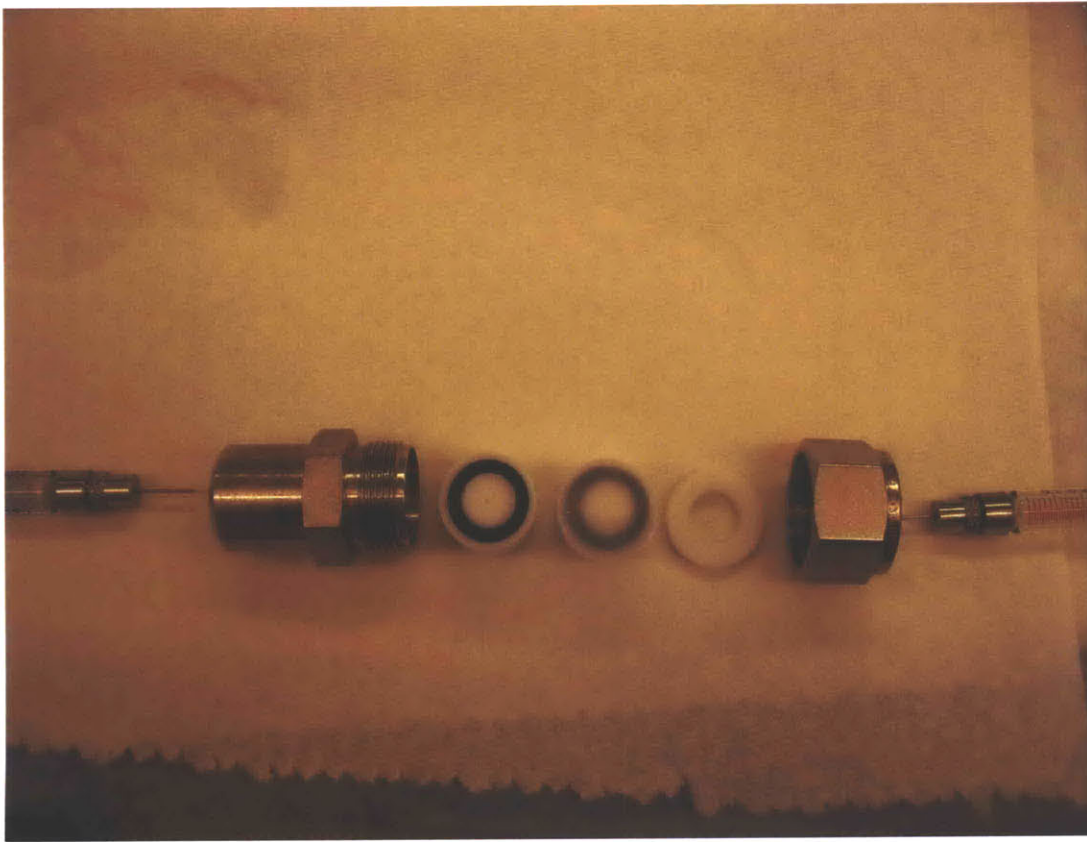


Figure B.2 Assembly of the extrusion apparatus: on each internal membrane support (white plastic part with a black O-ring) there is a filter support, with a polycarbonate track-etched membrane on top.



Figure B.3 Assembly of the internal membrane support parts with filter support and polycarbonate track-etched membrane in the middle.



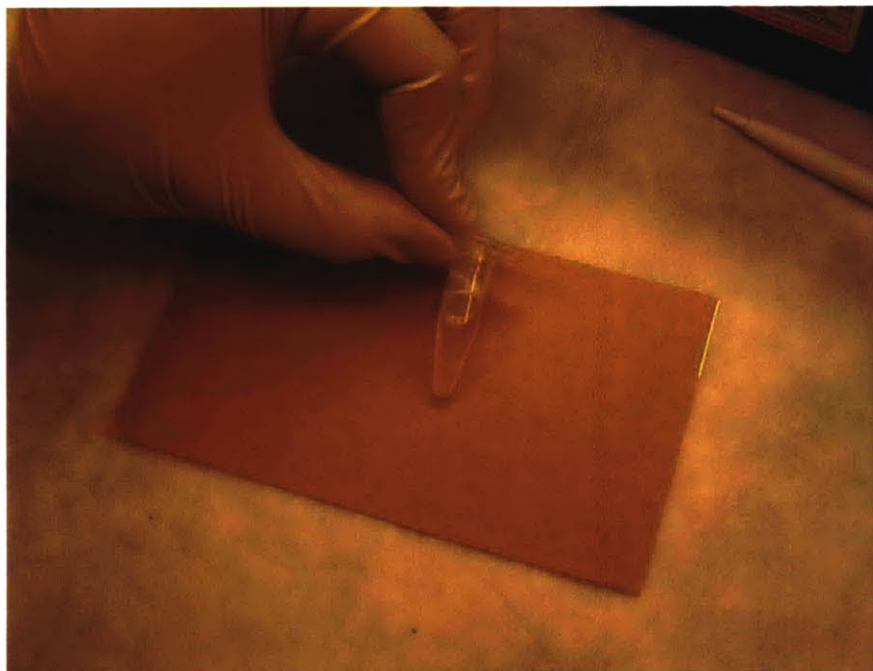
Figure B.4 Slowly push one syringe (left), so that all the solution in it goes through the hand-held mini-extruder to the other side, into the other syringe (right).

References

Hanczyc, M. M., Fujikawa, S. M., and Szostak, J. W. (2003). Experimental models of primitive cellular compartments: encapsulation, growth, and division. *Science* 302, 618-622.

Mayer, L. D., Hope, M. J., and Cullis, P. R. (1986). Vesicles of variable sizes produced by a rapid extrusion procedure. *Biochim Biophys Acta* 858, 161-168.

Preparation of Fatty Acid Micelles



Purpose

Here we describe a method for preparing fatty acid micelles. The method for adding micelles to a buffered solution containing fatty acid or phospholipid vesicles is also discussed.

Theory

When the carboxylate head groups of fatty acid amphiphiles are deprotonated, they aggregate into monolayer spherical structures with the hydrophilic head groups pointing outwards and the hydrophobic hydrocarbon chains pointing inwards. These fatty acid micelles, when added to fatty acid or phospholipid vesicles, can be incorporated into the vesicle membranes, leading to an increase of vesicle surface area (Berclaz et al., 2001; Hanczyc et al., 2003; Zhu and Szostak, 2009).

Equipment

Bench top vortex machine

Single depression glass slides

pH meter

1.5 ml Eppendorf tubes

Materials

Oleic acid

Myristoleic acid

NaOH

Deionized water

Solutions and Preparation

Buffers

NaOH solution (100 mM)

Component	Stock	Amount
NaOH solution	10 M	1 ml
Add water to 100 ml		

oleic acid/NaOH solution (100 mM each)

Component	Stock	Amount
oleic acid (pure)	>99%	32 ul
NaOH	100 mM	1 ml

myristoleic acid/NaOH solution (100 mM each)

Component	Stock	Amount
myristoleic acid (pure)	>99%	28 ul
NaOH	100 mM	1 ml

Protocol

Duration

Preparation	about 10 minutes
Protocol	about 1 hour

Preparation Fatty acids are often shipped in sealed glass ampoules. Break the ampoule and pipette the fatty acid into an Eppendorf tube for later use.

Caution Use paper towels or clean gloves to wrap the ampoule, to avoid injuries from broken glass pieces. All lipids should be stored at -20°C .

Step 1 Dissolving fatty acid in a NaOH solution

Overview Dissolving fatty acid in a NaOH solution, to 1:1 molar concentration ratio

Duration 20 min

1.1 Pipette an appropriate amount (see the Solutions and Buffers section) of fatty acid into the bottom of a 1.5 ml Eppendorf tube. Add NaOH solution, so that the final molar amounts of fatty acid and NaOH are equal in the solution.

Tip The sample should be maintained above the melting temperature of the fatty acid(s) used.

1.2 Vortex the sample using a bench top vortex machine for 30 seconds to fully disperse the fatty acid in the NaOH solution (Figure C.1). (Large, visible air bubbles may form during the process, as shown in Figure C.1 and Figure C.2).

Tip *Avoid light by wrapping aluminum foil around the sample. Avoid oxygen by flushing the container with argon or nitrogen gas.*

1.3 Allow the sample to sit for 1 hr, until the air bubbles disappear, and fatty acid micelles should have formed.

Step 2 Addition of fatty acid micelles to vesicles

Overview Addition of fatty acid micelles to fatty acid vesicles or phospholipid vesicles, for experiments on vesicle growth (Berclaz et al., 2001; Hanczyc et al., 2003; Zhu and Szostak, 2009).

Duration 10 min

2.1 To ensure rapid mixing of fatty acid micelles and vesicles, pipette an appropriate amount of micelles into a 1.5 ml Eppendorf tube first, and add a volume of vesicle suspension. Use the pipette tip to stir the solution for rapid mixing.

Tip *The vesicle suspension should be buffered to avoid pH changes upon the addition of fatty acid micelles that contain NaOH.*

2.2 For imaging, it is necessary to keep the vesicles in the field of view upon the addition of fatty acid micelles. A single depression glass slide can be used: pipette a drop of micelles onto the middle of the single depression glass slide, add

vesicles onto the slide, and briefly stir the sample with the pipette tip. Optical imaging of vesicle growth can be performed by an inverted epifluorescence microscope with extra long working distance (ELWD) objective lenses of 20X or 40X magnification.

Figures



Figure C.1 Vortex the sample using a bench top vortex machine for 30 seconds to fully disperse the fatty acid in the NaOH solution.

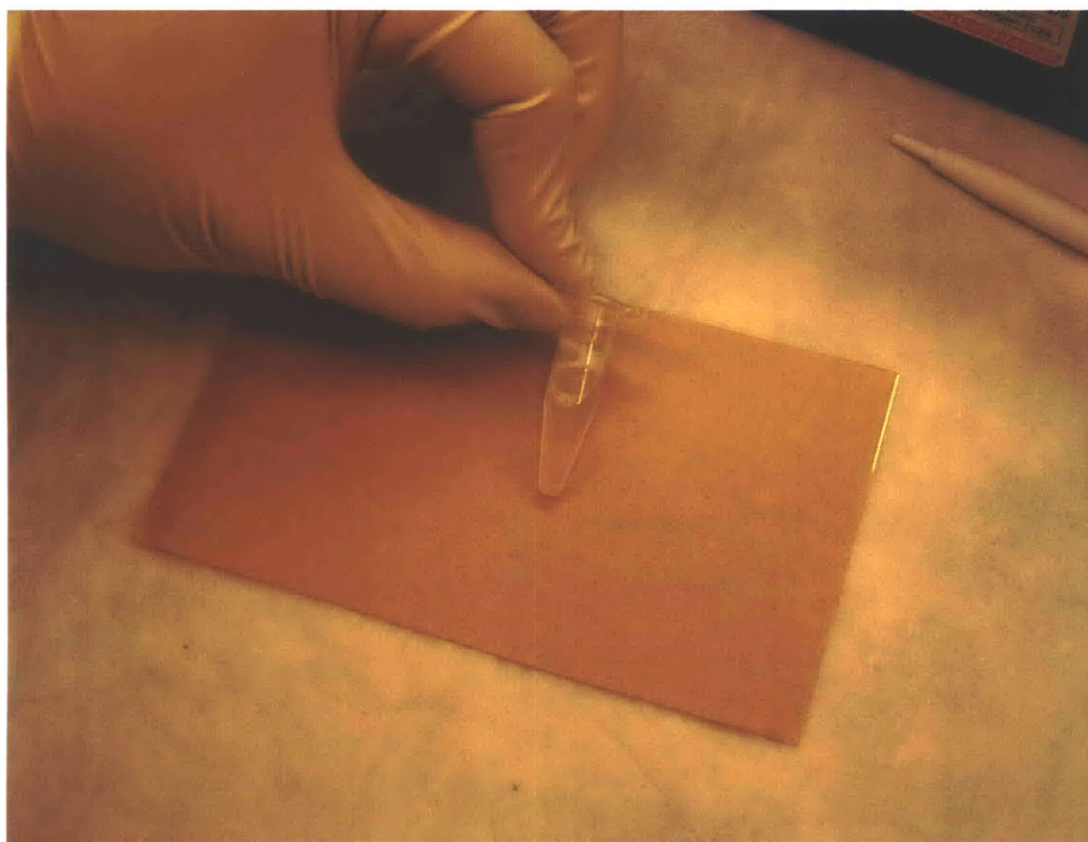


Figure C.2 Large, visible air bubbles appear after vortex.

References

Berclaz, N., Muller, M., Walde, P., and Luisi, P. L. (2001). Growth and transformation of vesicles studied by ferritin labeling and cryotransmission electron microscopy. *J Phys Chem B* *105*, 1056-1064.

Hanczyc, M. M., Fujikawa, S. M., and Szostak, J. W. (2003). Experimental models of primitive cellular compartments: encapsulation, growth, and division. *Science* *302*, 618-622.

Zhu, T. F., and Szostak, J. W. (2009). Coupled growth and division of model protocell membranes. *J Am Chem Soc* *131*, 5705-5713.